NASA Contractor Report 4105

An Experimental Investigation of Dynamic Ground Effect

Pai Hung Lee, C. Edward Lan,
and Vincent U. Muirhead

Flight Research Laboratory
The University of Kansas Center for Research, Inc.
Lawrence, Kansas

NASA

National Aeronautics
and Space Administration

Scientific and Technical
Information Division

1987

SUMMARY

A 60-degree delta wing, an F-106B, and an XB-70 models with and without flap deflections were tested in static and dynamic ground effect in the 36-by-51-inch subsonic wind tunnel at the University of Kansas. Dynamic ground effect was measured with movable sting support. For flow visualization, a tufted wire grid was mounted on the movable sting behind the model.

Test results showed that the lift and drag increments in dynamic ground effect were always lower than the static values. Effect of the trailing-edge flap deflections on lift increments was slight. The fuselage reduced the lift increments at a given ground height. From flow visualization under static conditions, the vortex core was seen to enlarge as the ground was approached.

TABLE OF CONTENTS

LIST OF FIGURES

LIST OF FIGURES, continued

LIST OF SYMBOLS

b   Wing span, ft

C_D Drag coefficient, $\dfrac{Drag}{qS}$

ΔC_D Drag-coefficient increment

C_L Lift Coefficient, $\dfrac{Lift}{qS}$

ΔC_L Lift-coefficient increment

C_m Pitching-moment coefficient

$\bar{c}$ Wing mean aerodynamic chord, ft

D   Drag force, lb,
or
Vortex core diameter, ft

H   Height of quarter chord of wing mean aerodynamic chord above ground, ft

$\dot{h}$ or VH   Vertical velocity, ft/sec

L   Lift force, lb

q   Dynamic pressure, lb/ft^2

RN   Reynolds number

S   Wing area, ft^2

T   Wind-tunnel test section temperature, $^\circ F$

t   Time, sec

x   Longitudinal axis distance, ft

y   Lateral axis distance, ft

z   Vertical axis, ft

α Angle of attack, deg

δ_f Flap deflection, deg

Subscripts:

r   Wing root

o   Initial value

∞ Free stream

Abbreviations:

B   Body (i.e. fuselage)

C   Canard

V   Vertical tail

W   Wing

1. INTRODUCTION

Flight tests to determine ground effect on the aerodynamic characteristics of an airplane are usually conducted with either the fly-by technique or the constant-angle-of-attack approach. Using the former method, a constant ground height is maintained in each flight. It has been found that results obtained from this technique agreed well with those from conventional static wind-tunnel test (References 1-3). On the other hand, with the latter method, constant angle-of-attack and power setting are maintained while the ground height varies continuously in the same flight (Reference 4). It was found in Reference 4 that a significant difference was present in the incremental lift coefficient determined by these two methods for a modified F5D-1 configuration. The main advantage of the constant angle-of-attack technique is that it represents a better simulation of an actual landing operation. In addition, it requires fewer test runs for the same ground-height and angle-of-attack range (Reference 4).

To simulate the constant angle-of-attack technique in a wind tunnel, a test technique of moving a model toward a ground board was developed in Reference 5. Five wing models, including those of the F-104A and the XB-70, were tested. It was found that for configurations with low sweep, dynamic test results agreed well with static data. However, for highly swept, low-aspect-ratio wings, the lift increment from static ground effects tests was found to be considerably higher than that from dynamic testing. In addition,

1

dynamic wind-tunnel test results correlated well with flight test results by the constant angle-of-attack technique. Since only plain wings were tested, it was not certain how a complete configuration with flap deflections would affect the correlation.

In the present investigation, an F-106B and an XB-70 aircraft models were tested to determine dynamic ground effect for wing alone and wing-body combinations, with and without flap deflections. In addition, a 60-degree delta wing was also tested for direct comparison with dynamic ground effect data obtained in the NASA Langley Vortex Research Facility.

2. APPARATUS AND PROCEDURE

2.1 Models

Three basic models were used for the experimental study (Figures 1, 2, and 3). The 60-degree delta wing model had been previously tested by Chang (Reference 5) and Wentz (Reference 7). The 1/48 scale model of the F-106 was constructed from parts of a plastic kit with a wing machined from aluminum. The important geometric features of the aircraft were closely simulated. The model was equipped with flaps which could be set at angles of ±30°, ±15°, or 0°.

The wind-tunnel model of the XB-70-1 was a 1/100 scale model. The wing and canard were constructed from aluminum. The wing flaps

could be set to ±30°, ±15°, or 0°. The fuselage was from a plastic scale model so that important geometric features of the aircraft were closely simulated.

2.2 Mounting

The models were mounted in an inverted position on a movable sting support (Figure 4). Figure 5 shows the sting support with model positioned in the 36" x 51" test section of the University of Kansas wind tunnel. A fixed ground board was placed 4.4" below the wind tunnel's upper surface. By raising the model support with a cable (Figure 6), the model approached the ground board.

For flow visualization, a tufted wire grid was mounted on the movable sting behind the model, as shown in Figure 29.

2.3 Tests

The tests were conducted in the 36" x51" wind tunnel at Reynolds numbers of 300,000 to 750,000. The Reynolds number was controlled by adjusting the wind-tunnel airspeed. Tests were conducted at angles of attack from 0° to 34° and ground heights of an H/b = 1.6 to a low ground-board height determined by the model length and angle of attack. Wing flap angles of 0°, 15°, and -30° were used in the tests.

Two data acquisition systems were used in recording the test data. The analog signals from the sensors during the static tests

were scanned at a rate of 40 channels per second and the voltages fed to a Hewlett Packard 9826 computer. One hundred data points from each channel were averaged to make the calculations for the coefficients.

The dynamic test data were recorded by a twelve-channel visacorder and the Hewlett Packard 9826 computer at a rate of 100,000 samples per second. Each 30 samples from each channel were averaged for coefficient calculations and the calculated data stored. These data contained an oscillatory signal from the natural vibration of the sting during the dynamic tests. To overcome this problem, a computer program based upon the running average of data points was utilized to remove the vibration data. The same method was used in Reference 5.

3. ANALYSIS OF TEST RESULTS

3.1 60-Degree Delta Wing

The longitudinal characteristics of the 60-degree delta wing out-of- and in-ground effect are presented in Figures 7A - 7C. Lift data in Figure 7A show that the present results without ground effect are consistent with Wentz's, except for $\alpha > 25$ degrees. At these high α's, the present results are larger in magnitude by 8-9 percent, probably because of differences in vortex-breakdown characteristics. However, the lift coefficients measured in the

4

Langley Vortex Research Facility (VRF) tend to be lower and the drag coefficients tend to be higher as shown in Figure 7B. Exact reasons for the discrepancy are not known.

Static ground-effect data with H/b = 0.30 are also presented in Figures 7A-7C. The results show that the lift coefficients are always increased, the drag coefficients are decreased, and the longitudinal stability is increased (i.e., $\partial C_m/\partial C_L$ becomes more negative) as the ground height is reduced from H/b = 1.60 to 0.30. Note that in free air, the leading-edge vortices tend to move inboard as the angle of attack is increased, so that the loading near the tips is reduced even before vortex breakdown to produce a less negative pitching moment. From Figure 7C it may be conjectured that in ground effect the leading-edge vortices not only become stronger but also stay more outboard (see also "Flow Visualization," Section 3.4), perhaps because of reduced streamwise velocity due to ground-induced backwash. As a result, the pitching moment becomes more negative. For a configuration without much vortex lift, such as the F-104, this type of change in pitching moment in ground effect did not occur (Reference 5).

Static and dynamic ground effect data on lift and drag are compared in Figures 8A and 8B at α = 14 degrees. As expected, both lift and drag coefficients with dynamic effect are lower than the values under static conditions. It is of interest to note from the Langley Vortex Research Facility (VRF) test data shown in Figure 8A that increasing the sink rate tends to decrease the lift further. This is perhaps caused by the increased vortex lag effect as the

5

sink rate is increased. Data in Figures 8A and 8B are replotted in Figure 9A and 9B in percent increase in C_L and C_D. At high ground heights, all incremental C_L data (Figure 9A) are comparable in magnitude. At lower ground heights the dynamic values are definitely lower than the static ones, and the Langley VRF data show still lower values with higher sink rate. A similar conclusion is applicable to incremental C_D as shown in Figure 9B.

3.2. F-106

The longitudinal characteristics of a clean configuration of the F-106B out of ground effect are presented in Figures 10. The lift coefficients obtained in the Langley 12-foot tunnel are always lower than the present results (Figure 10A), although the vortex-breakdown characteristics appear to be quite similar. In addition, the drag coefficients are higher (Figure 10B) and the pitching moments are more positive (Figure 10C) from the 12-foot tunnel. For the latter, since the slopes of the moment curves for both sets of data are nearly the same, the discrepancy is not caused by the difference in the location of moment center.

As expected, the wing-body lift is lower than that of the wing alone (Figure 10A) and the wing-body drag is higher (Figure 10B). Although the longitudinal stability of the wing-body configuration, as evidenced by the reduced moment-lift slope, is lower than that of the wing alone, the zero-lift moment of the former is much more negative. This is probably caused by the nose camber of the fuselage.

6

The static ground effect on longitudinal aerodynamic characteristics is presented in Figures 11A-11C. As expected, the lift is increased and the drag is reduced in ground effect as shown in Figures 11A and 11B. Longitudinal stability is increased substantially (Figure 11C).

Comparing the results with flap deflection in and out of ground effect (Figures 12 and 13) indicates that lift is increased as usual by ground effect. However, at a given C_L, C_D is not much different in ground effect (see Figures 12B and 13B) at low C_L. Again, the longitudinal stability is increased by ground effect (Figures 12C and 13C).

In Figure 14, variation of longitudinal characteristics with ground height in the static and dynamic tests are presented at an α of 14 degrees. With a positive flap angle of 15 degrees, lift increases more rapidly (Figure 14A); and the drag increase is much smaller (Figure 14B) as the ground height is reduced, when compared with a flap angle of -30 degrees. Meanwhile, the lift and drag coefficient with dynamic effect are always slightly lower than the static data. On the other hand, the static pitching moment becomes much more negative with a positive flap angle as the ground board is approached (see Figure 14C). Comments about the pitching moment in ground effect for the 60-degree delta wing are also applicable for the F-106B configuration.

The percent increases in lift and drag at α = 14 degrees with ground height are presented in Figure 15. Although the lift

7

increments for flap angles of ±15 degrees and -30 degrees are approximately the same, the change in C_D is much lower with a positive flap angle, as it was indicated in Figure 14. This is perhaps because with a positive flap angle, the leading-edge vortex flow is stronger and the conical camber of the F-106 will produce the effect of a vortex flap to reduce the drag. In addition, the lift and drag coefficients with dynamic effect are lower than the static data (Figure 15). Again, vortex lag may be the contributing factor.

Fuselage effectiveness on lift coefficient, in static and dynamic ground effect is presented in Figure 16. In lift increment, the wing-alone value is always larger than the wing + body + vertical tail configuration in both static and dynamic ground effect.

3.3 XB-70-1 Configuration

The longitudinal characteristics of the XB-70-1 with various ground heights are presented in Figures 17. The lift coefficients obtained in the present (KU) tests are always higher than those from the Langley 7-by-10-foot-tunnel results (Figure 17A). However, the lift-curve slope is seen to be in good agreement. In addition, the drag coefficients are higher (Figure 17B) and the pitching moments are more positive (Figure 17C) from the 7 x 10 foot tunnel. But the slopes of the moment curves for both sets of data are nearly the same.

8

The static ground effect on longitudinal aerodynamic
characteristics of wing alone, wing-body-vertical-tail, and wing-
body-vertical-tail-canard configurations are presented in Figures
18A-18C, Figures 19A-19C, and Figures 20A-20C, respectively. As
expected, the lift is increased in ground effect (Figures 18A, 19A,
and 20A) and the drag is reduced in ground effect at a given C_L
(Figures 18B, 19B, and 20B). Meanwhile, the longitudinal stability
is increased by ground effect (Figures 18C, 19C, and 20C).

From Figures 19C and 20C, it is seen that the canard reduces
the longitudinal stability substantially. Once the lift coefficient
reaches 0.6 ($\alpha > 12°$), the pitching-moment slope relative to the
quarter mean aerodynamic chord starts to change from a negative to a
positive value (Figure 20C). This variation of the pitching-moment
slope indicates that the XB-70-1 has a longitudinal instability in
the high angle-of-attack range.

Comparing the results with flap deflection in and out of ground
effect (Figures 21 and 22) indicates that lift is increased as usual
by ground effect at low C_L (Figures 21A and 22A). Again, the
longitudinal stability is increased by ground effect (Figures 21C
and 22C). However, unlike the F-106B configuration, which produces
a more linear variation for the moment curves in ground effect up to
high angles of attack (Figures 11C and 13C), the pitching moment
curves for the XB-70-1 configuration are quite nonlinear (Figures
20C, 21C, and 22C). This is caused by the canard because without it
the pitching moment curves are much more linear (Figures 18C and
19C).

The lift and drag coefficients in static and dynamic ground effect are shown in Figure 23. Variation with ground height is presented at an α near 14 degrees. The lift and drag are increased as the ground height is reduced. While the lift coefficients with dynamic effect are lower than the static values (Figure 23A), similar to those for the F-106B configuration (Figure 14A), the drag coefficients in dynamic ground effect tend to be higher than the static values, contrary to the results for the F-106B configuration (Figure 14B). This is perhap because the F-106B is equipped with a conical camber similar to a vortex flap, but not the XB-70-1 configuration. The pitching moment becomes more negative as the ground board is approached (Figure 23C). The variation is more rapid with a negative flap deflection. This again can be explained with the more rapidly increasing vortex lift near the tips as the ground is approached. Note that the dynamic pitching moment data are not presented because they are judged to be not reliable. In addition, the lift increment at a flap angle of -30 degrees is higher than that at a flap angle of +15 degrees (Figures 24A, 24B). However, the drag increment with the negative flap angle is lower (Figure 24B). Some dynamic test results are also presented in Figure 24. Again, the lift and drag increments with dynamic effect are always lower than the static test values.

The lift coefficient of the static and dynamic test data with fuselage effect are shown in Figure 25. The wing + body + vertical tail + canard configuration produces less lift increment than the wing alone in both static and dynamic tests.

10

In Figure 26, flight and wind tunnel static and dynamic ground-effect data are compared at an angle of attack of about 9.5 degrees. The general trend for the increase in lift is the same for all four sets of data. However, there is considerable disparity in magnitudes.

3.4 Flow Visualization

The results of the tests to locate vortex core center due to ground effect are presented in Figures 27 and 28. The vortex core was visualized with a tufted screen which was mounted just behind the model's trailing edge.

As the ground height (H/b) was reduced, the vortex core center tended to move outboard (Figures 27A and 28A). Meanwhile, as the flap deflection increased from −30° up to +15° down, the vortex core center shifted inboard (Figures 27A and 28A) and moved closer to the wing upper surface (Figures 27B and 28B). In addition, the vortex core (D/b = Dia/span) was enlarged due to ground height reduction (Figure 29).

4. CONCLUDING REMARKS

A 60-degree delta wing, an F-106B, and an XB-70 models with and without flap deflections have been tested in static and dynamic ground effect. From these test data, the following conclusions could be made.

1. The present data on lift coefficients for the 60-degree delta wing and the XB-70 model were always higher than the Langley (7-by-10-foot or VRF) results, both in the static and dynamic tests. However, the lift-curve slopes appeared to be in good agreement.

2. The lift and drag increments in dynamic ground effect were always lower than the static values.

3. Trailing-edge flap deflection affected the lift increments due to ground effect only slightly. However, the vortex core center tended to move slightly more inboard and closer to the wing upper surface due to flap deflection in ground effect.

4. Comparing the results with wing alone and wing-body data, the fuselage was found to reduce the lift coefficient and lift increments at a given ground height.

5. From flow visualization, the vortex core diameter was seen to increase as the ground height was reduced.

5. REFERENCES

1. Pelagatti, C., Pilon, J. C., and Bardaud, J., "Analyse Critique des Comparaisons des Resultats de Vol aux Previsions de Soufflerie pour des Avions de Transport Subsonique et Supersonique," paper 23, AGARD CP-187, Flight/Ground Testing Facilities Correlation, 1975.

2. O'Leary, C. O., Flight Measurements of Ground Effect on the Lift and Pitching Moment of a Large Transport Aircraft (Comet 3B) and Comparison with Wind Tunnel and Other Data," British ARC R&M 3611, June 1968.

3. Rolls, L. S., and Koenig, D. G., "Flight-Measured Ground Effect on a Low-Aspect Ratio Ogee Wing Including a Comparison With Wind-Tunnel Results," NASA TN D-3431, 1966.

4. Baker, P. A., Schweikhard, W. G., and Young, W. R., "Flight Evaluation of Ground Effect on Several Low-Aspect-Ratio Airplanes," NASA TN D-6053, October 1970.

5. Chang, R. C., and Muirhead, V. U., "Effect of Sink Rate on Ground Effect of Low-Aspect-Ratio Wings," Journal of Aircraft, Vol. 24, March 1987, pp. 176-180.

6. Fink, Marvin P., and Lastinger, James L., "Aerodynamic Characteristics of Low-Aspect-Ratio Wings in Close Proximity to the Ground," NASA TN D-926, 1961.

7. Wentz, William H., Jr., and Kohlman, David L. "Wind Tunnel Investigations of Vortex Breakdown on Slender Sharp-Edged Wings," NASA CR-98737, 1968.
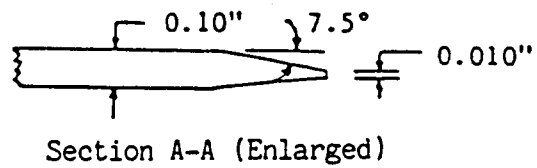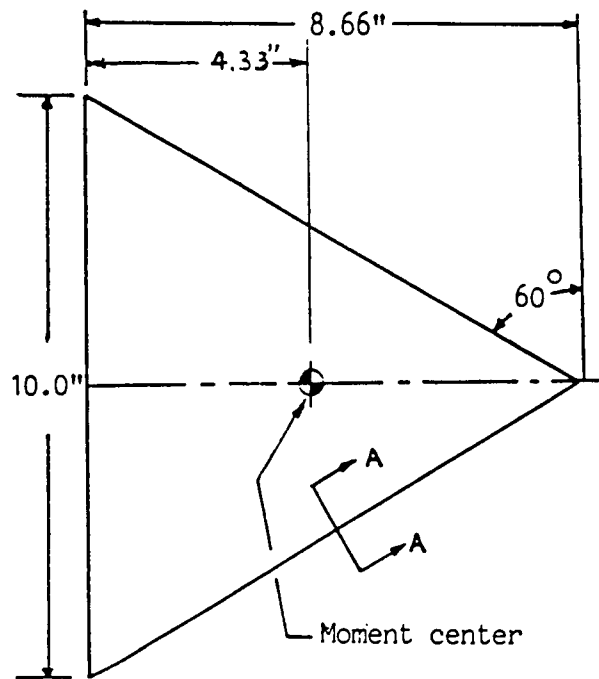
Note: Section A-A is typical of all edges

Figure 1: Model Geometry of a 60-Degree Delta Wing

14
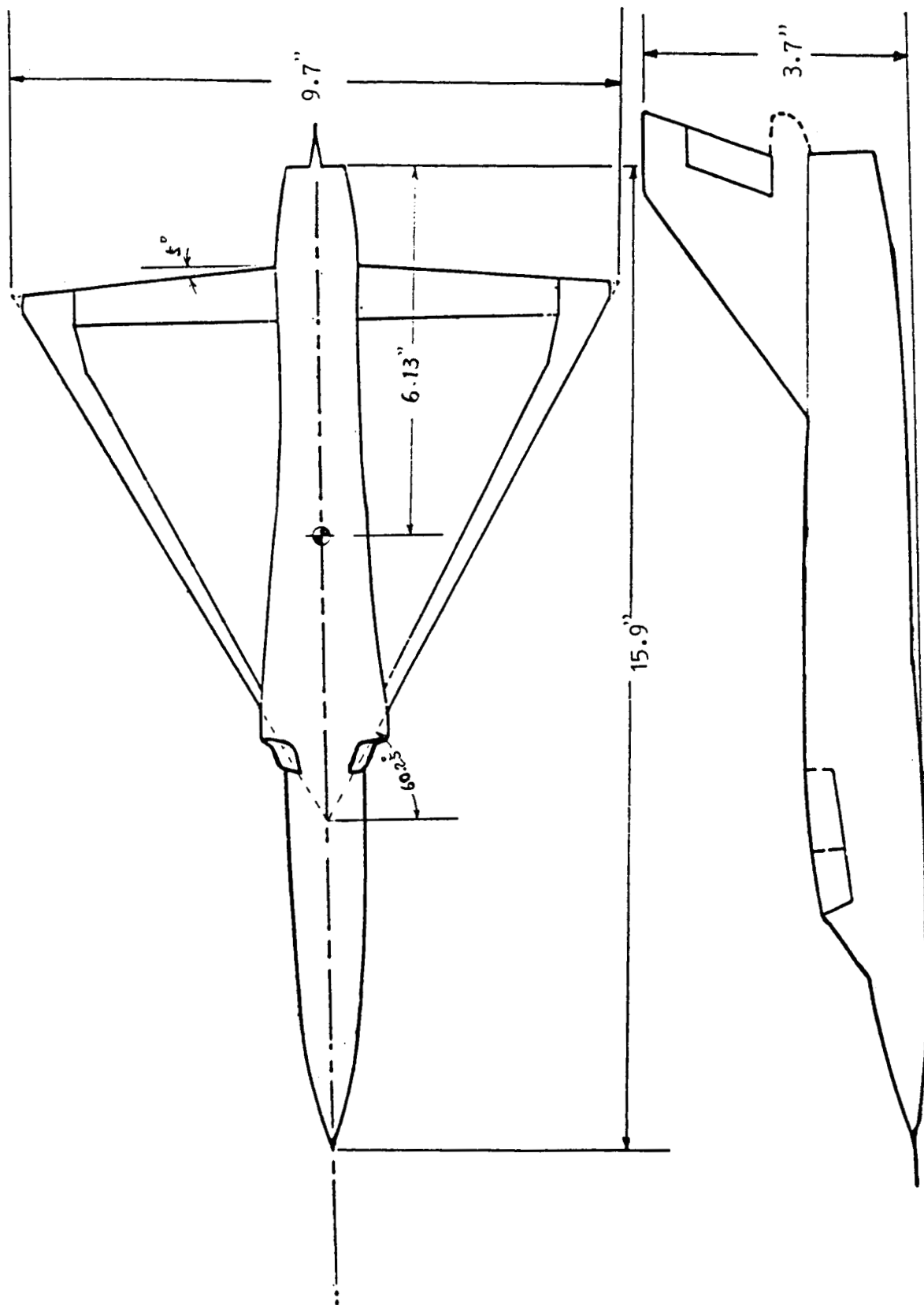
Figure 2: Model Geometry of an F-106 Model

9.7"

6.13"

15.9"

3.7"

60.25°

4°

Note: All dimensions are in inches
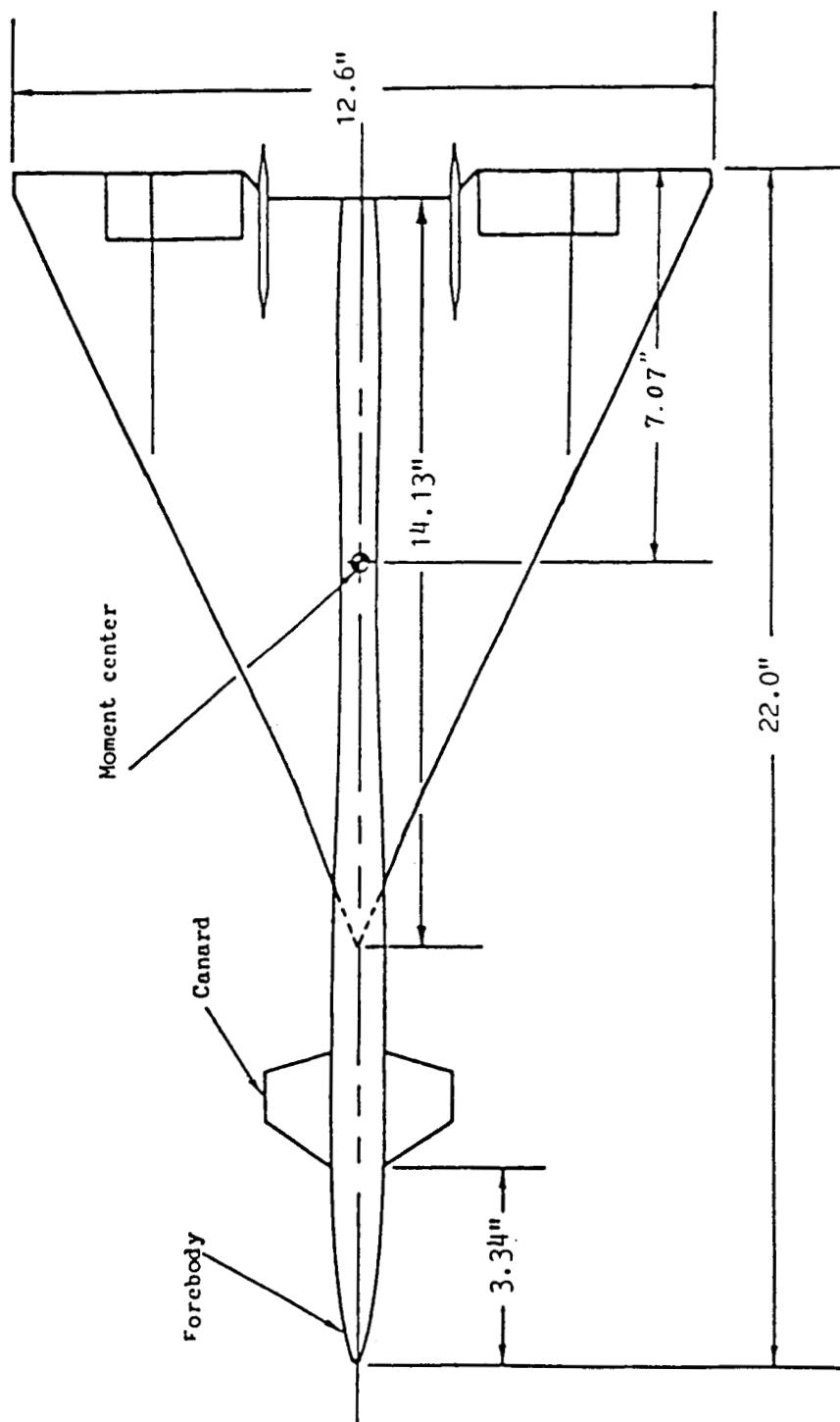
Figure 3: Model Geometry of an XB-70-1 Model

16

Section of
Strain Gage Location

$$I_Z = \frac{\overline{b}\overline{h}^3}{12}$$

Arrangement of
Strain Gages
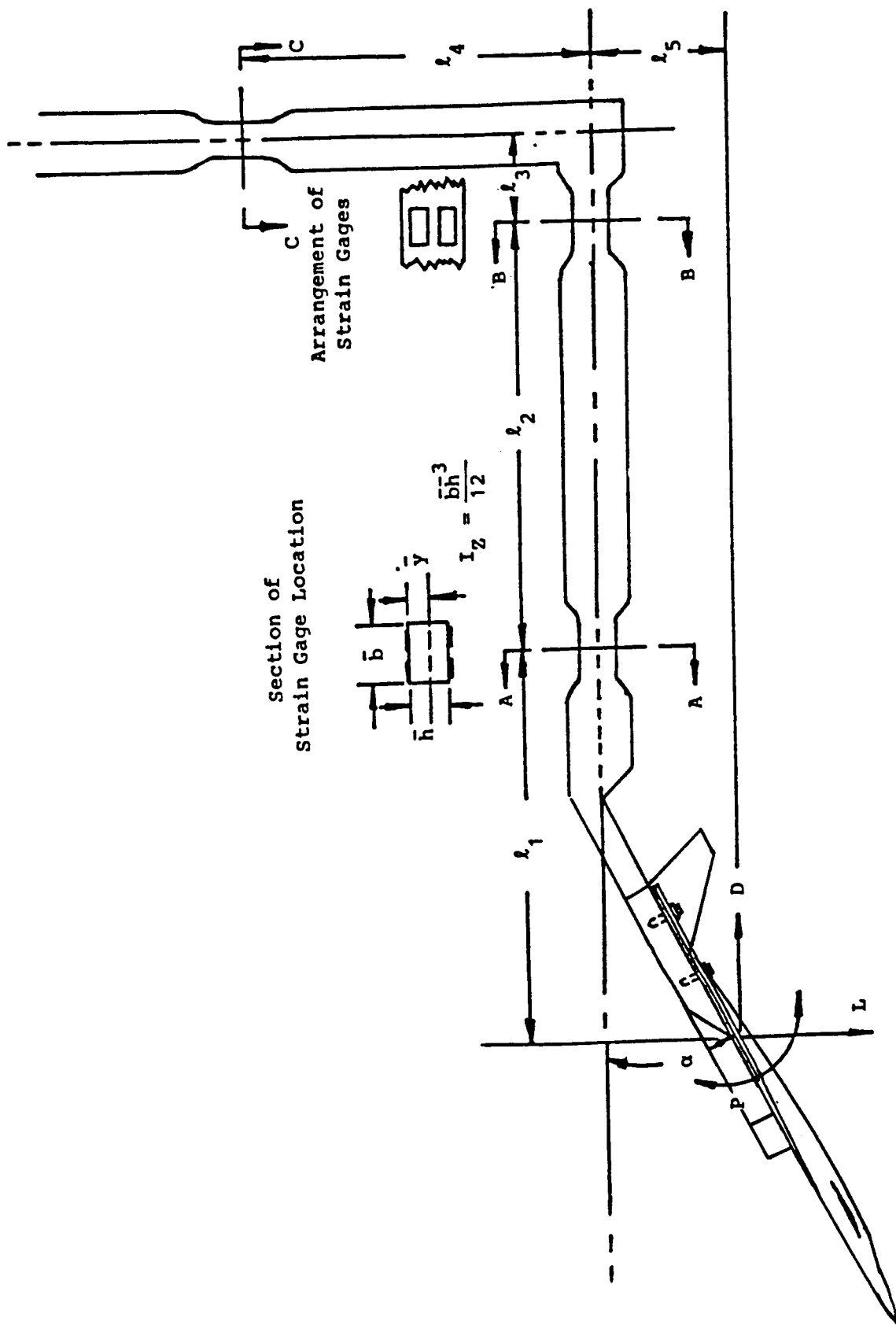
Figure 4: Sting Support and Strain Gage Arrangement

17
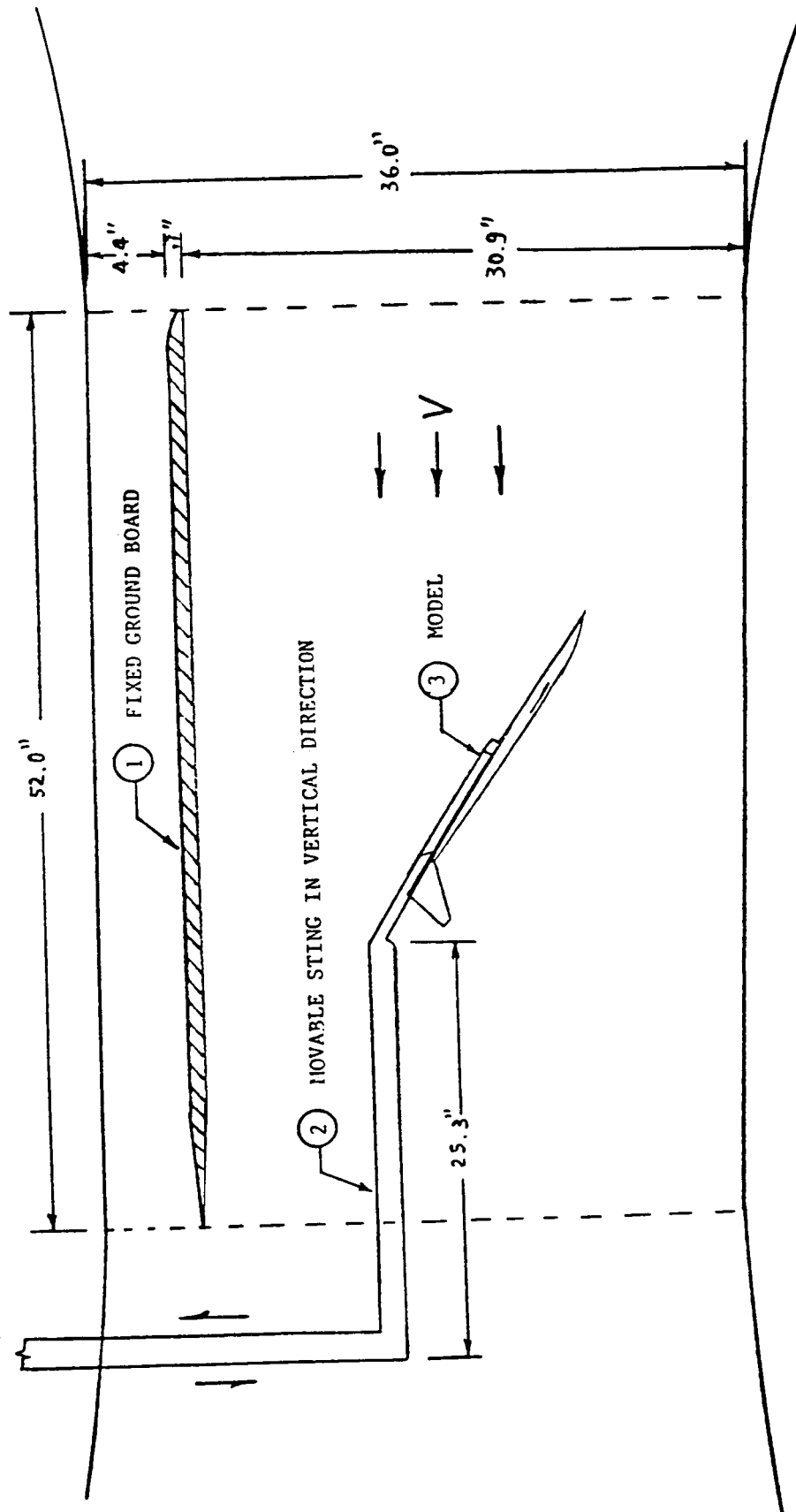
Figure 5: Test Section with Model Support and Ground Board in the KU Wind Tunnel
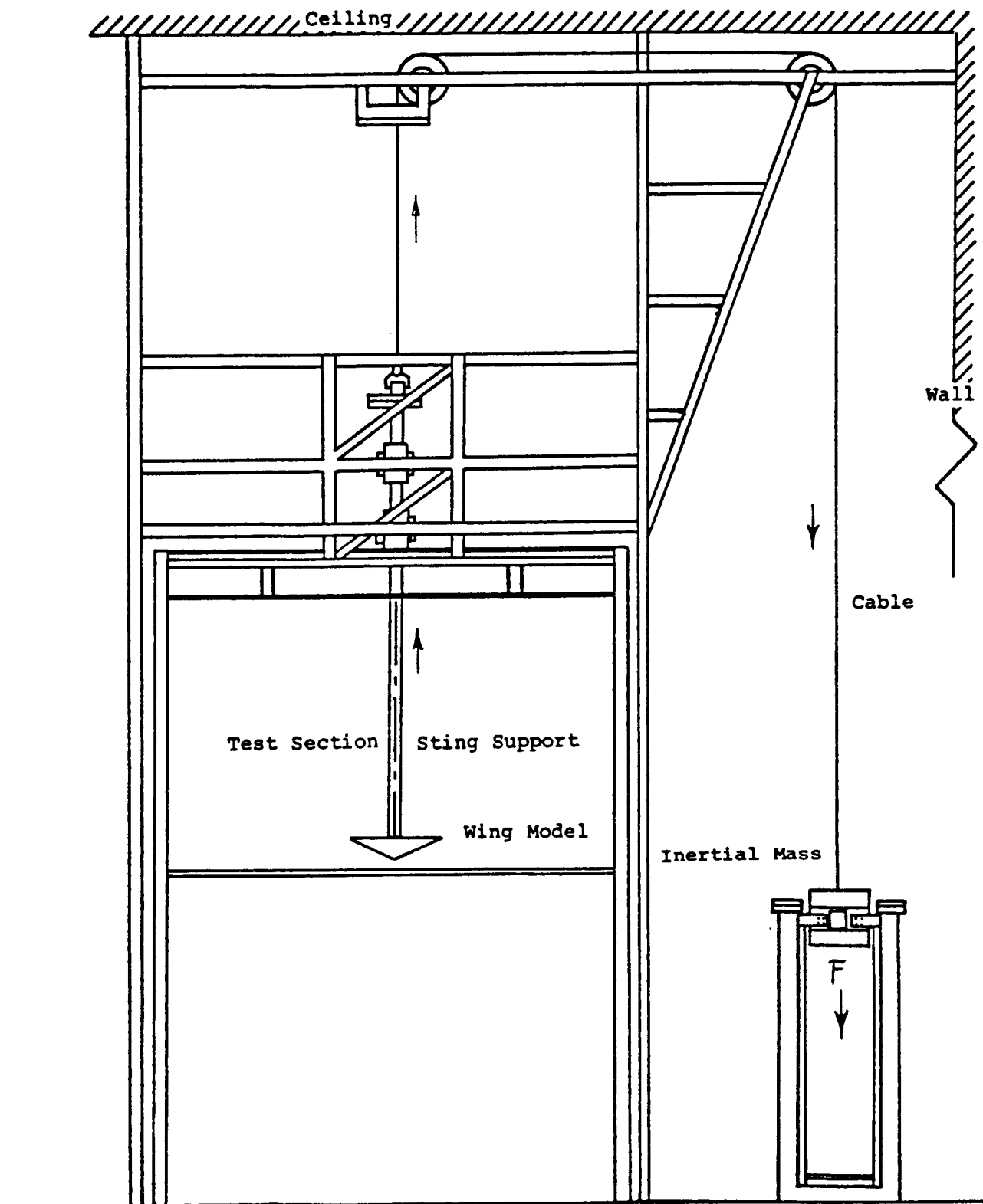
Figure 6: Dynamic ground effect test stand.
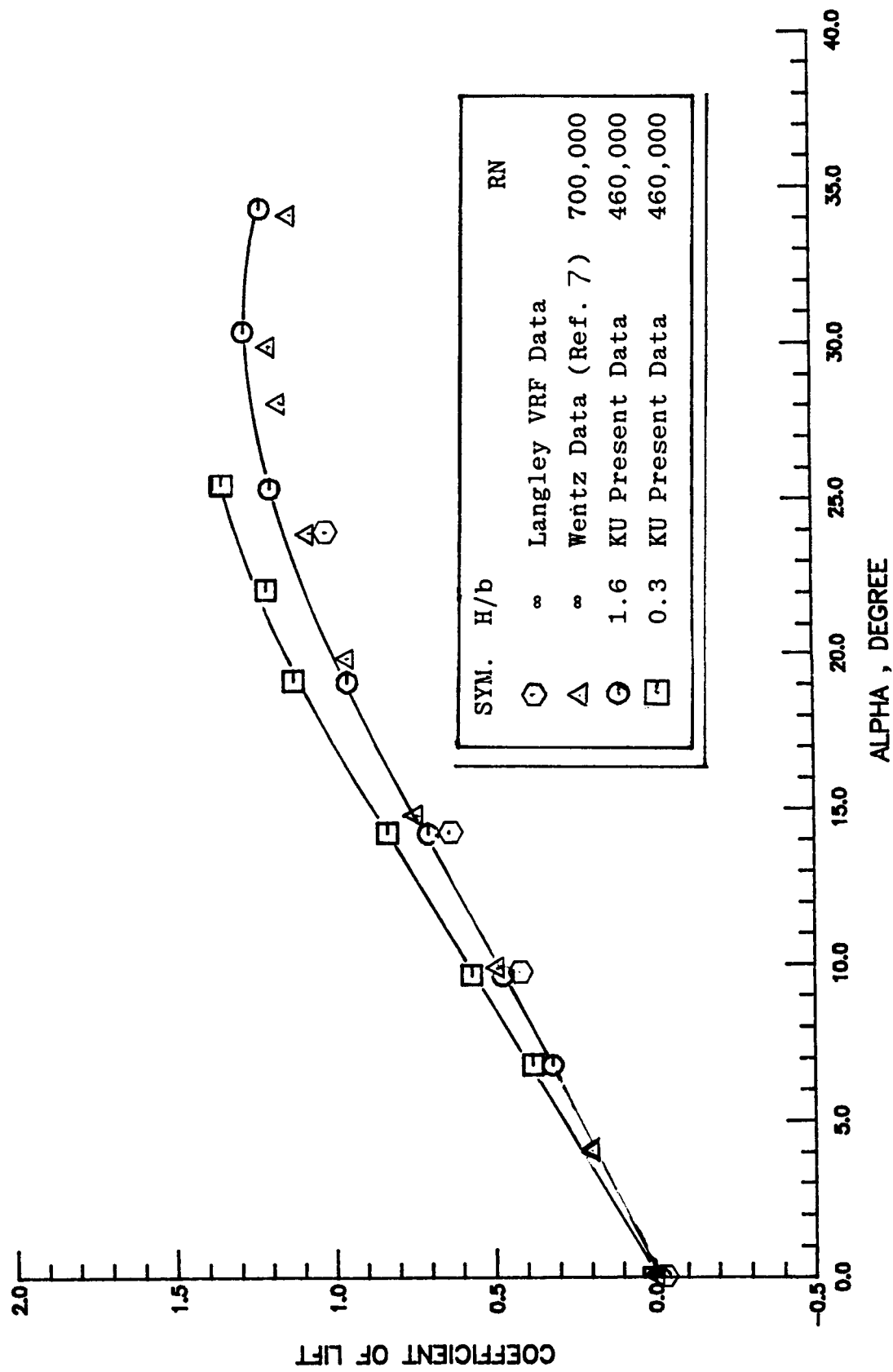
Figure 7 Longitudinal Aerodynamic Characteristics for a
60°-Delta Wing Model in Static Ground Effect

(A) C_L vs α

COEFFICIENT OF DRAG

COEFFICIENT OF LIFT

SYM.	H/b		RN
⬡	∞	Langley VRF Data	
△	∞	Wentz Data (Ref. 7)	700,000
⊖	1.6	KU Present Data	460,000
⊟	0.3	KU Present Data	460,000

(B) C_L vs C_D

Figure 7 Continued.

(C) $C_{m(1/4\bar{c})}$ vs C_L

Figure 7 Concluded.

22

SYM	V_∞(fps)	$\dot{h}$(fps)	
⊙	170.	0.	KU W.T.
– – –	100.	2.85	KU W.T.
———	70.	4.90	Langley VRF
–·–·–	90.	6.30	Langley VRF
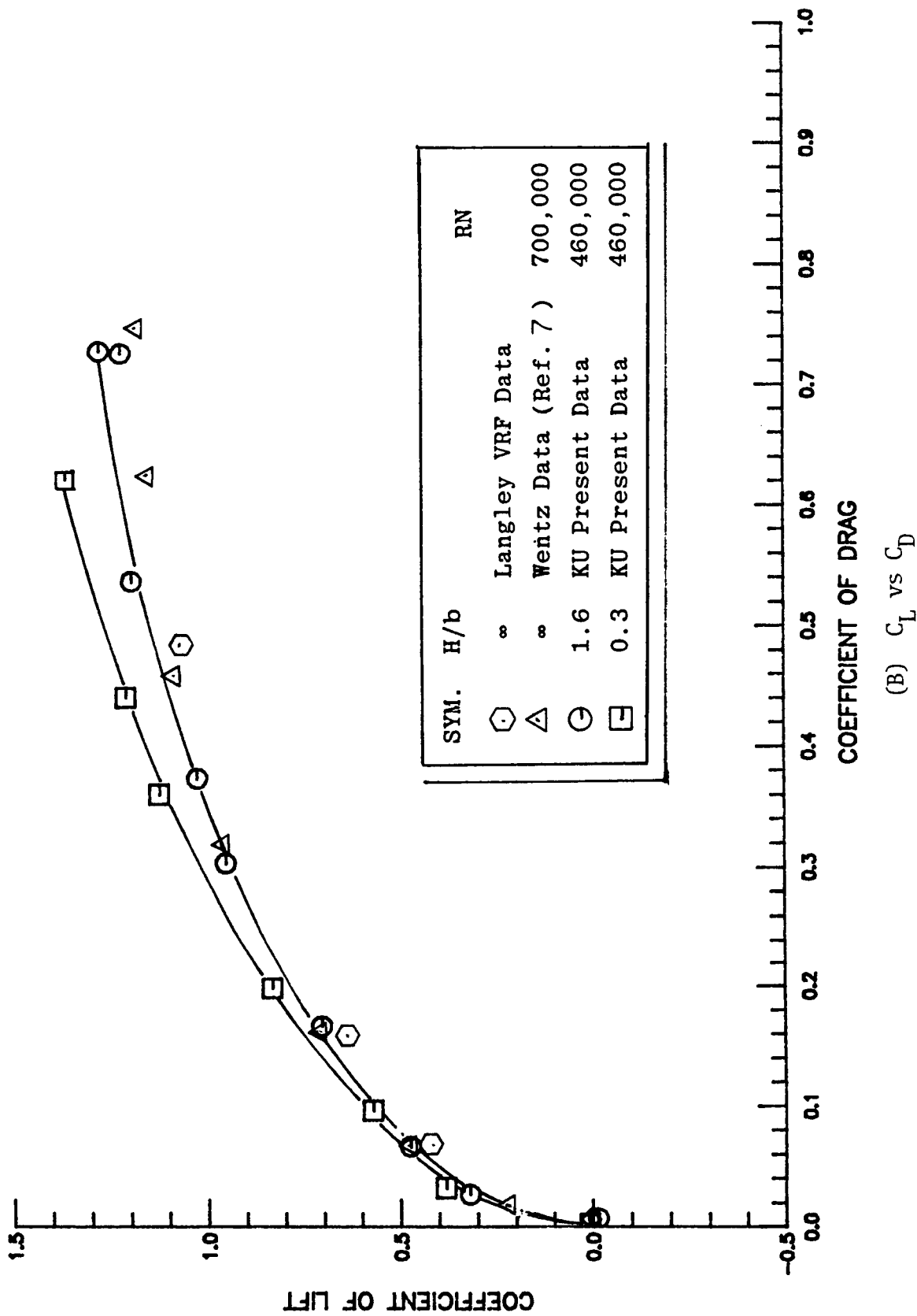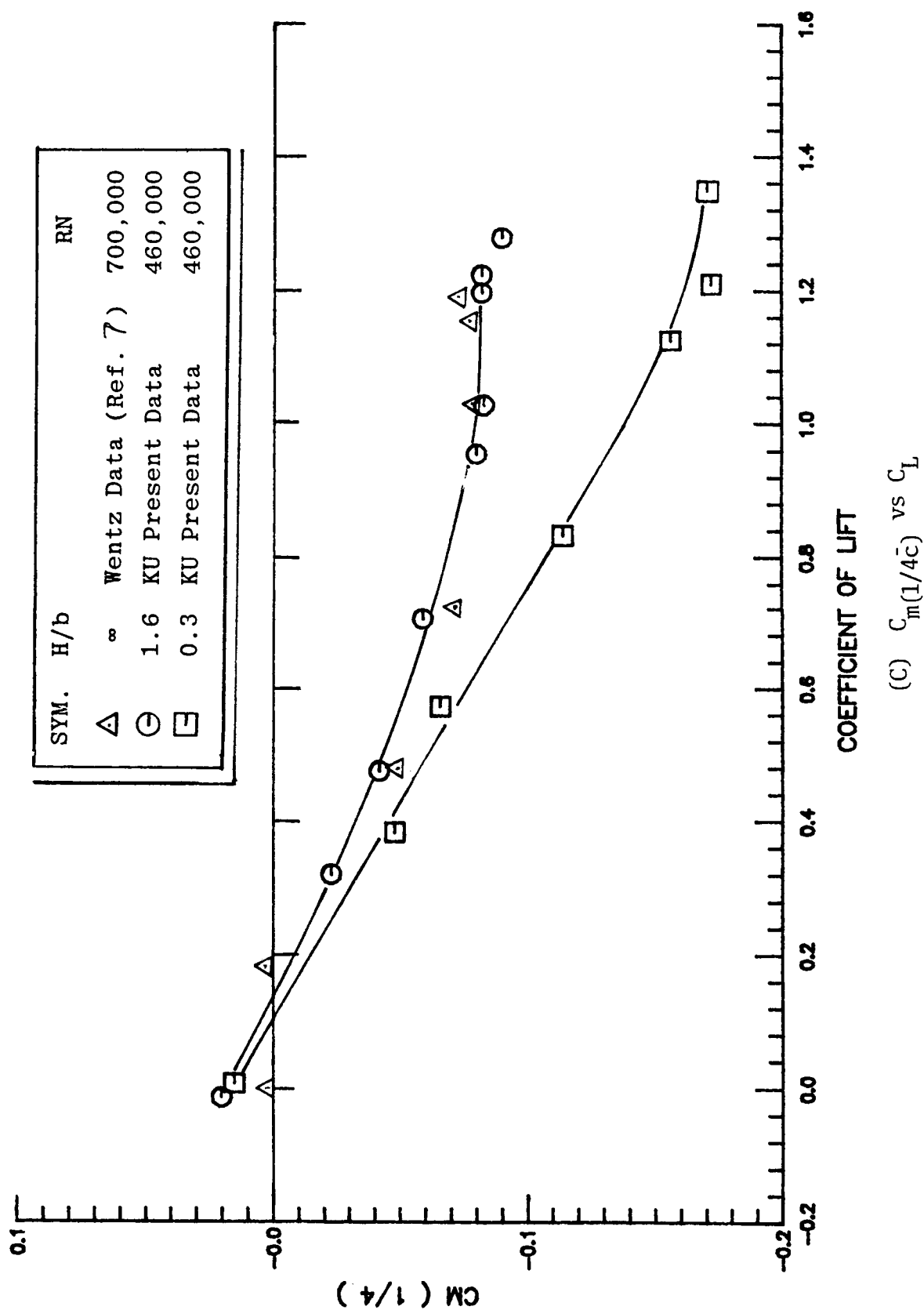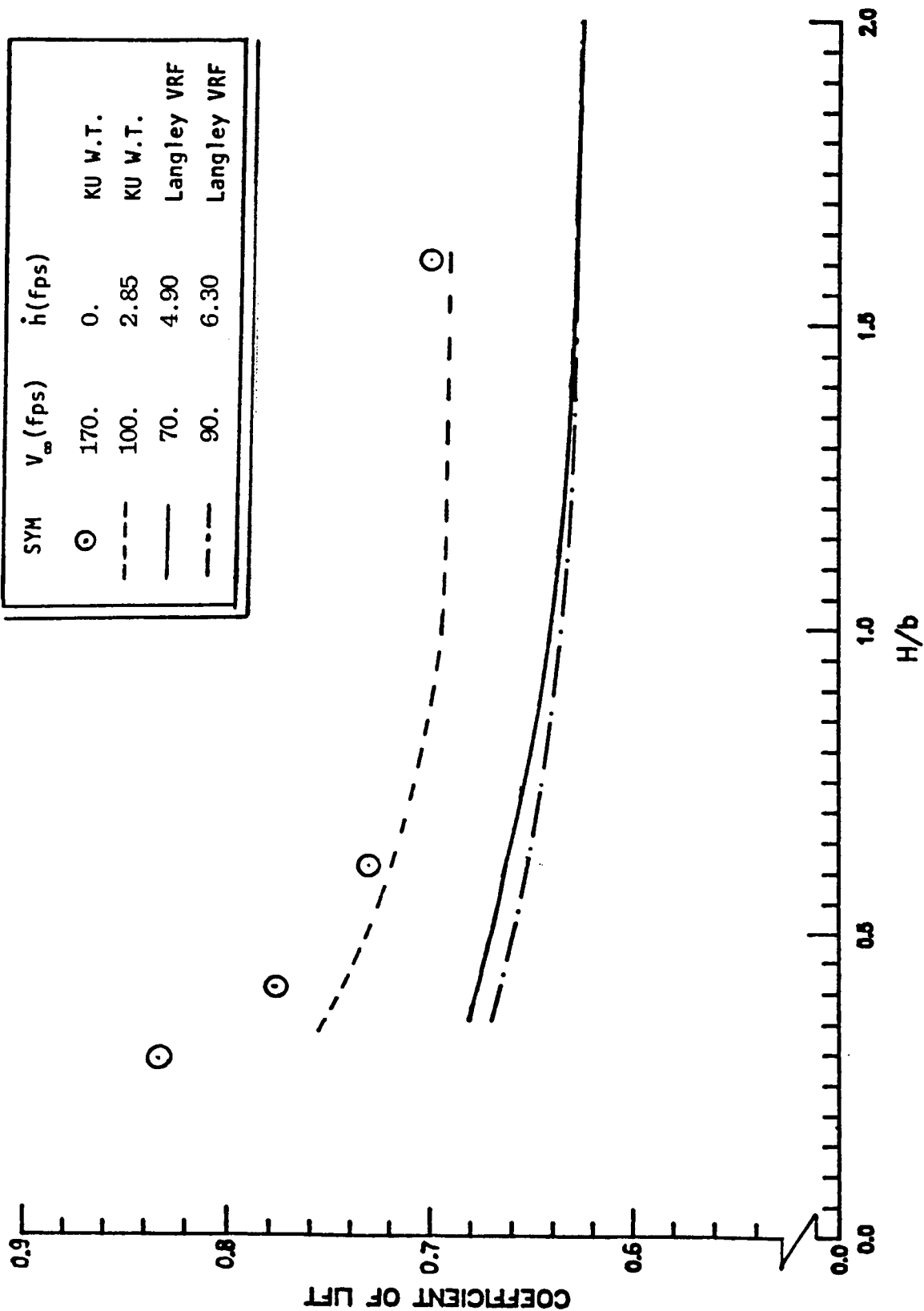
(A) C_L vs H/b

Figure 8   Longitudinal Aerodynamic Characteristics for a 60°-Delta Wing Model in Static and Dynamic Ground Effect at Different Ground Heights. α = 14 degrees.
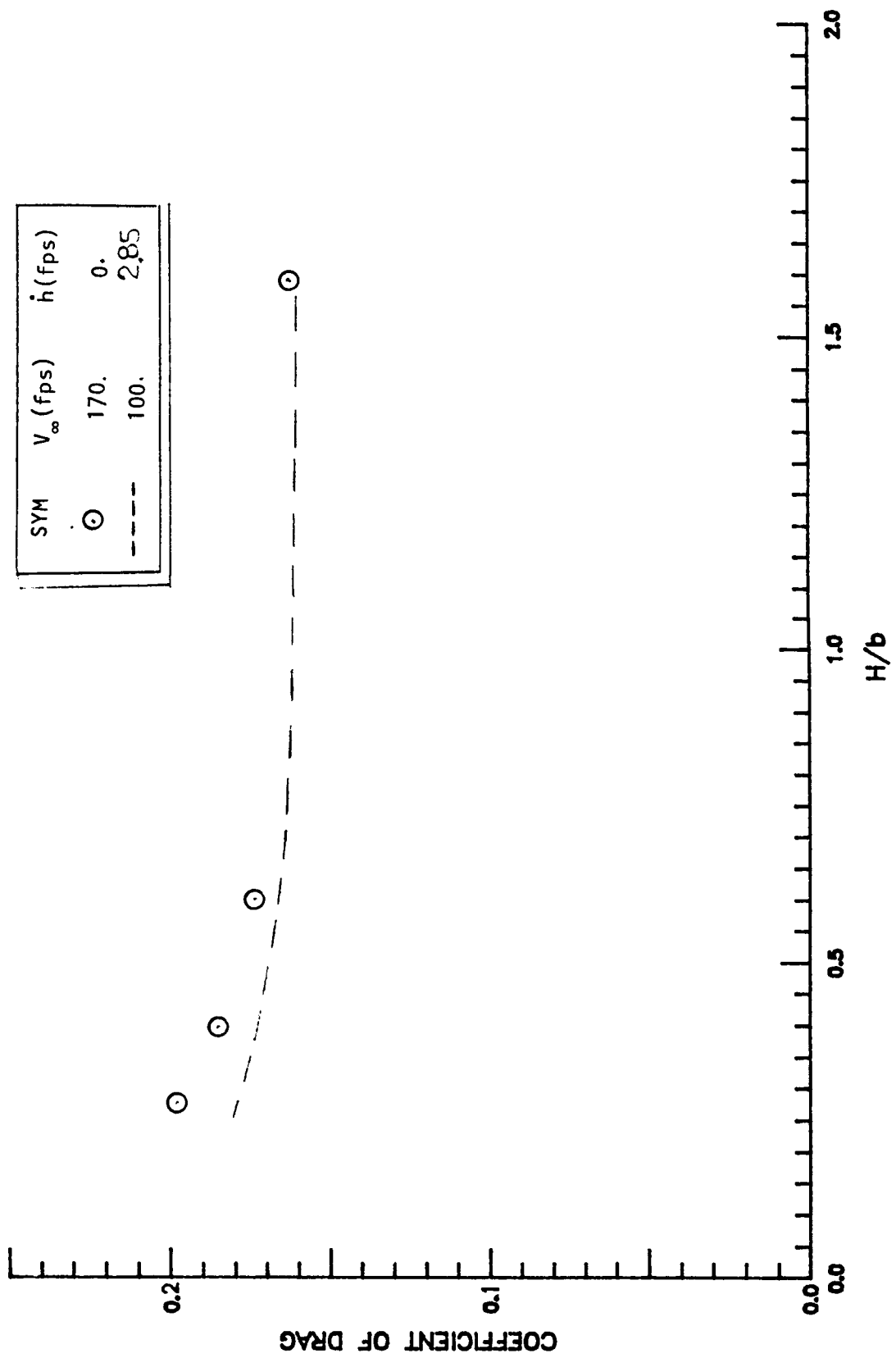
(B) C_D vs H/b

Figure 8   Concluded.

24
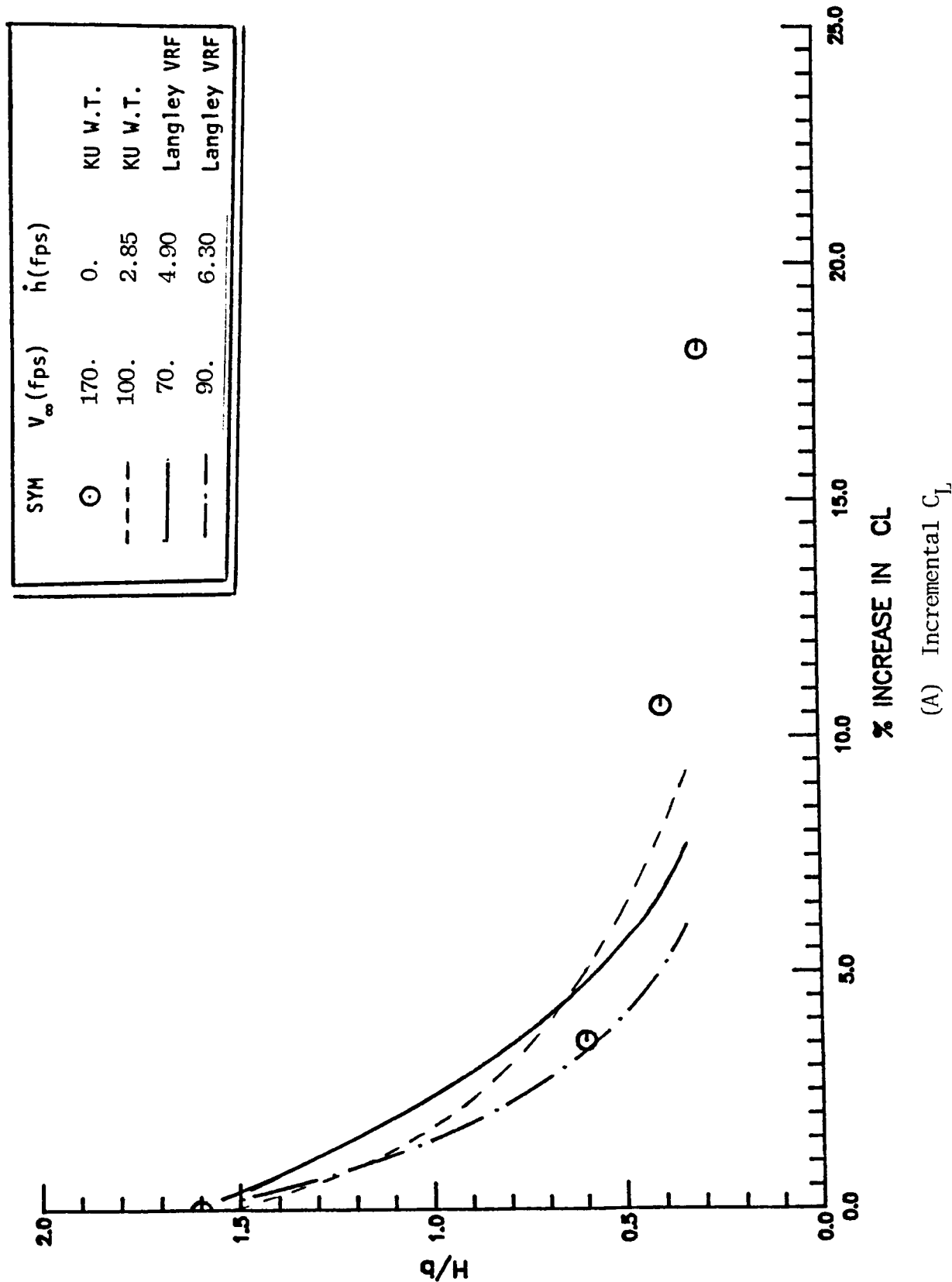
Figure 9 Incremental Lift and Drag Coefficients for a 60°-Delta Wing Model in Static and Dynamic Ground Effect at α = 14 degrees.
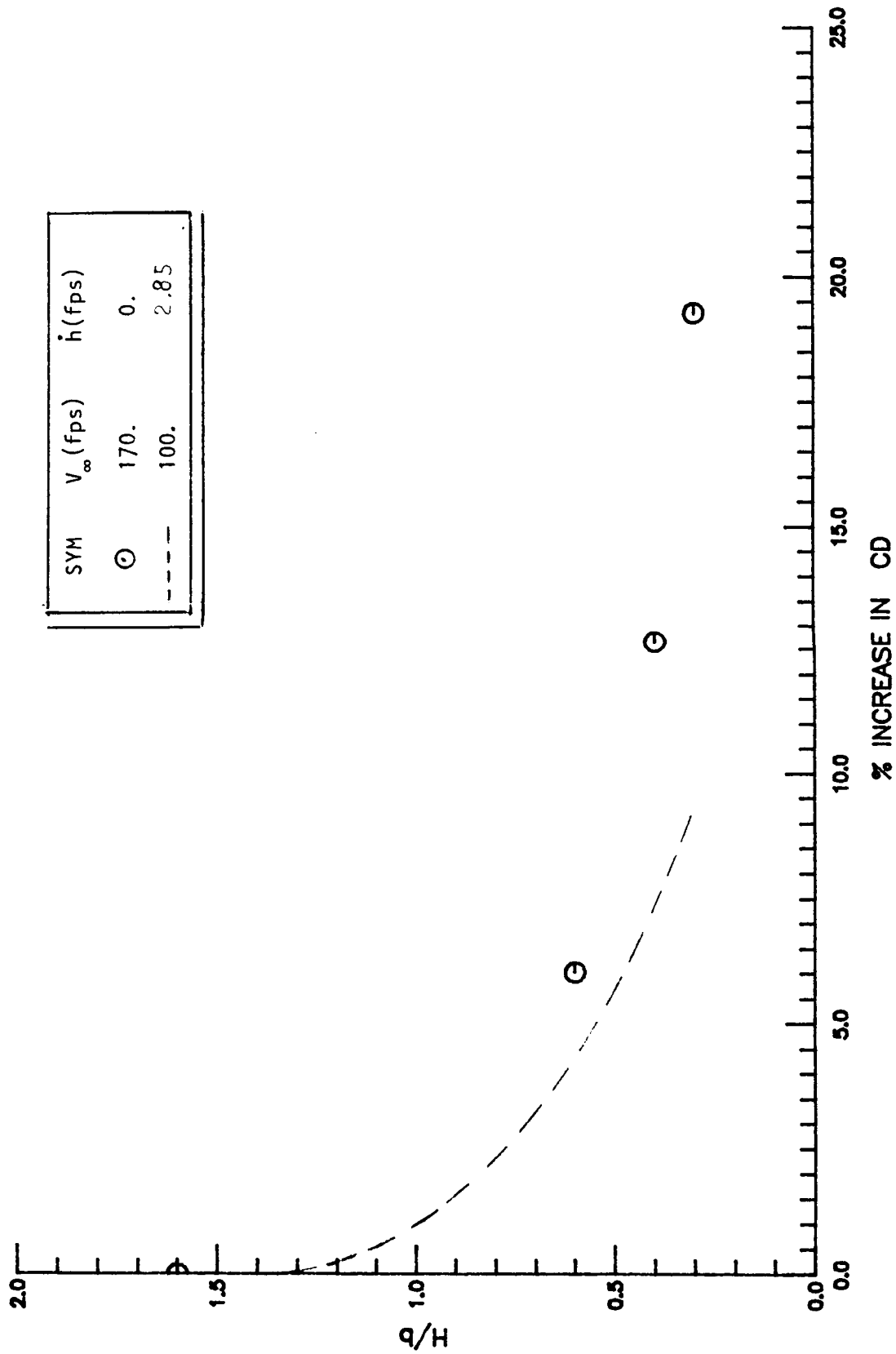
(A) Incremental C_L

(B) Incremental C_D

Figure 9 Concluded.
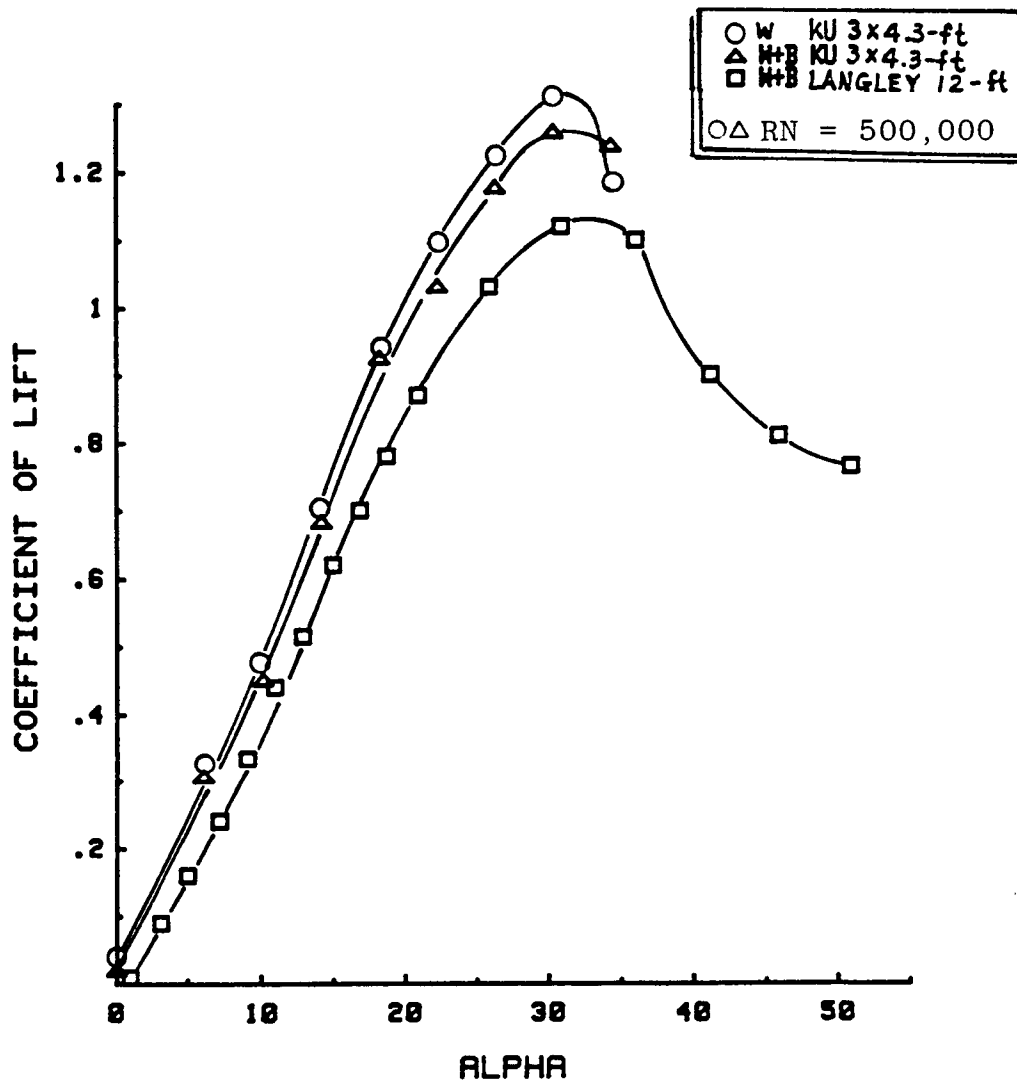
(A) C_L vs α

Figure 10   Longitudinal Aerodynamic Characteristics for an F-106 Model in Out-of-ground Effect

27

COEFFICIENT OF DRAG
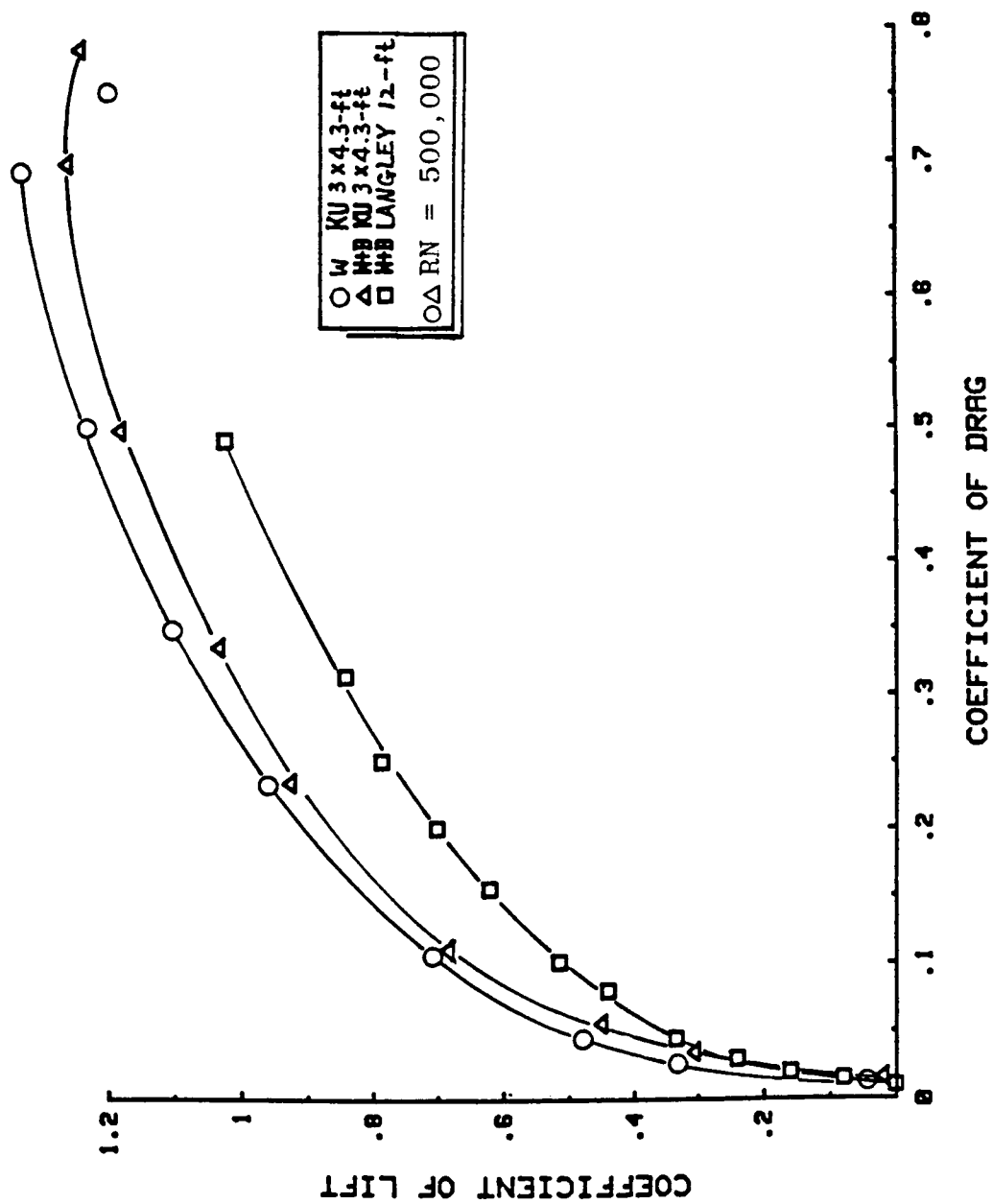
(B) C_L vs C_D

Figure 10   Continued.

28
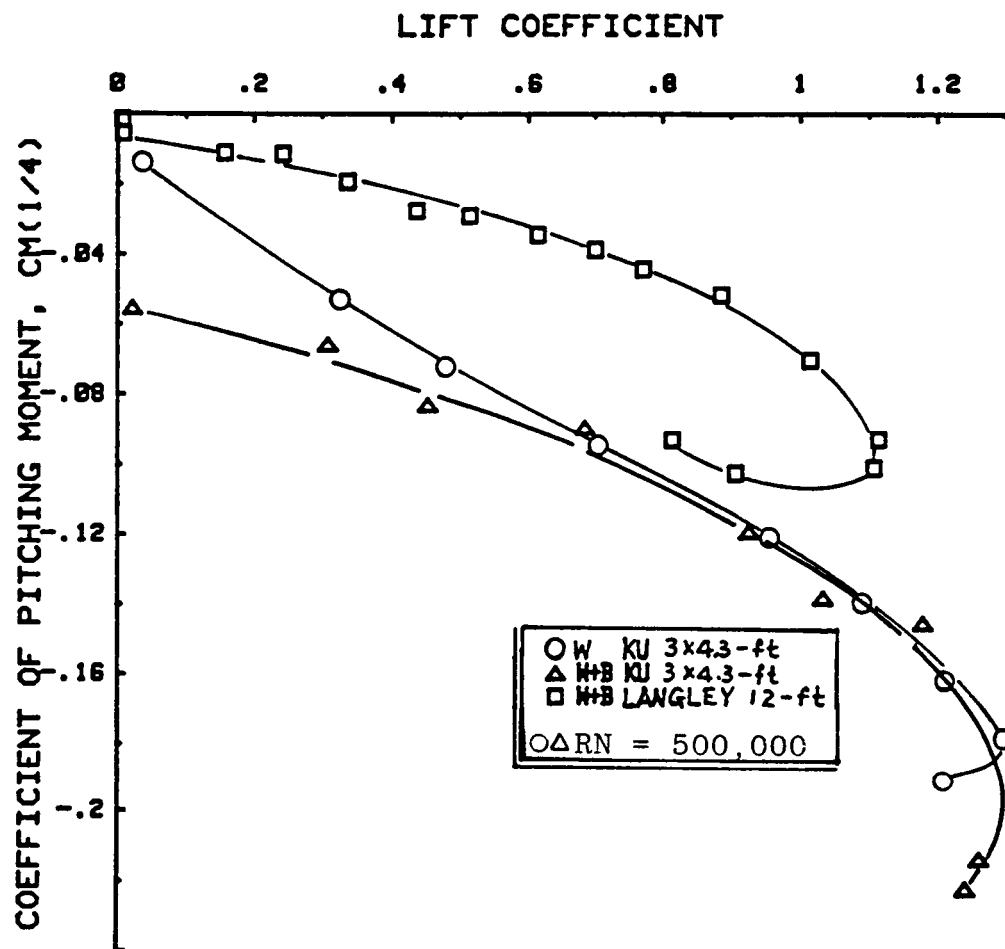
(C) $C_{m(1/4\bar{c})}$ vs C_L

Figure 10   Concluded.
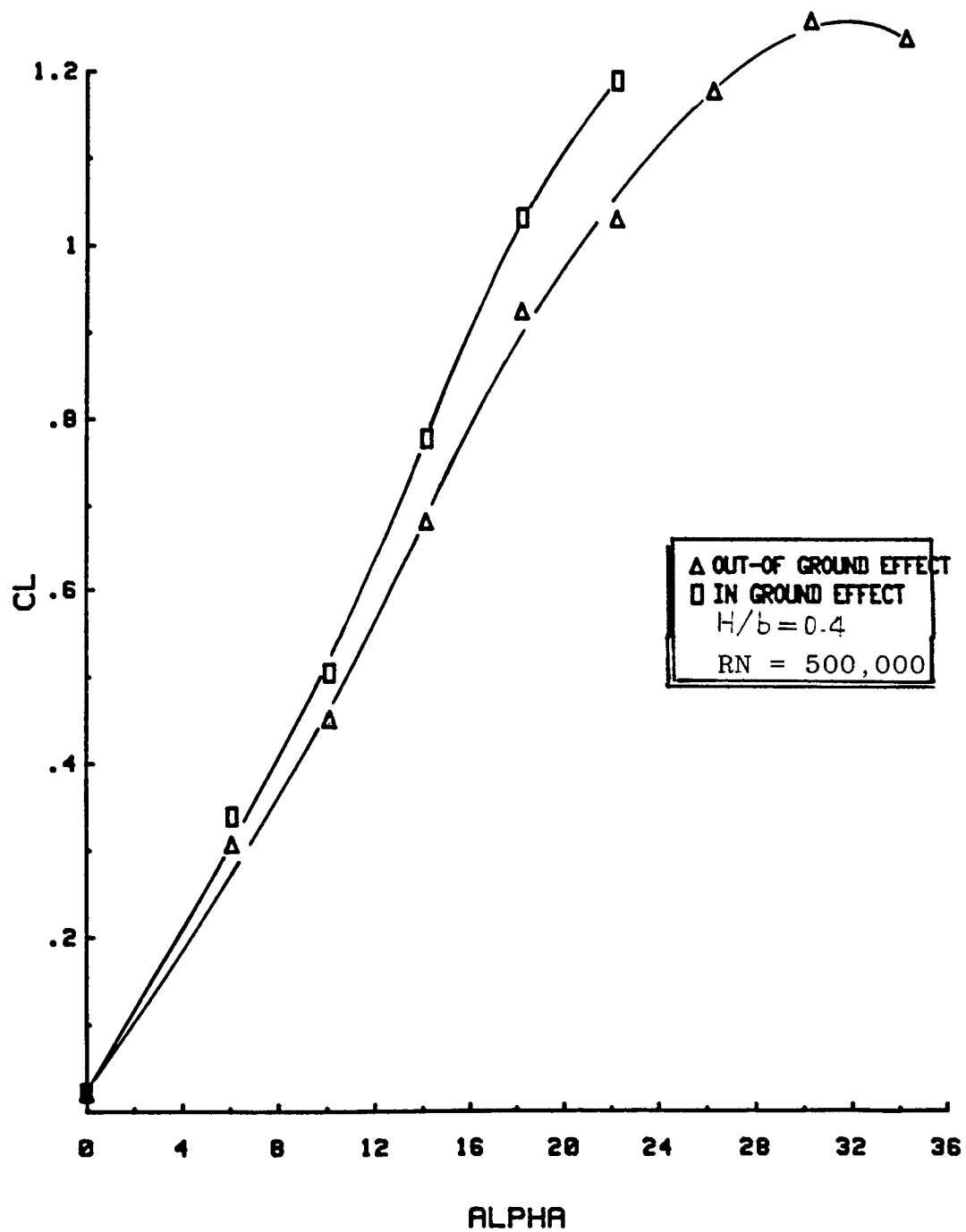
(A) C_L vs α

Figure 11   Longitudinal Aerodynamic Characteristics for an F-106
Model in Static Ground Effect. H/b = 0.4.
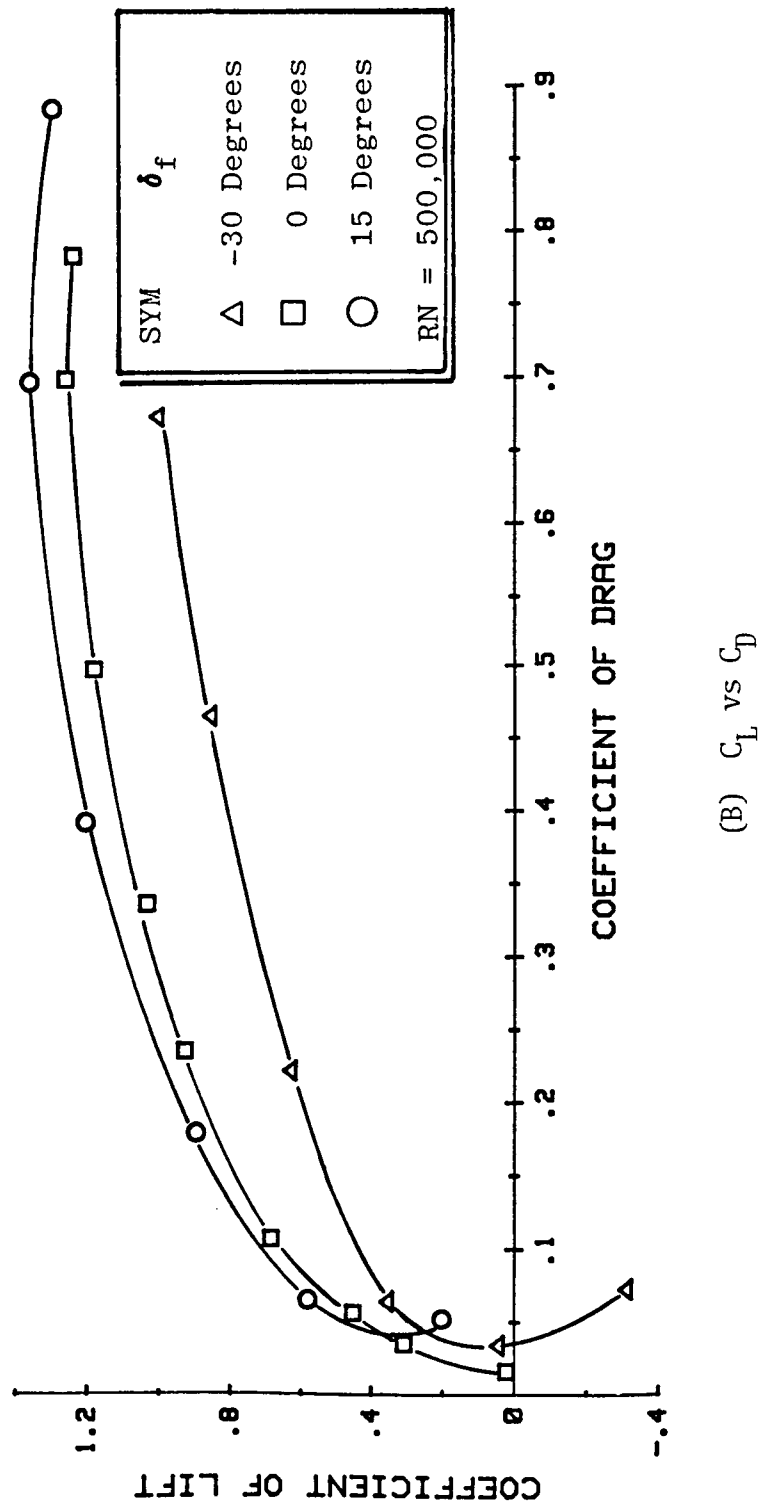
30
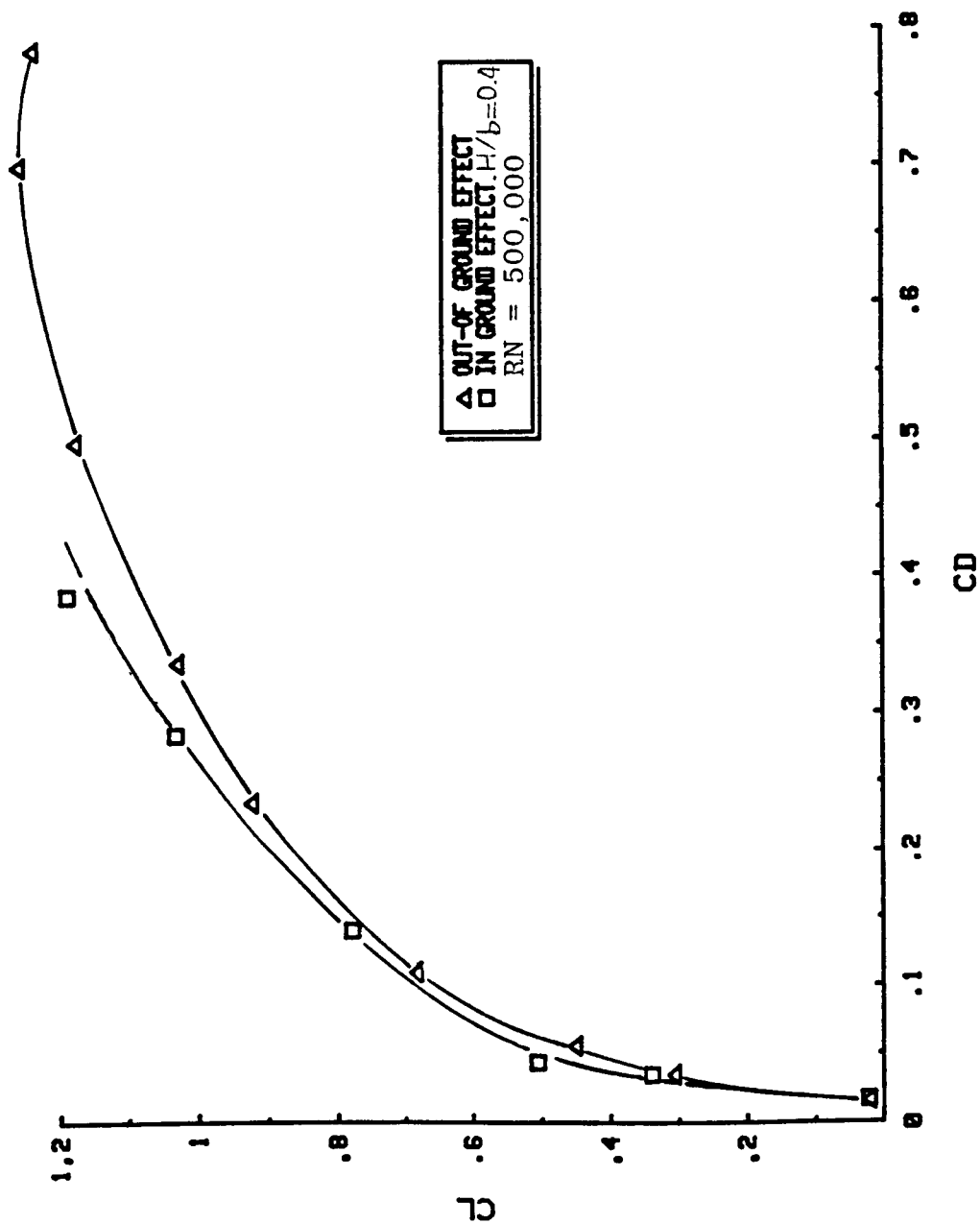
(B) C_L vs C_D

Figure 11 Continued.
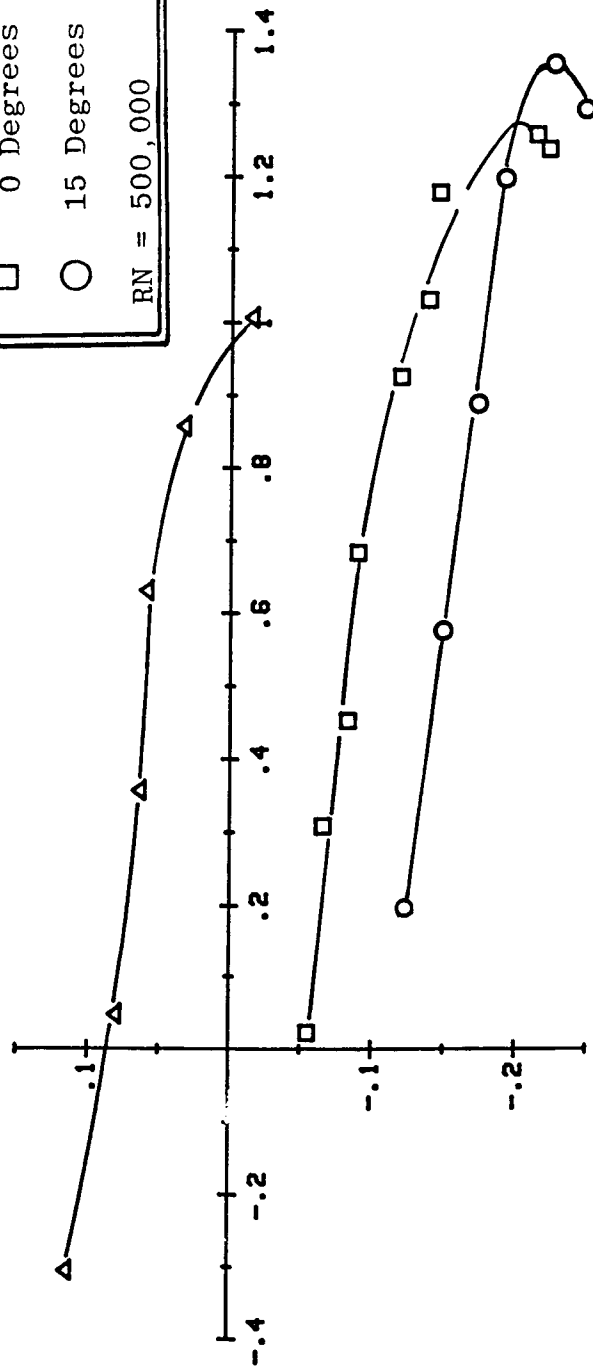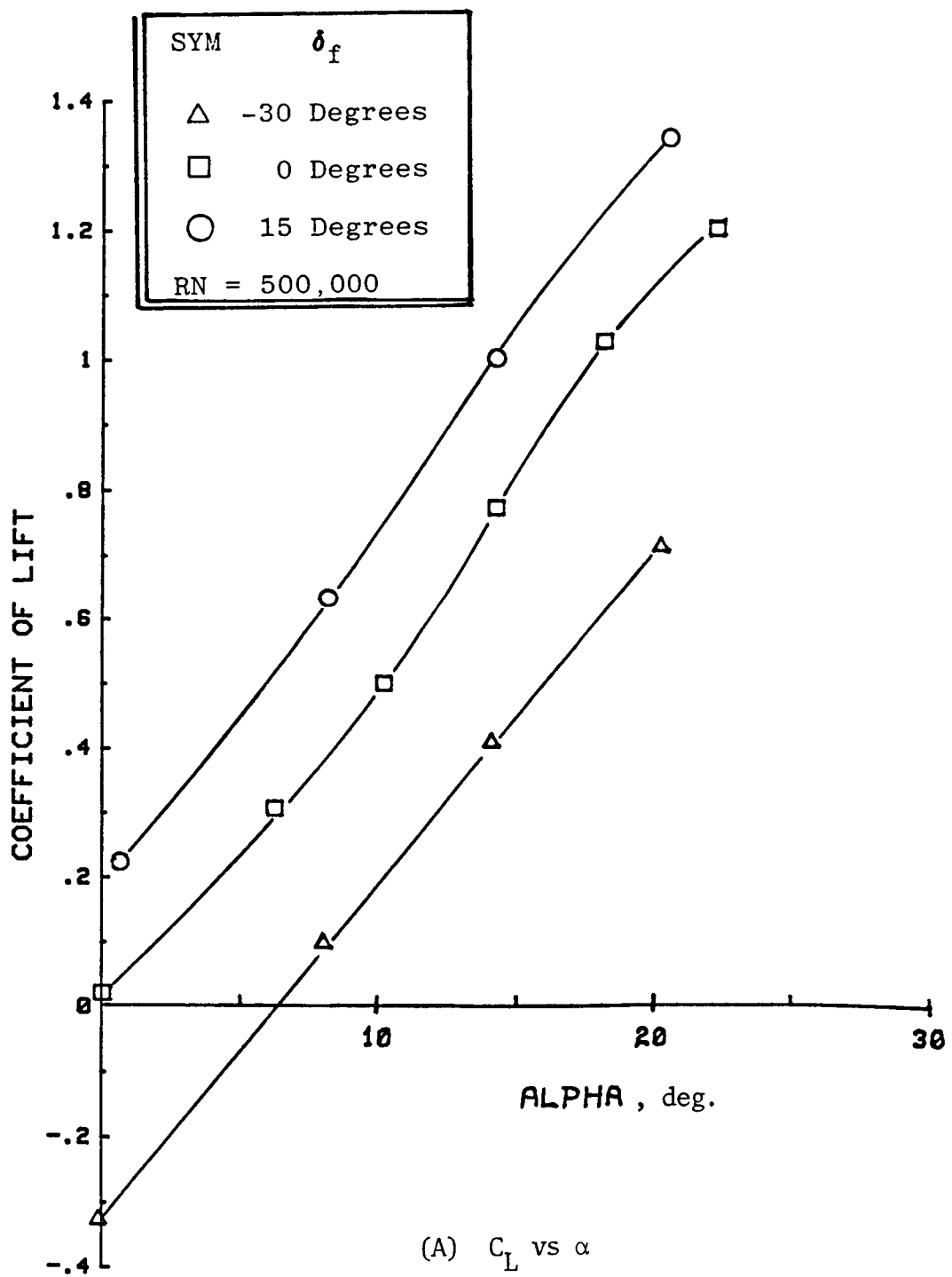
31
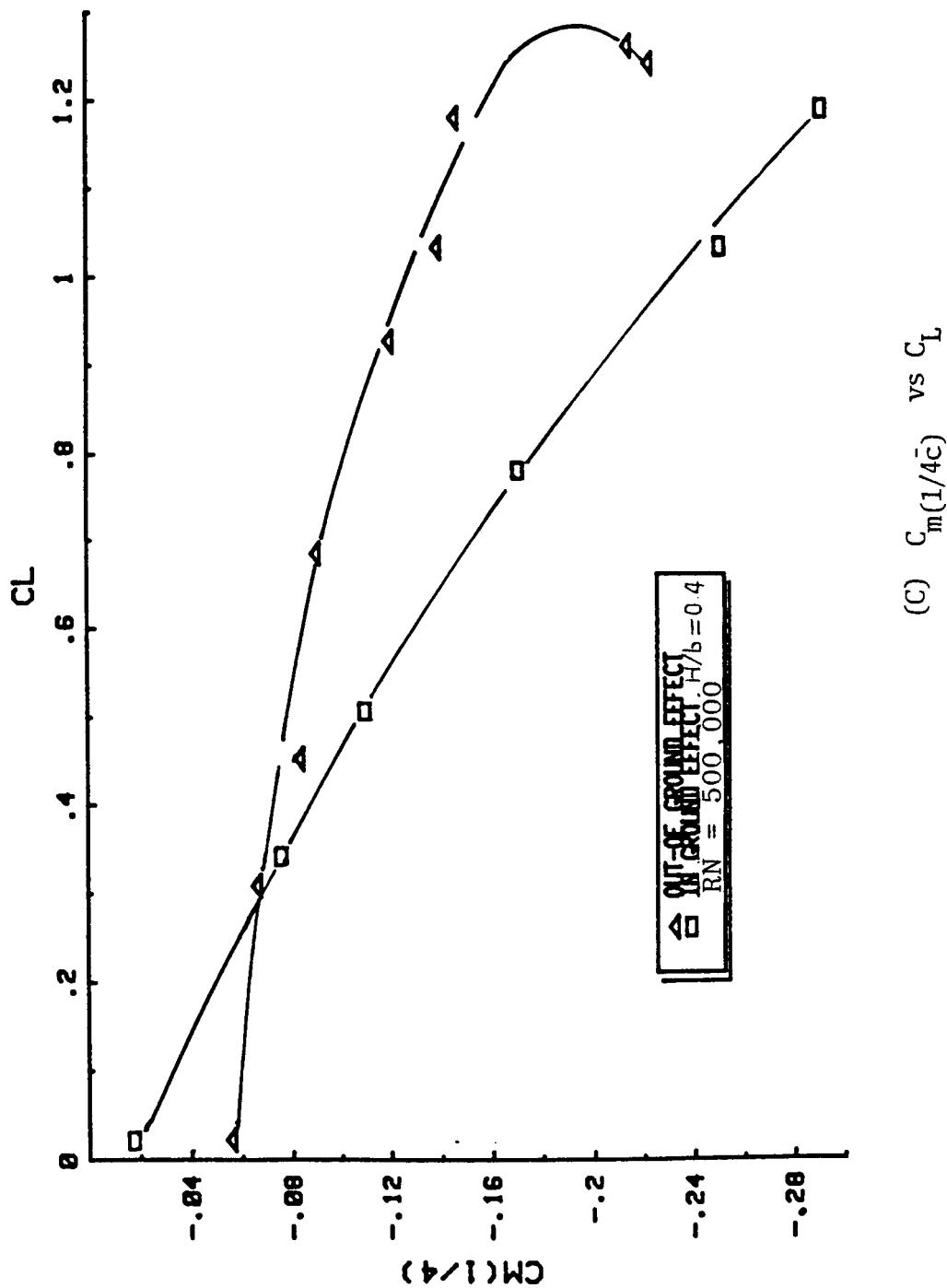
(C) $C_{m(1/4\bar{c})}$ vs C_L

Figure 11 Concluded.

32

SYM δ_f

△ -30 Degrees

□   0 Degrees

○ 15 Degrees

RN = 500,000

COEFFICIENT OF LIFT

1.2

.8

.4

-.4

4   8   12   16   20   24   28   32   36

ALPHA, deg.
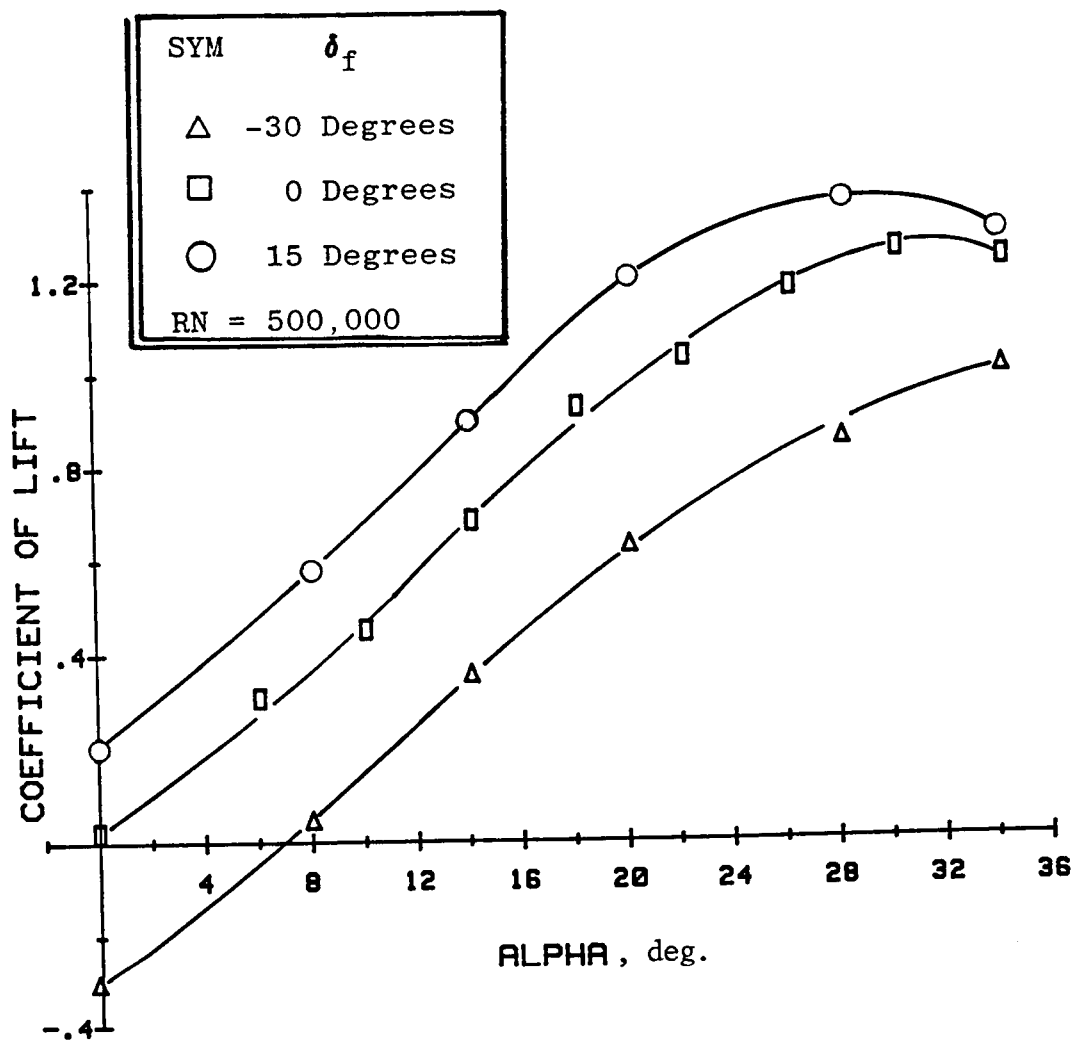
(A) C_L vs α

Figure 12   Longitudinal Aerodynamic Characteristics for
an F-106 Model in Out-of-Ground Effect with
Flap Deflections

(B) C_L vs C_D

Figure 12 Continued.

34

COEFFICIENT OF LIFT

(C) $C_{m(1/4\bar{c})}$ vs C_L

Figure 12 Concluded.

SYM δ_f

△   -30 Degrees

□   0 Degrees

○   15 Degrees

RN = 500,000

COEFFICIENT OF LIFT

ALPHA , deg.

(A) C_L vs α

Figure 13   Longitudinal Aerodynamic Characteristics
for an F-106 Model with Flap Deflections in
Static Ground Effect. H/b = 0.4.
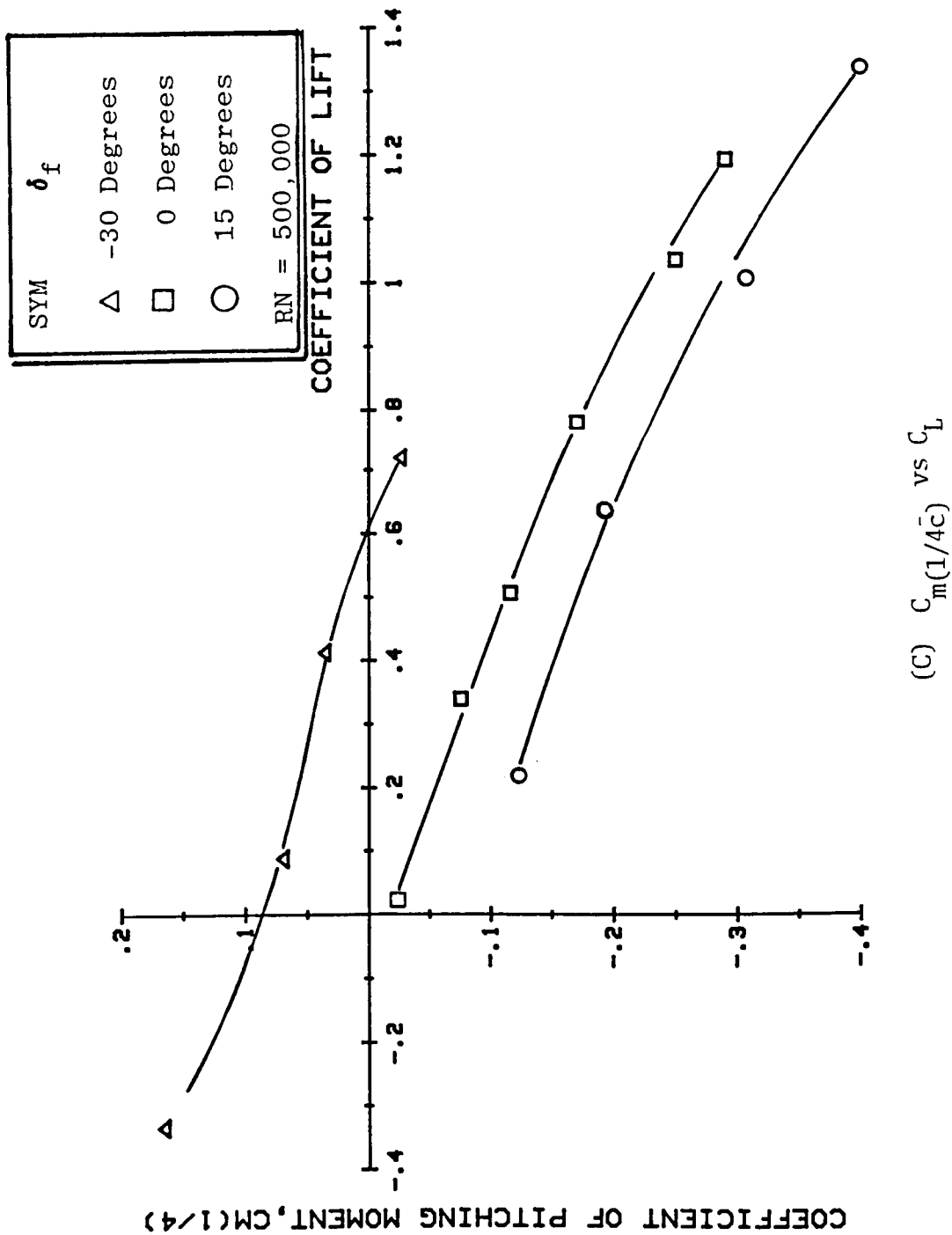
36
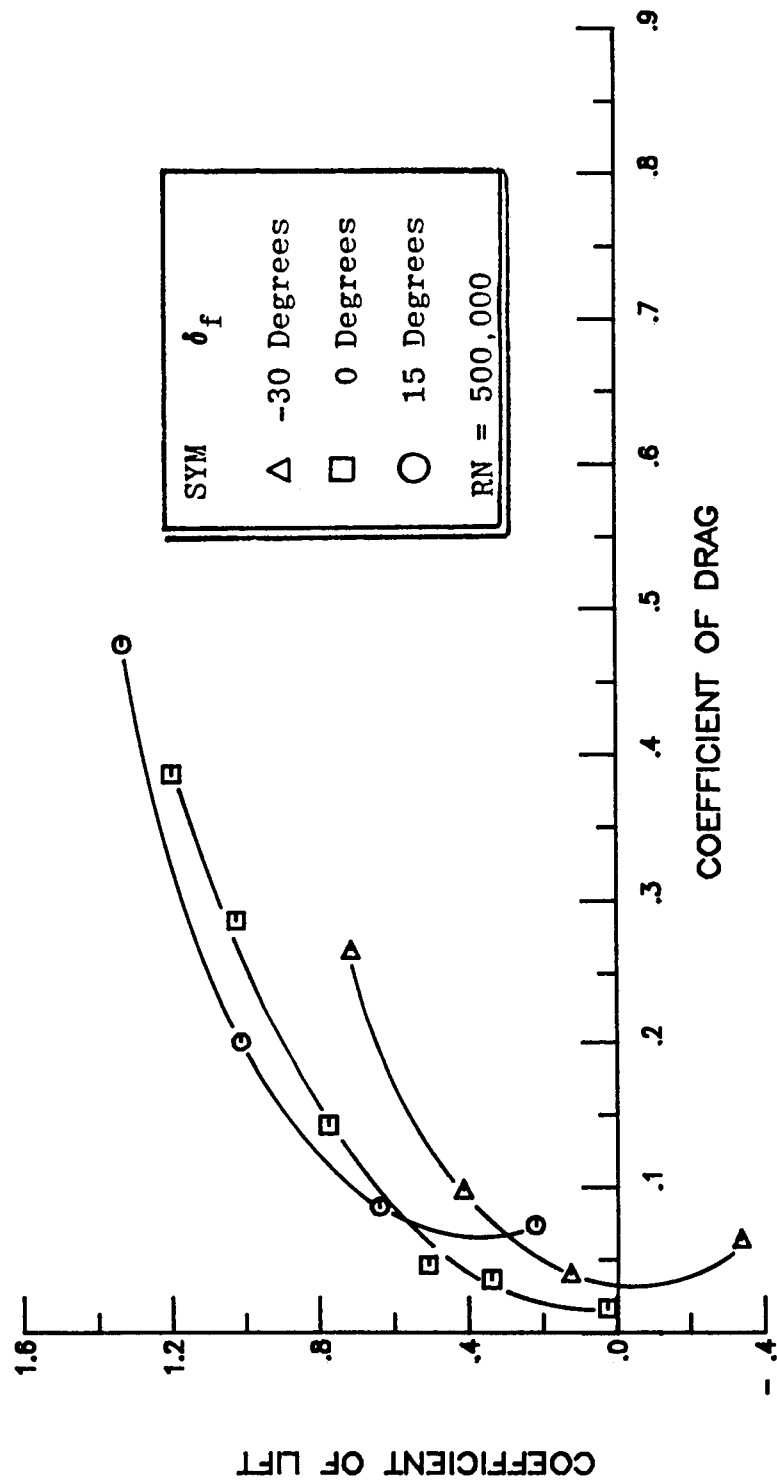
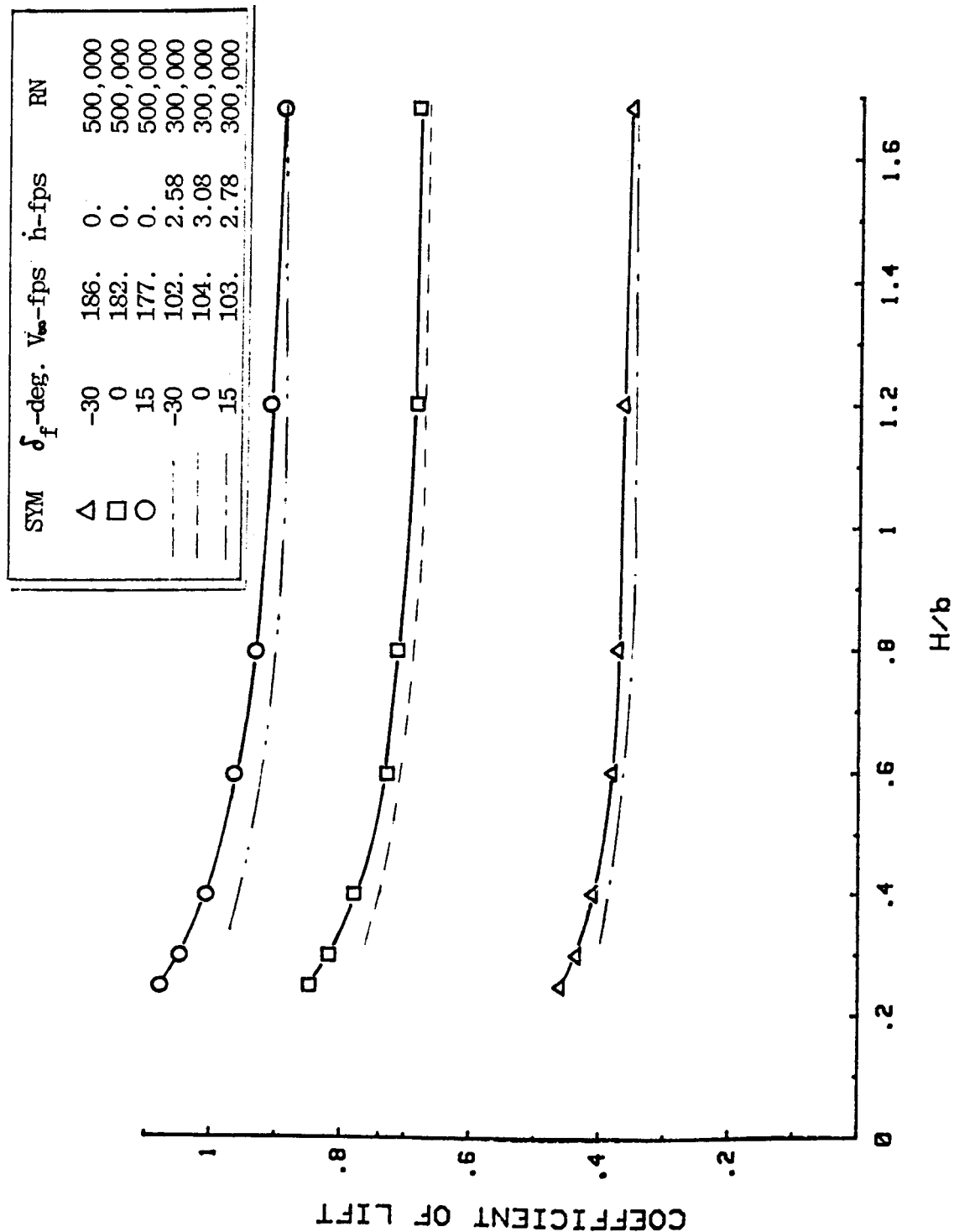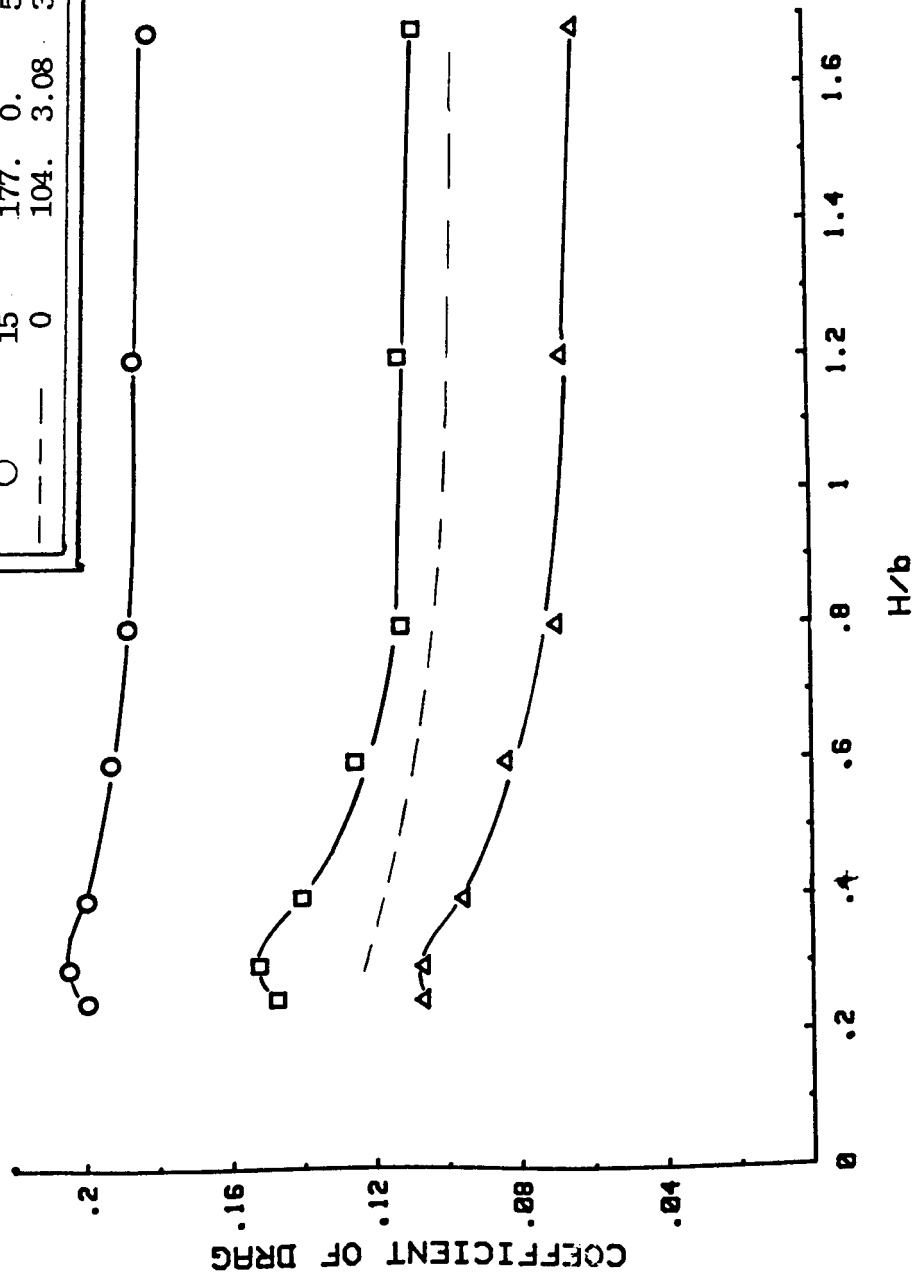(B) C_L vs C_D

Figure 13 Continued.

37

(C) $C_{m(1/4\bar{c})}$ vs C_L

Figure 13 Concluded.

38

SYM	δ_f-deg.	V_∞-fps	$\dot{h}$-fps	RN
△	-30	186.	0.	500,000
□	0	182.	0.	500,000
○	15	177.	0.	500,000
	-30	102.	2.58	300,000
	0	104.	3.08	300,000
	15	103.	2.78	300,000

COEFFICIENT OF LIFT

H/b

(A) CL VS H/b

Figure 14   Longitudinal Aerodynamic Characteristics for an F-106 Model with Flap Deflections in Static and Dynamic Ground Effect at Different Ground Heights. $\alpha \cong 14$ Degrees.

SYM	δ_f-deg.	V_∞-fps	$\dot{h}$-fps	RN
△	-30	186.	0.	500,000
□	0	182.	0.	500,000
○	15	177.	0.	500,000
– – –	0	104.	3.08	300,000

(B) <u>CD VS H/b</u>

Figure 14   Continued.

40
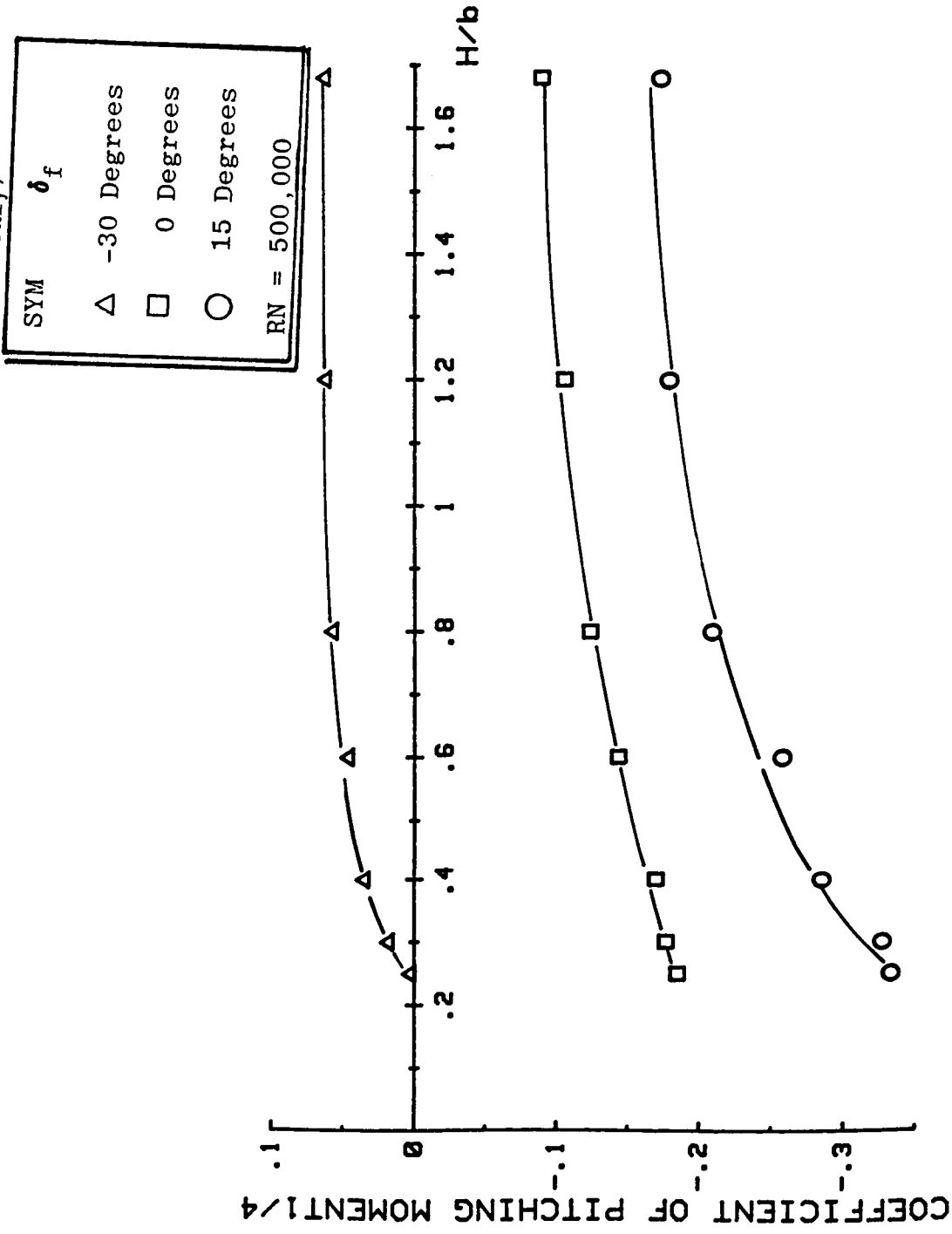
(C) $\underline{C_{M(1/4\bar{c})} \text{ VS } H/b}$

Figure 14   Concluded.

41

SYM	δ_f-deg.	V_∞-fps	$\dot{h}$-fps	RN
O	-30	186.	0.	500,000
△	0	182.	0.	500,000
□	15	177.	0.	500,000
—·—·	-30	102.	2.58	300,000
— —	0	104.	3.08	300,000
—··—	15	103.	2.78	300,000

% INCREASE IN CL

H/b
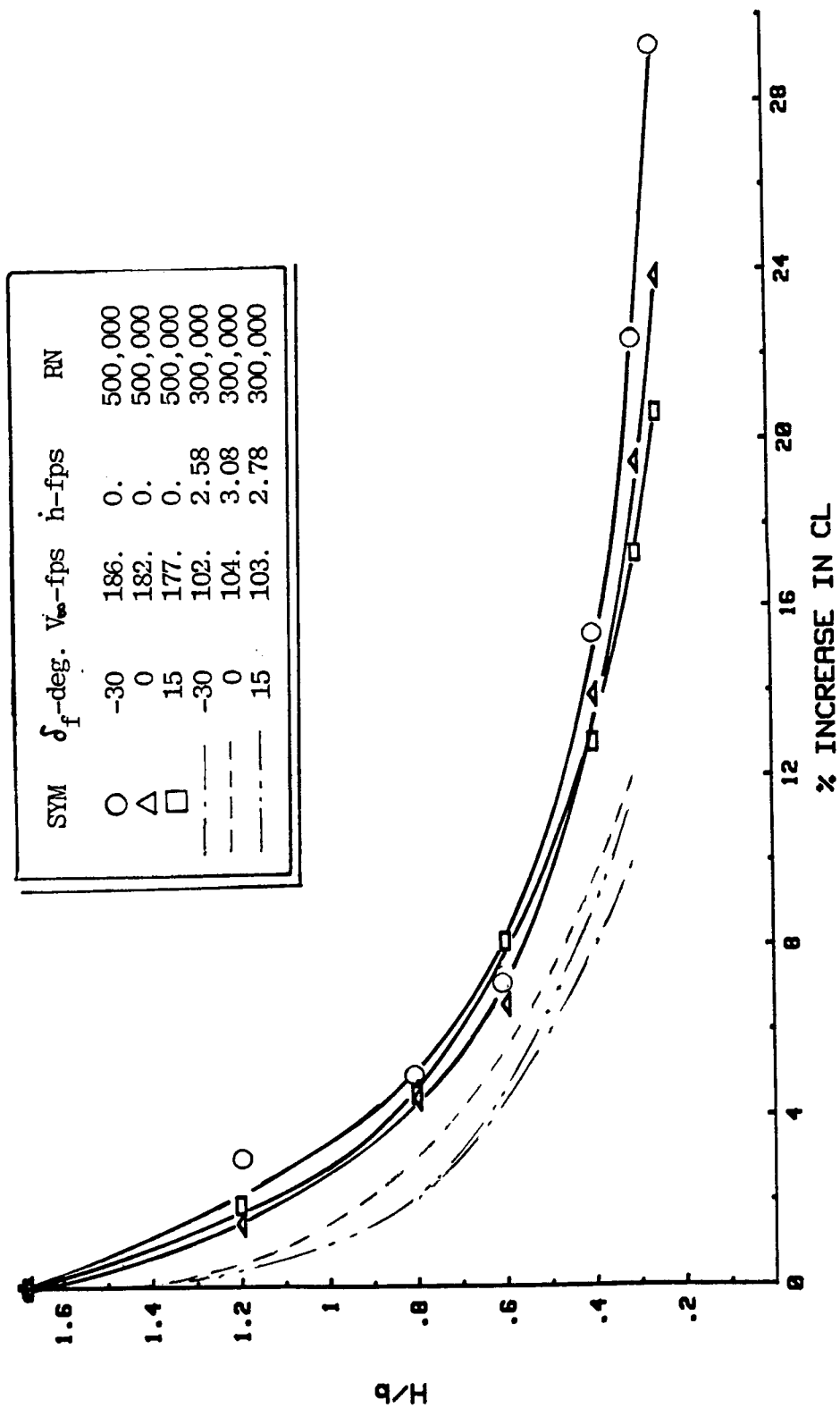
(A) H/b VS ΔCL%

Figure 15   Incremental Lift and Drag for an F-106 Model with Flap Deflections in Static and Dynamic Ground Effect at $\alpha \simeq$ 14 Degrees.

SYM	δ_f-deg.	V_∞-fps	$\dot{h}$-fps	RN
O	-30	186.	0.	500,000
△	0	182.	0.	500,000
□	15	177.	0.	500,000
— —	0	104.	3.08	300,000

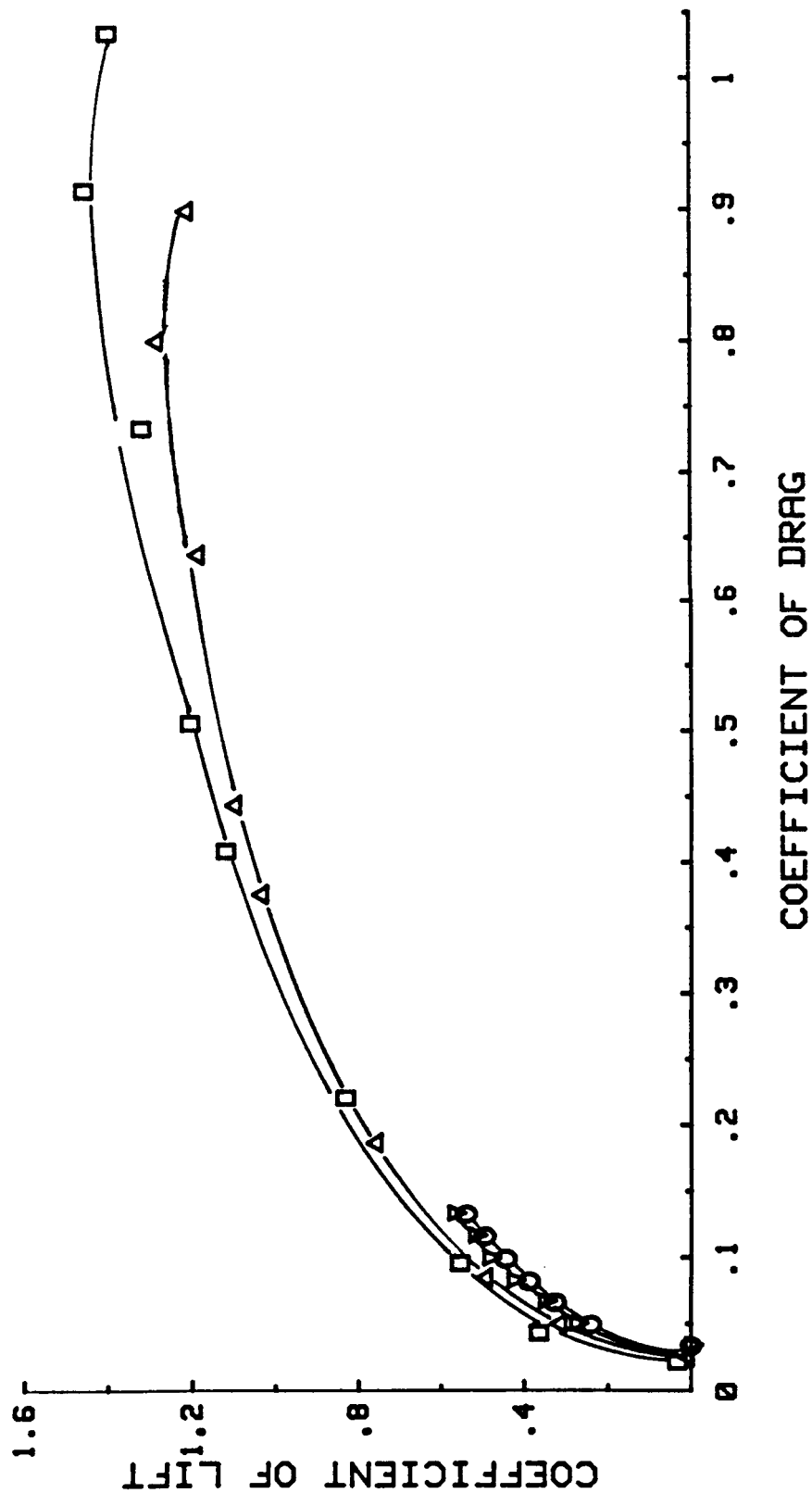H/b

% INCREASE IN CD
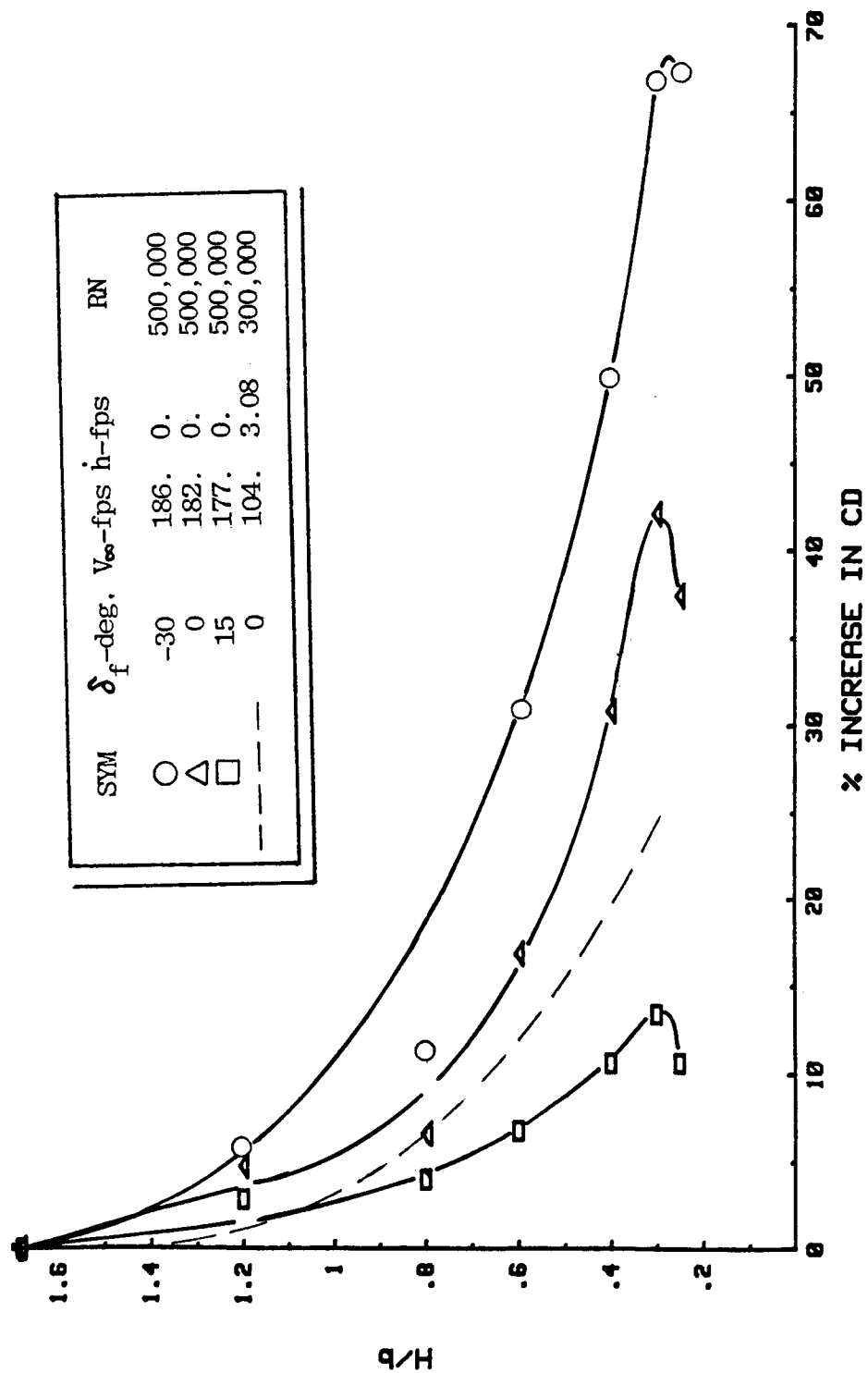
(B)   H/b VS ΔCD%

Figure 15   Concluded.
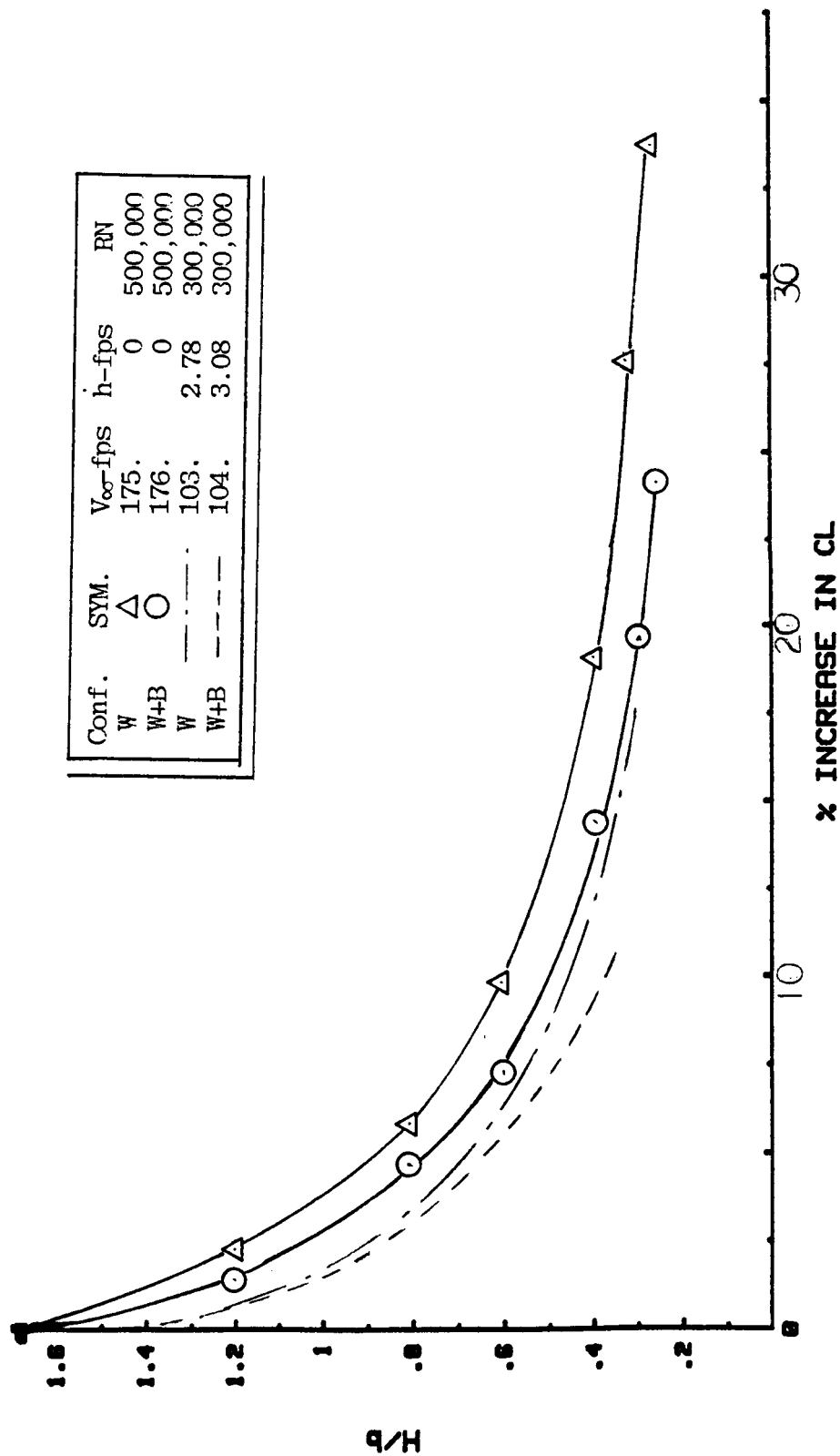
Figure 16   Incremental Lift for an F-106 Model Due to Fuselage Effectiveness in Static and Dynamic Ground Effect at $\alpha = 14$ degree.
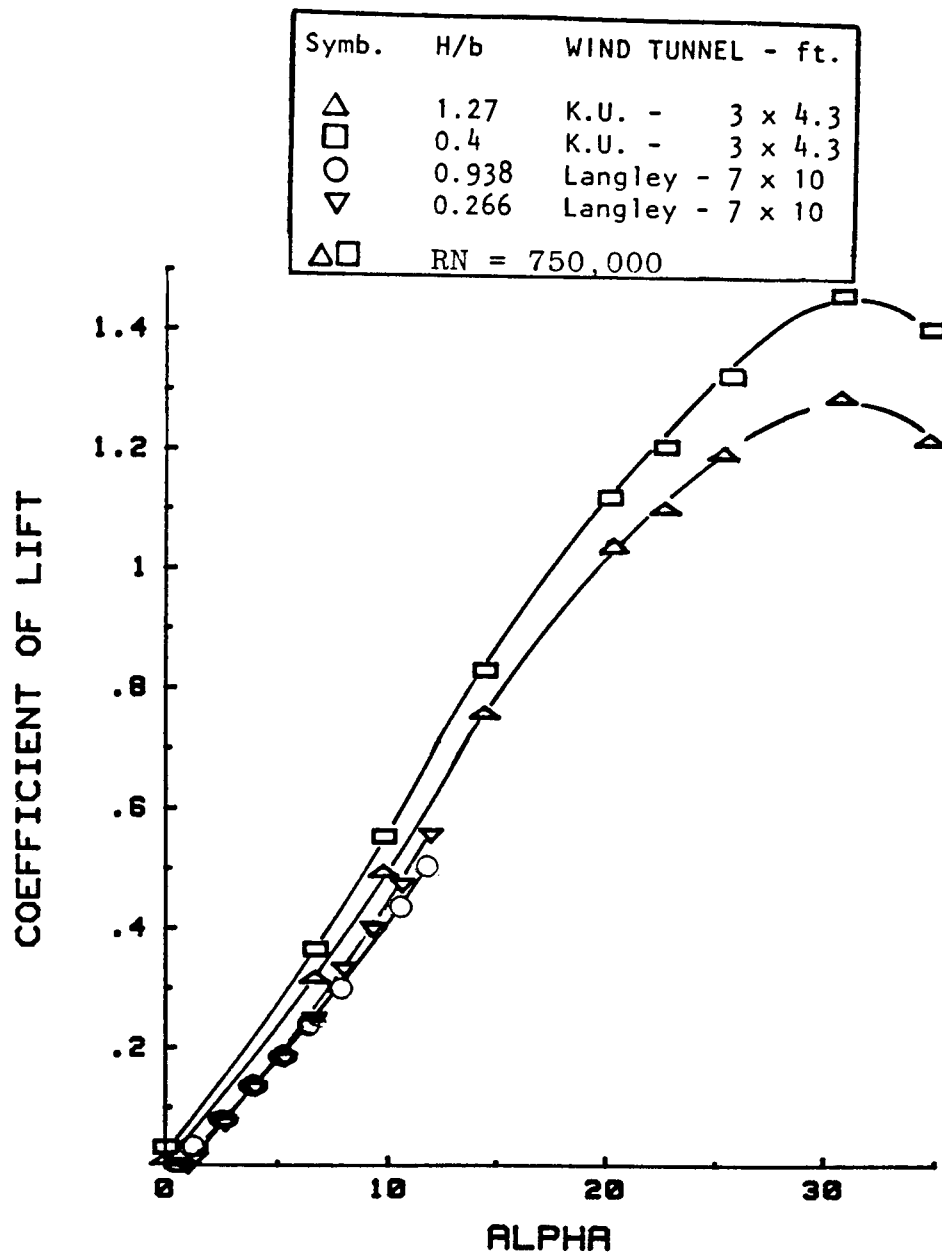
Figure 17   Comparison of Some Static Ground Effect
Data for the XB-70-1 Configuration from the
KU and Langley 7 x 10 Tunnels

45

(B) CL VS CD

Figure 17 Continued.

Symb.	H/b	WIND TUNNEL - ft.
△	1.27	K.U. - 3 × 4.3
□	0.4	K.U. - 3 × 4.3
○	0.938	Langley - 7 × 10
▽	0.266	Langley - 7 × 10
△□	RN = 750,000	

(C) CM (1/4c̄) VS CL
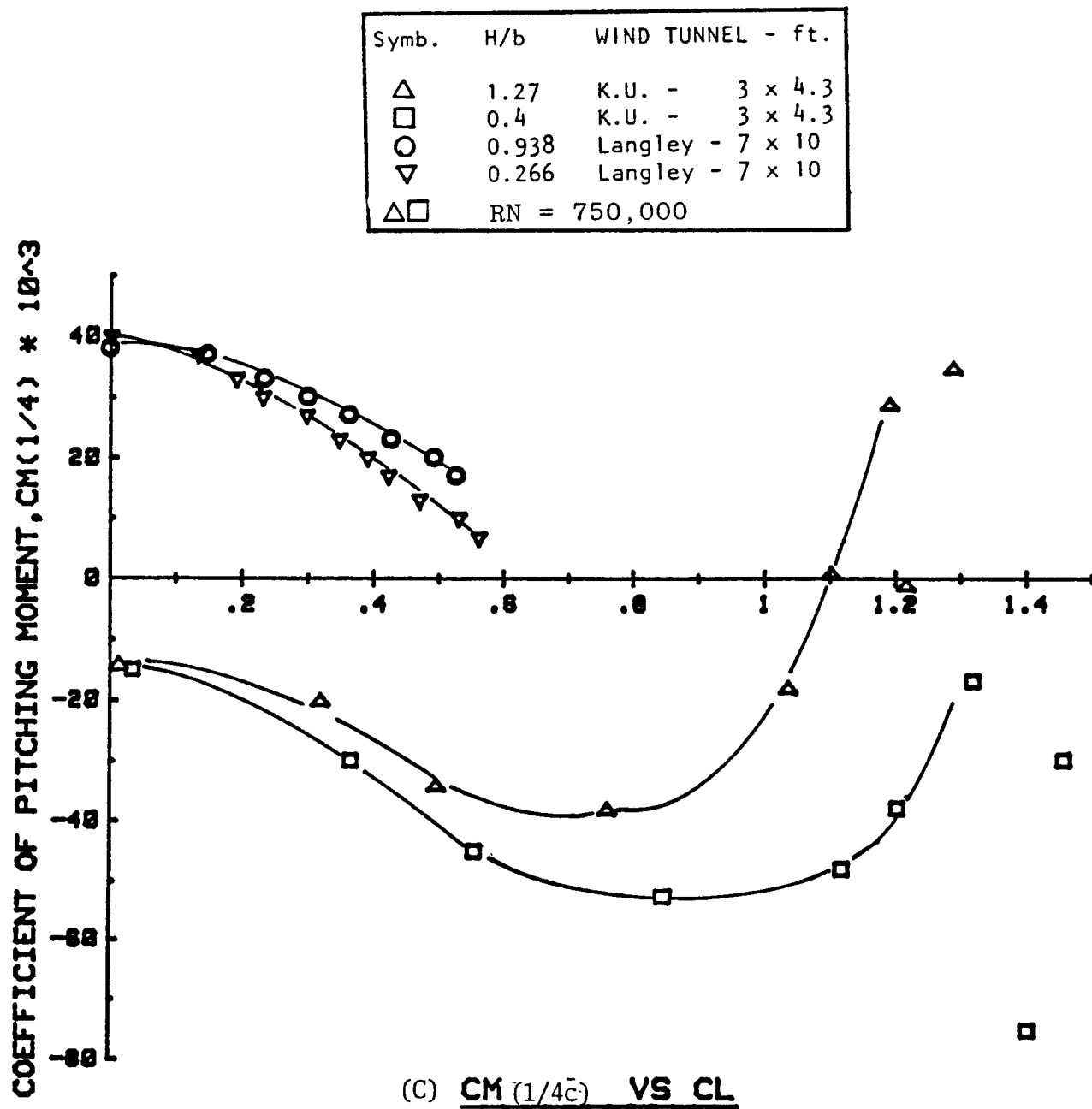
Figure 17 Concluded.

47
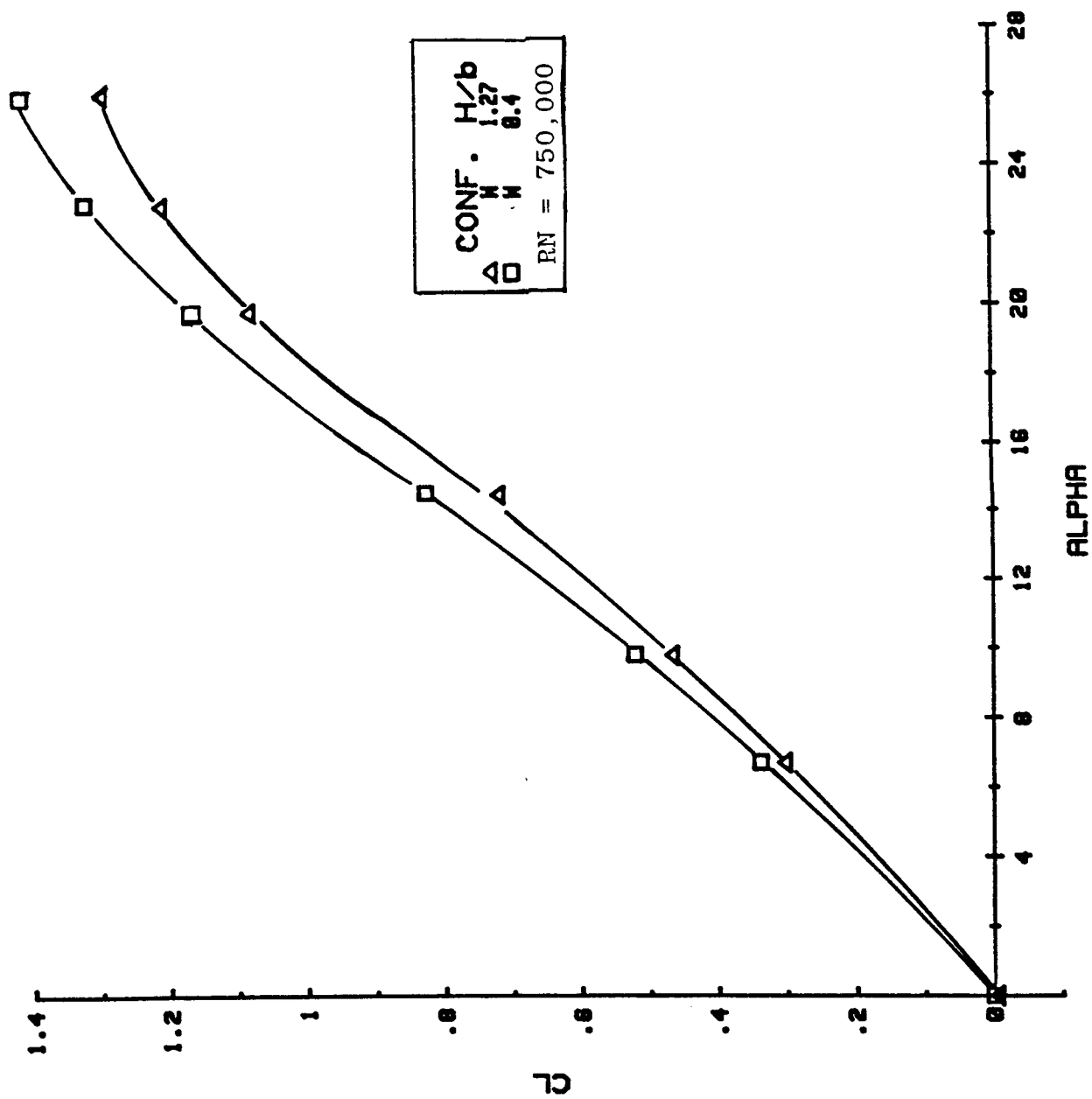
Figure 18   Longitudinal Aerodynamic Characteristics for an XB-70-1 Model
            with Wing Alone in Static Ground Effect
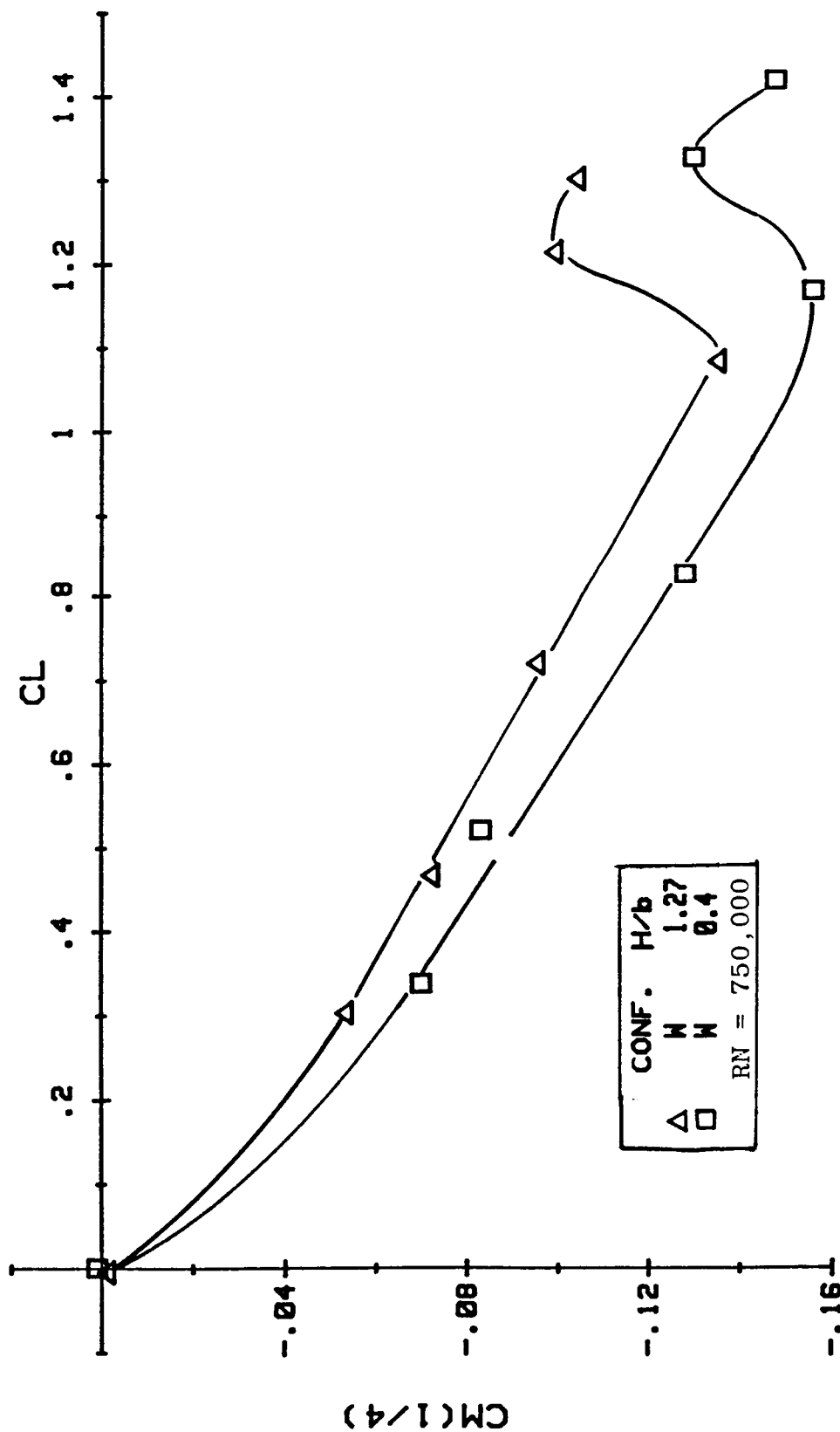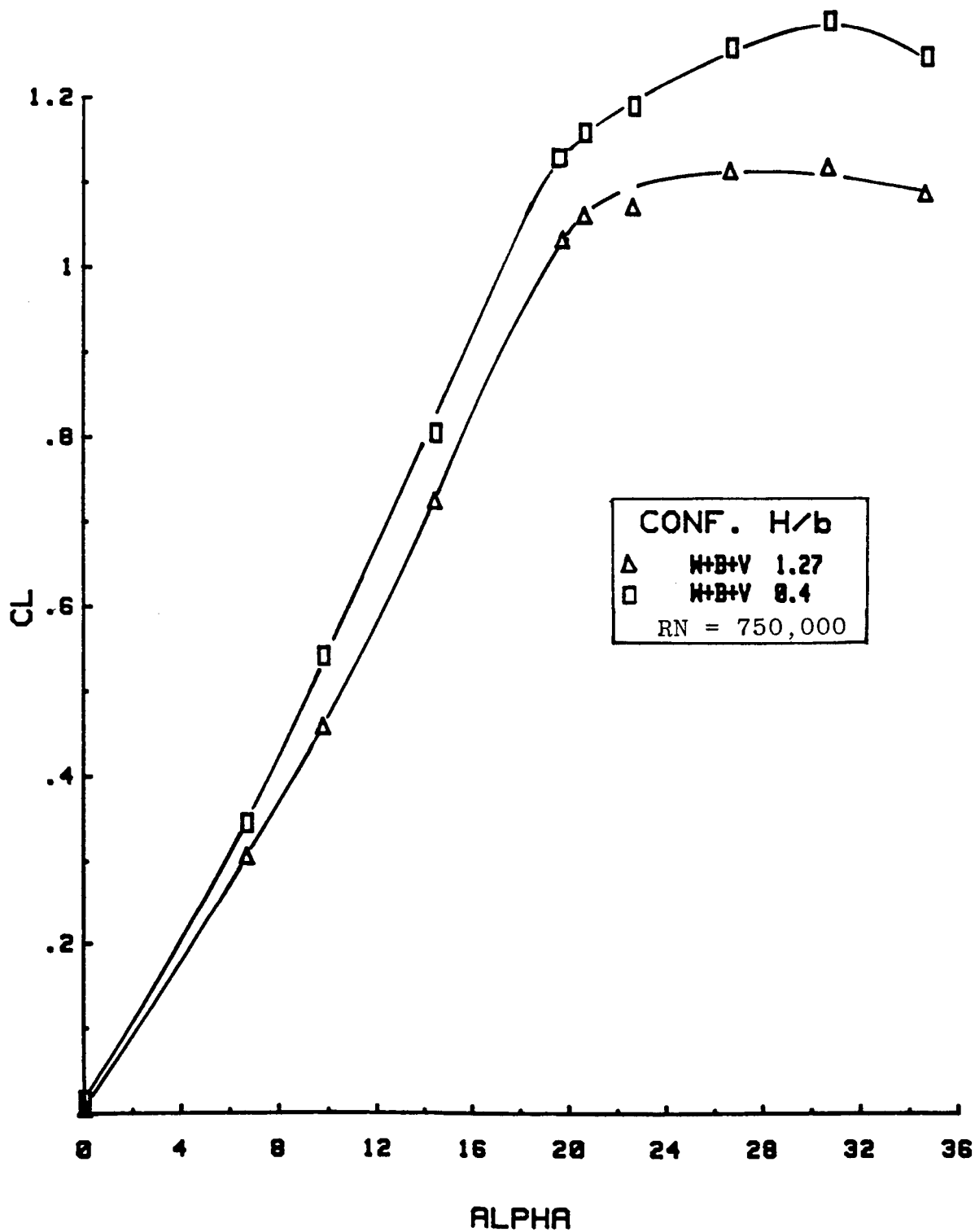
48

(B) CL VS CD
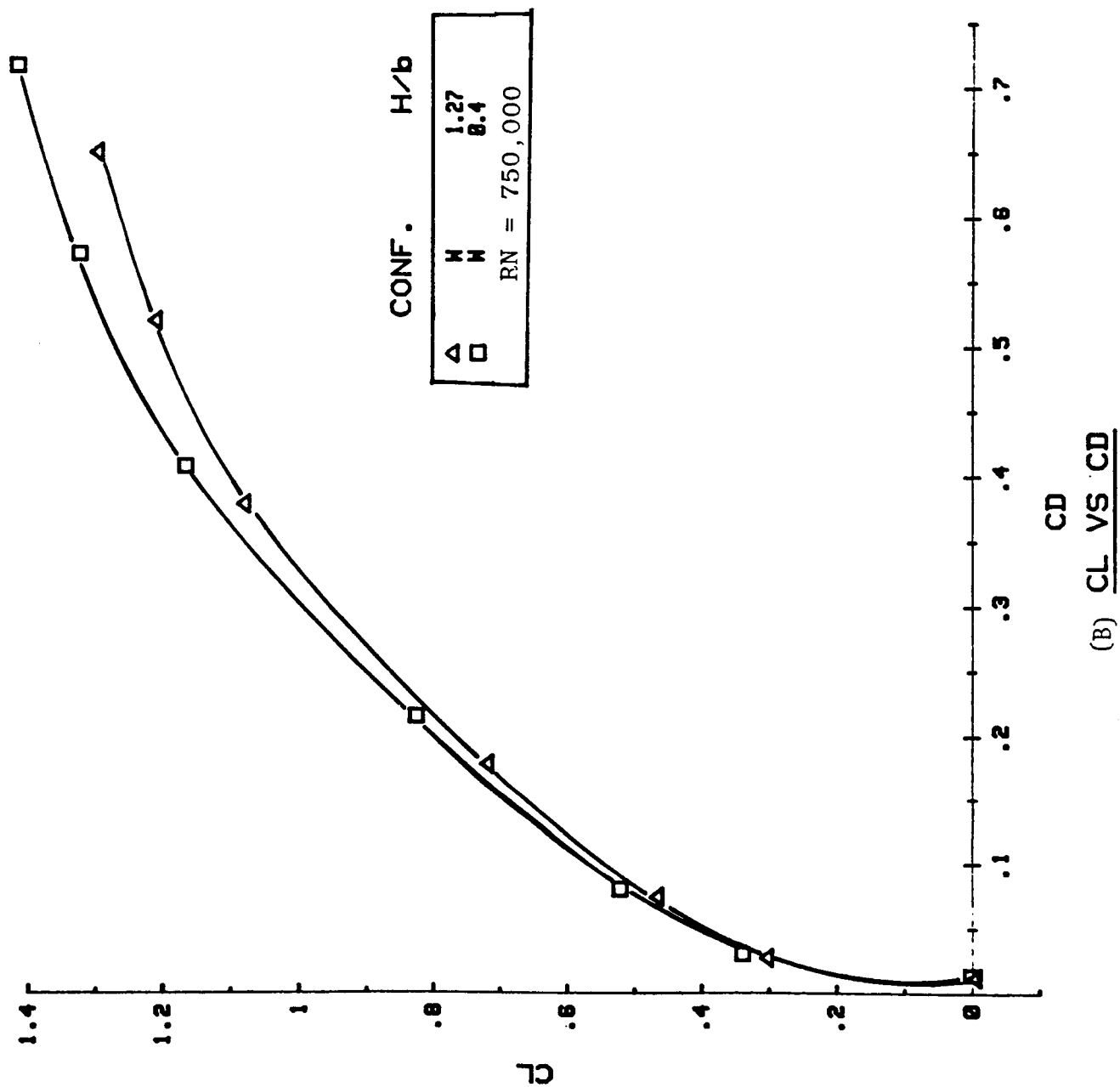
Figure 18   Continued.

49

(C) **CM(1/4c̄) VS CL**

Figure 18   Concluded.

(A) CL VS ALPHA

Figure 19   Longitudinal Aerodynamic Characteristics for an XB-70-1 Model (W + B + V) in Static Ground Effect
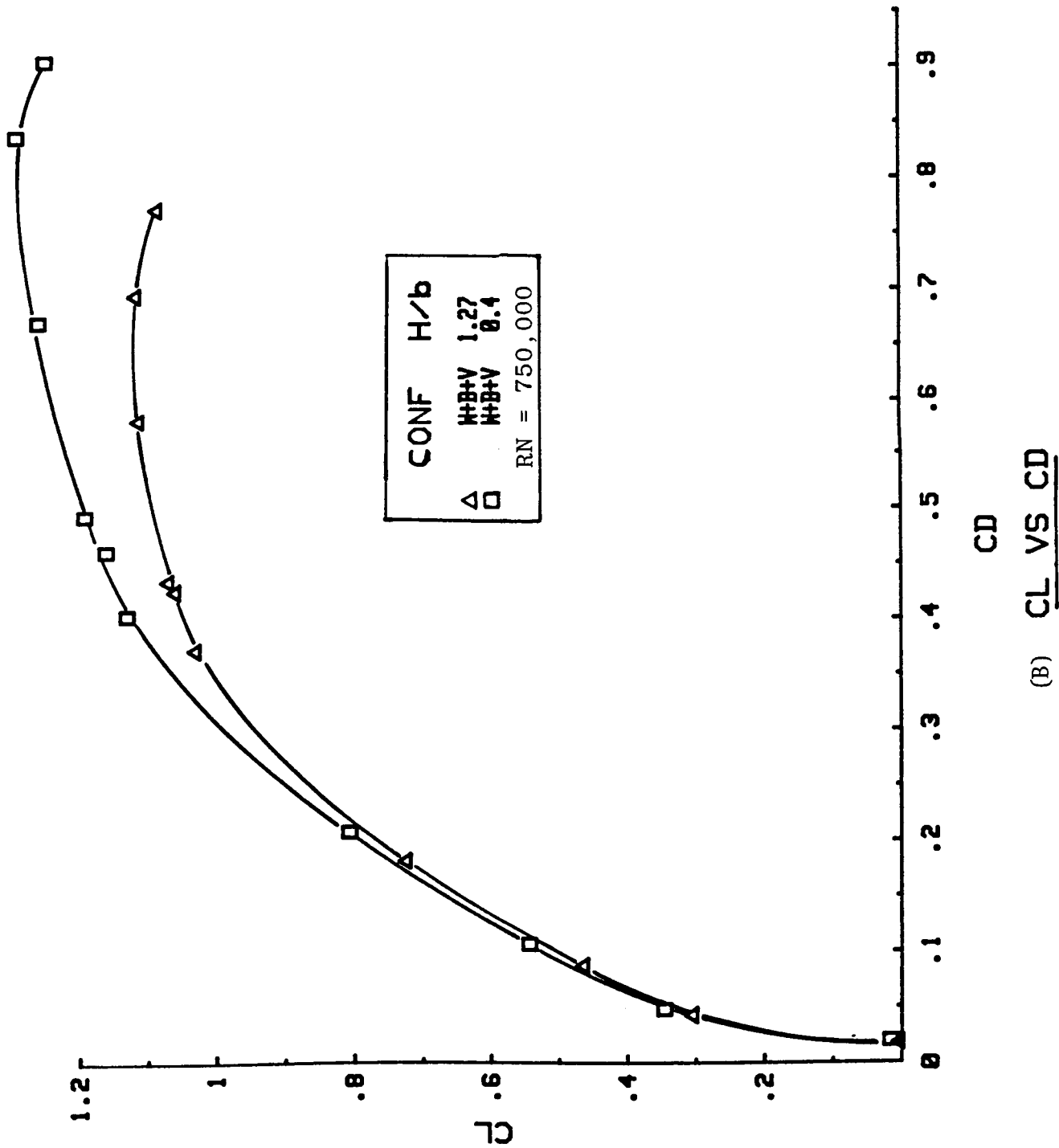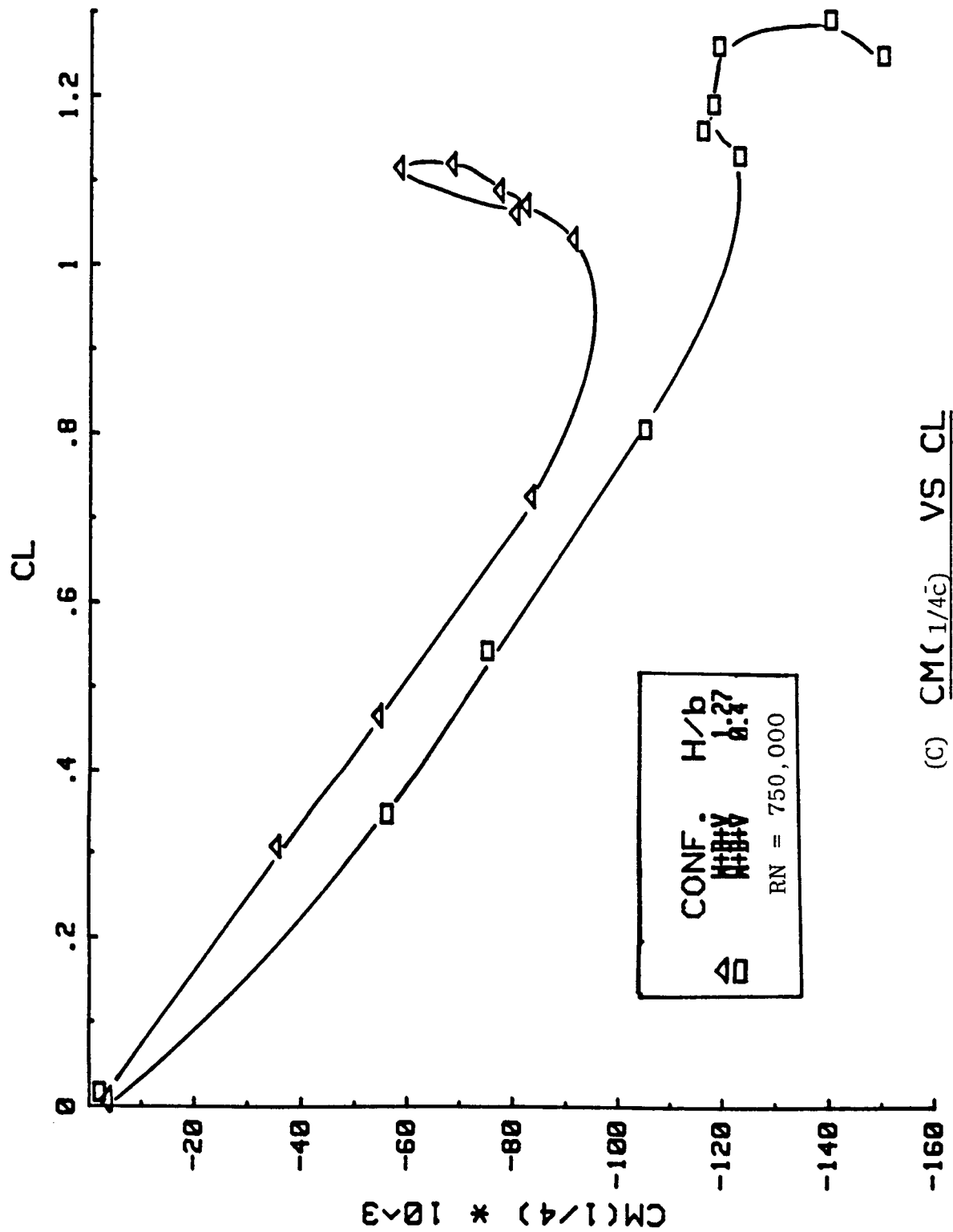
(B) CL VS CD

Figure 19   Continued.

52

(C) $\underline{CM(_{1/4\bar{c}})}$ $\underline{VS}$ $\underline{CL}$
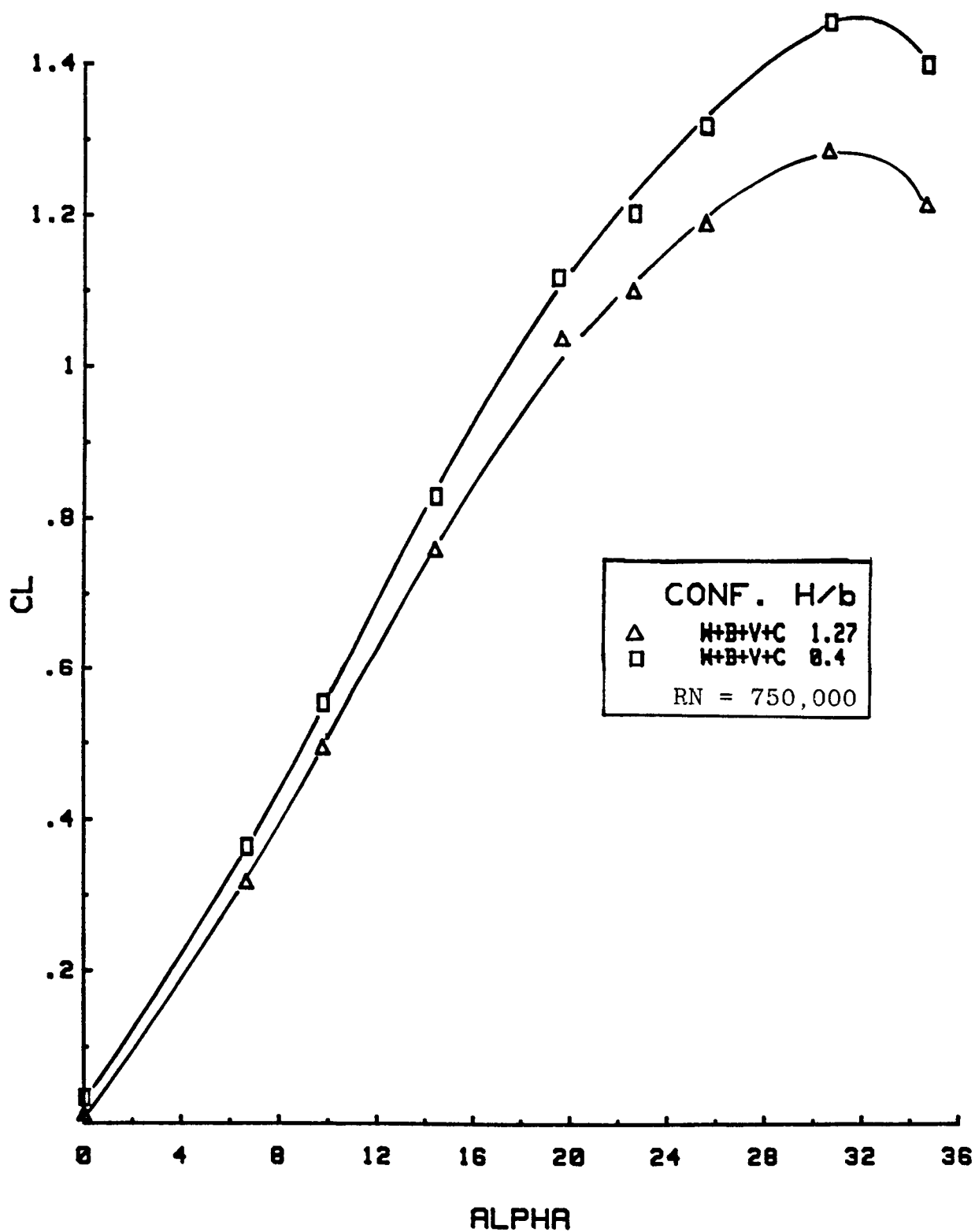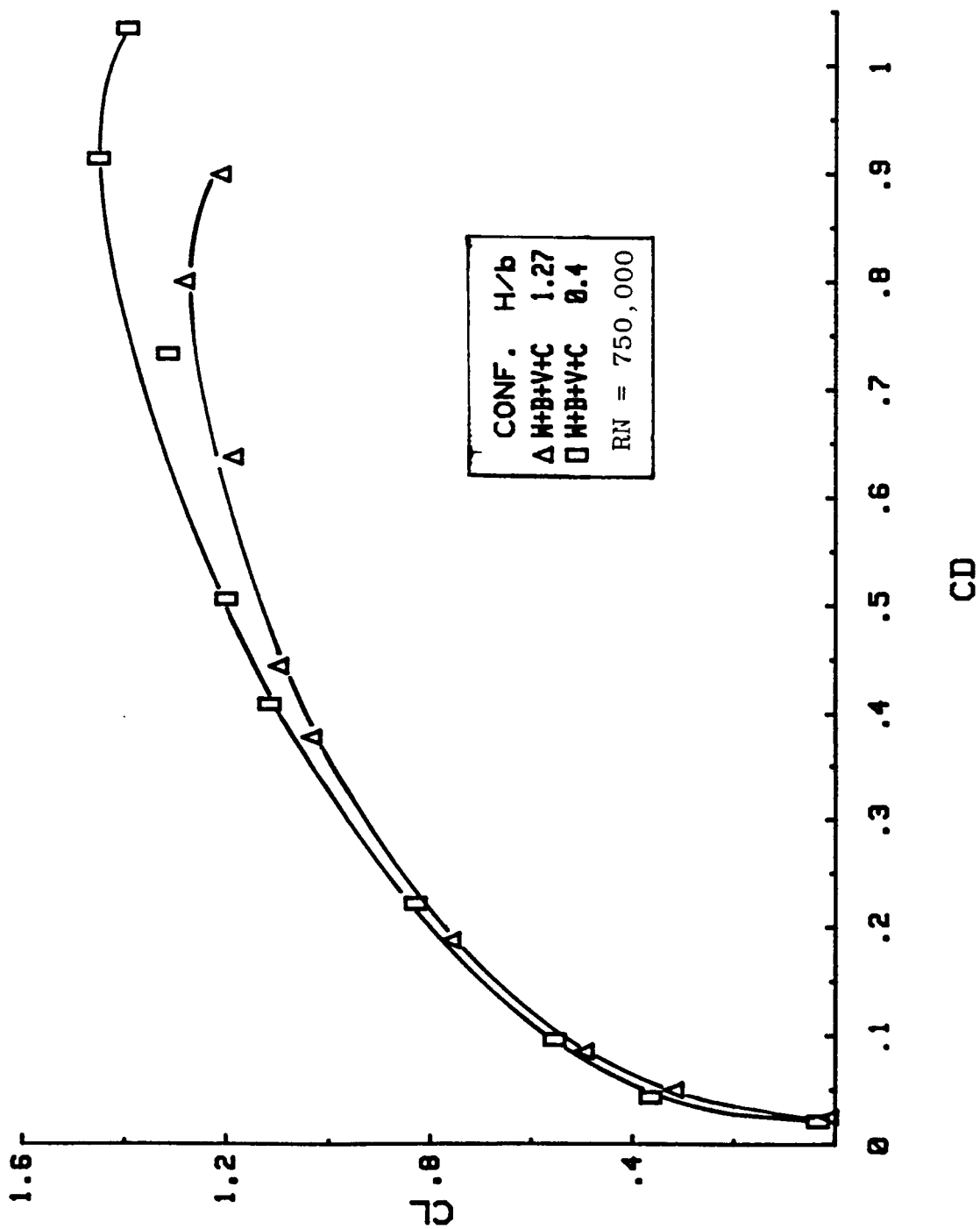
Figure 19   Concluded.

53

(A) CL VS ALPHA
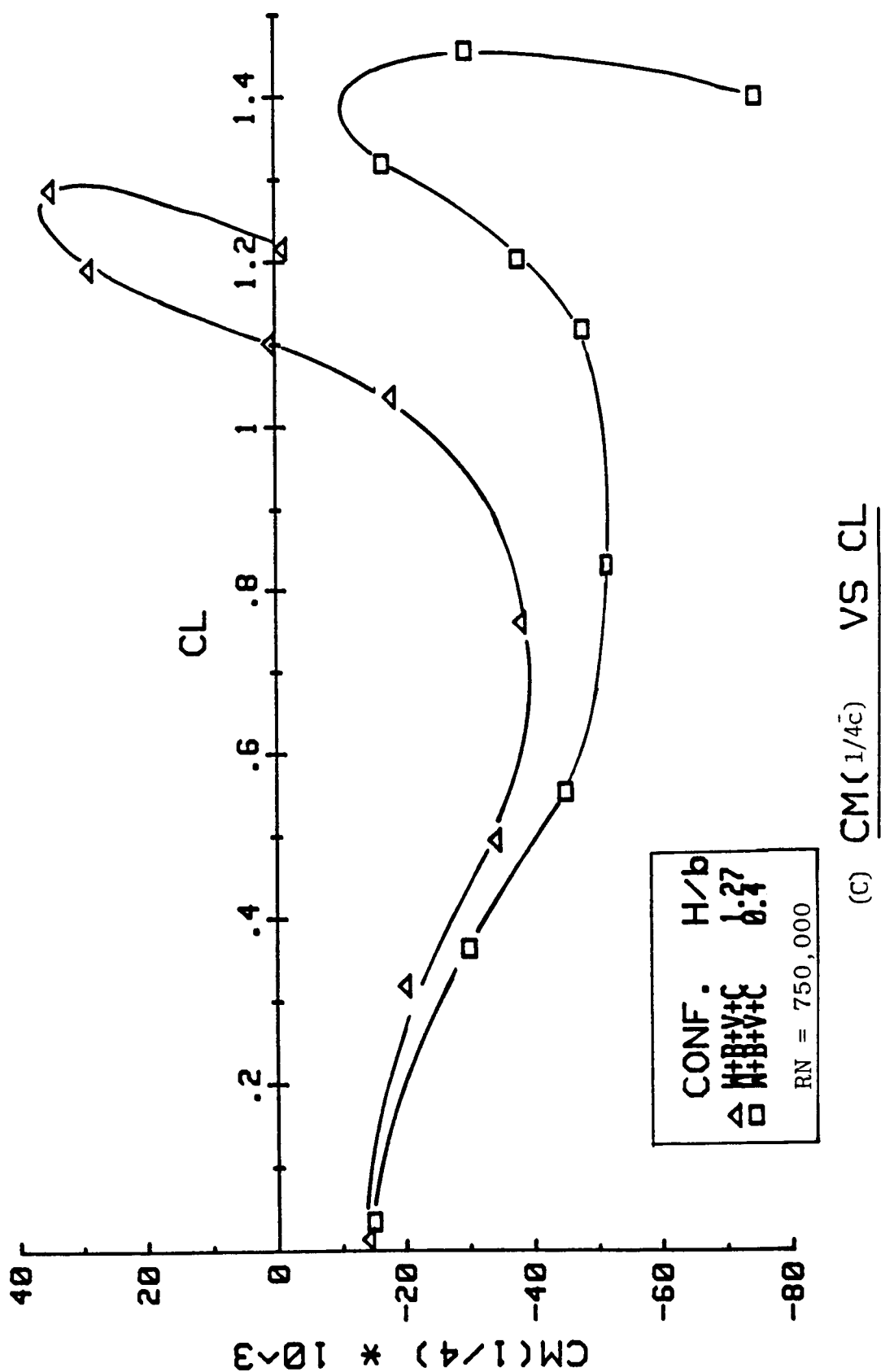
Figure 20   Longitudinal Aerodynamic Characteristics
             for an XB-70-1 Model (W + B + V + C) in
             Static Ground Effect

(B) CL VS CD

Figure 20. Continued

55

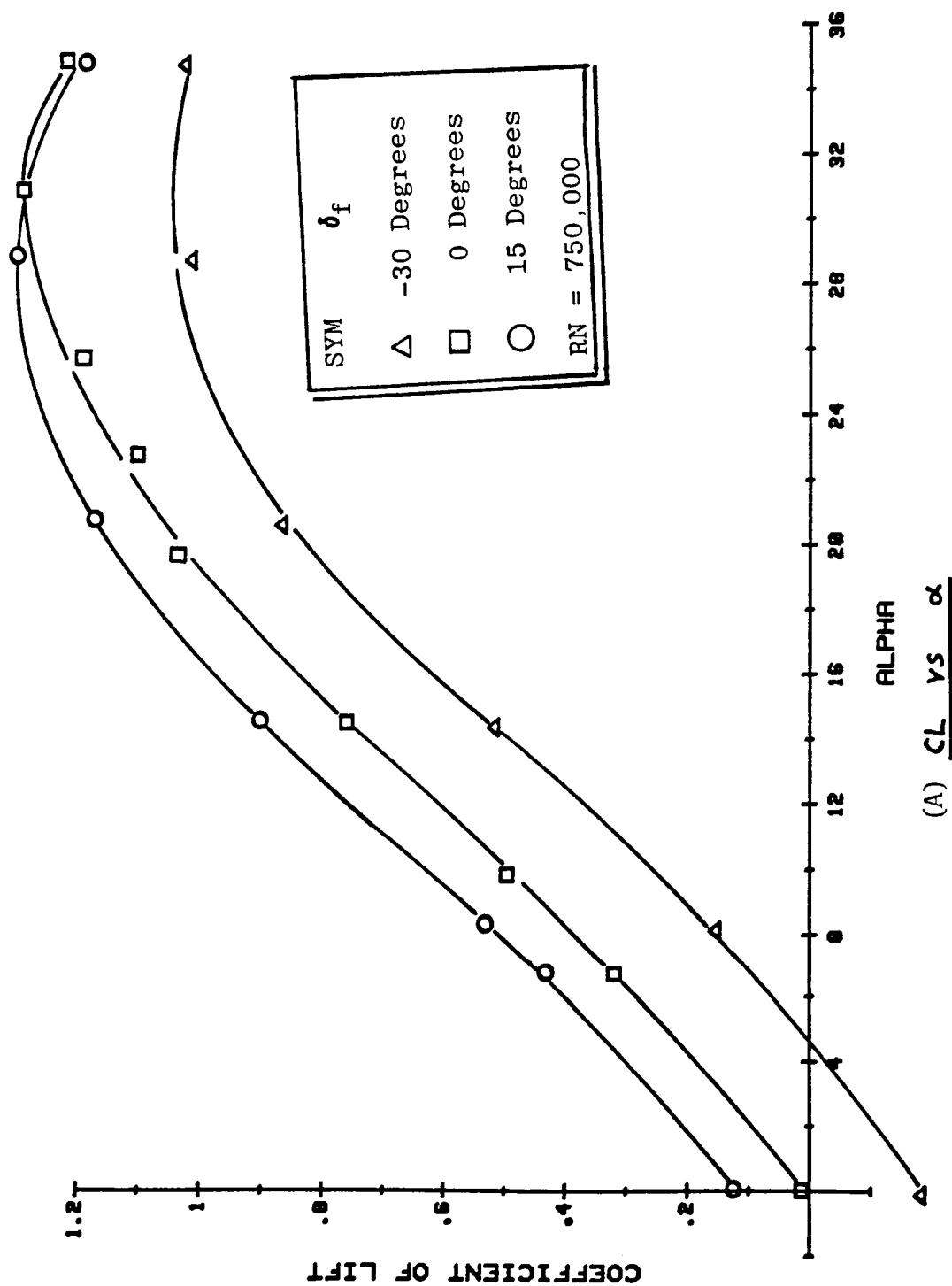(C) $\underline{CM(1/4\bar{c})}$ $\underline{VS}$ $\underline{CL}$

Figure 20   Concluded.

56

Figure 21   Longitudinal Aerodynamic Characteristics for an XB-70-1 Model
(W + B + V + C) with Flap Deflections in Out-of-Ground Effect
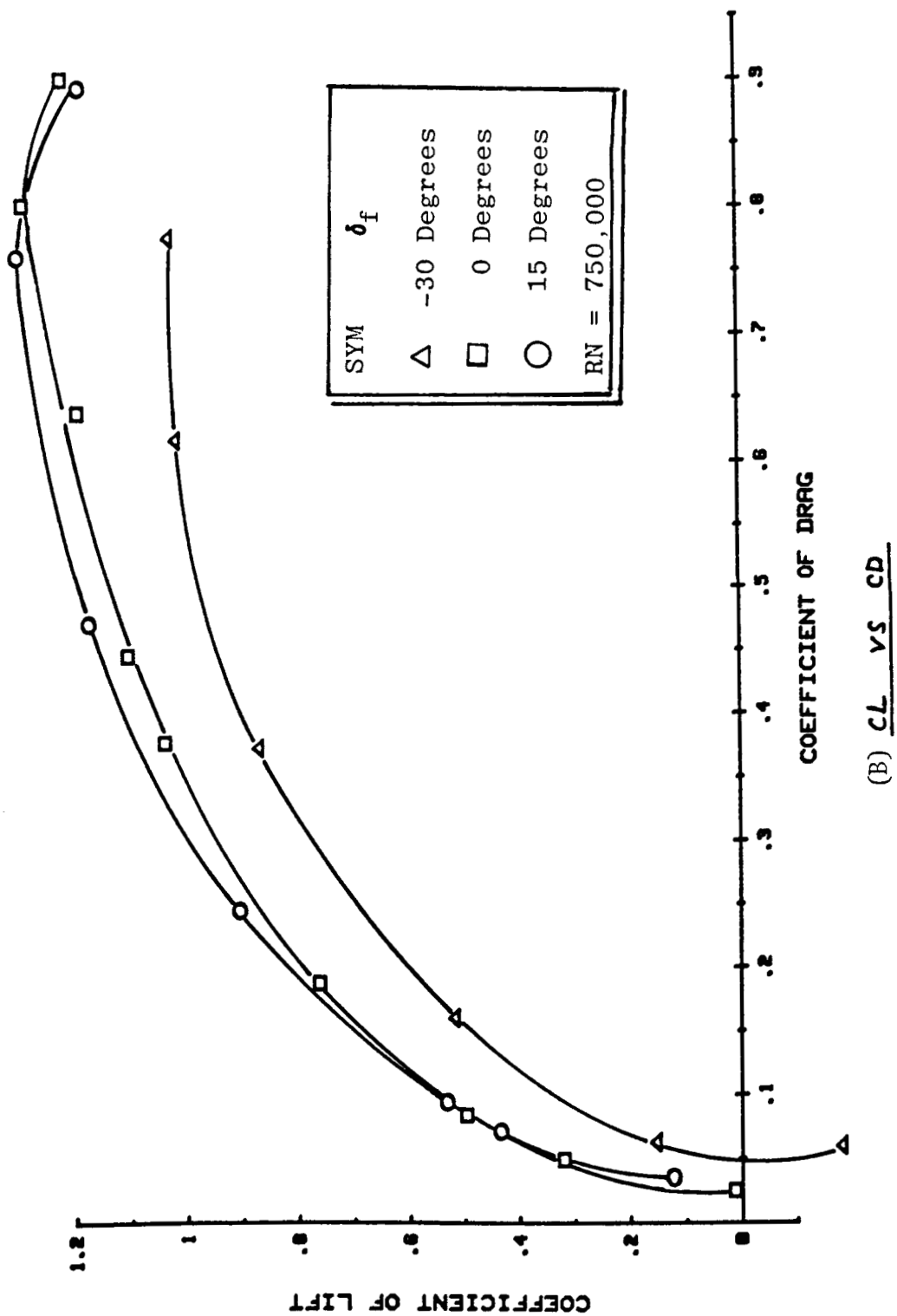
57

COEFFICIENT OF DRAG

SYM | δ_f
△ | -30 Degrees
□ | 0 Degrees
○ | 15 Degrees

RN = 750,000

COEFFICIENT OF LIFT

(B) *CL vs CD*

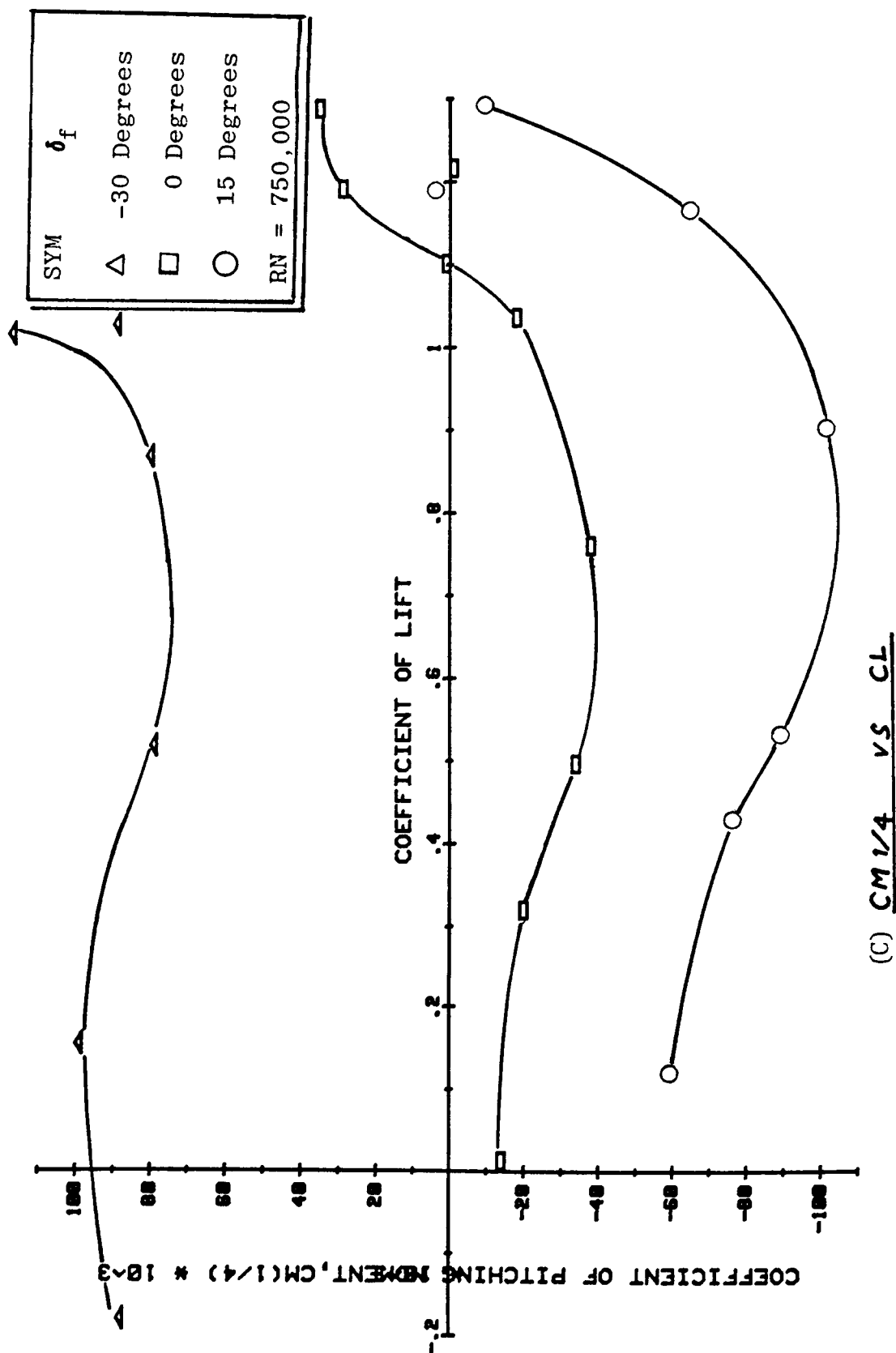Figure 21   Continued.
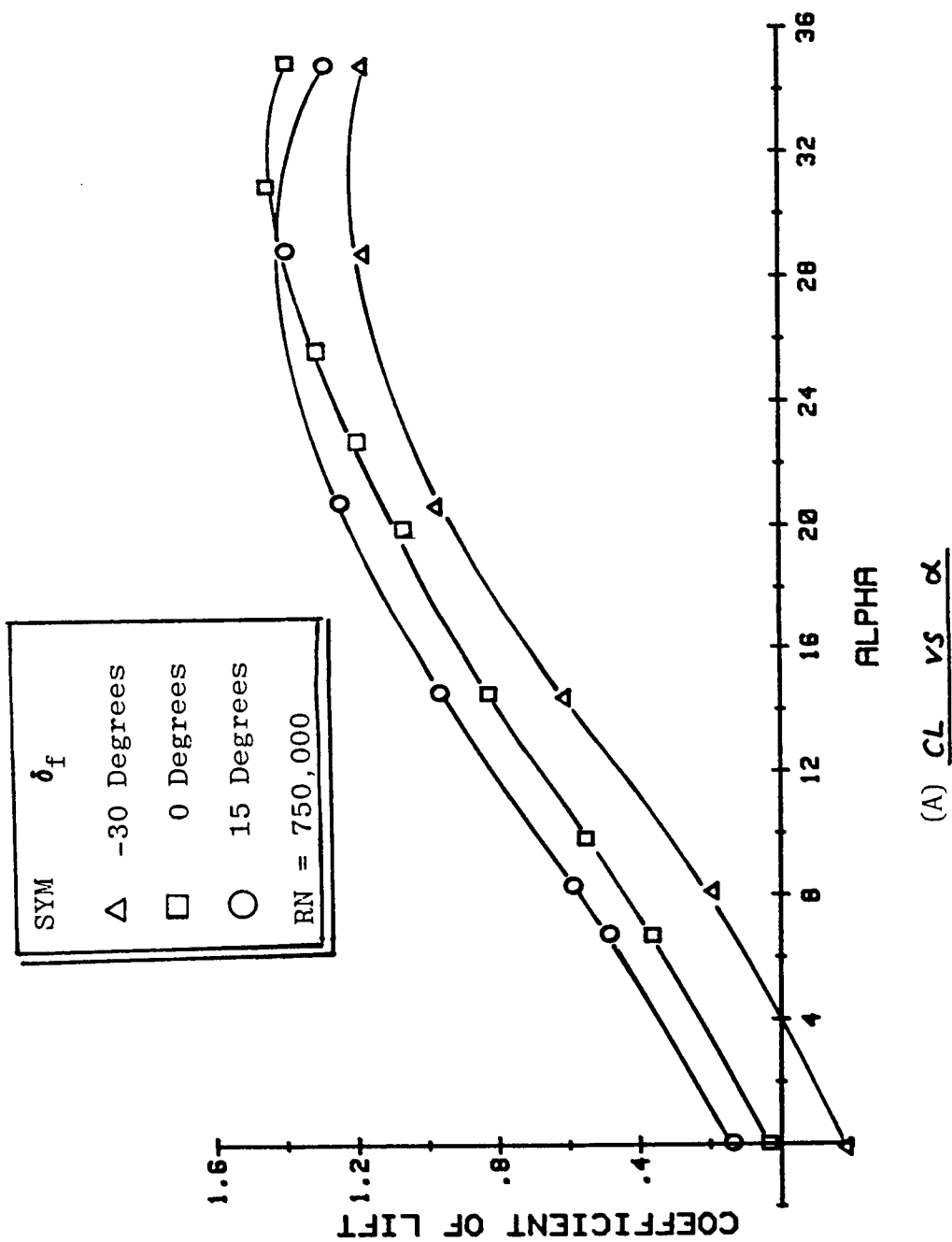
(C) <u>CM 1/4 vs CL</u>

Figure 21   Concluded.

59

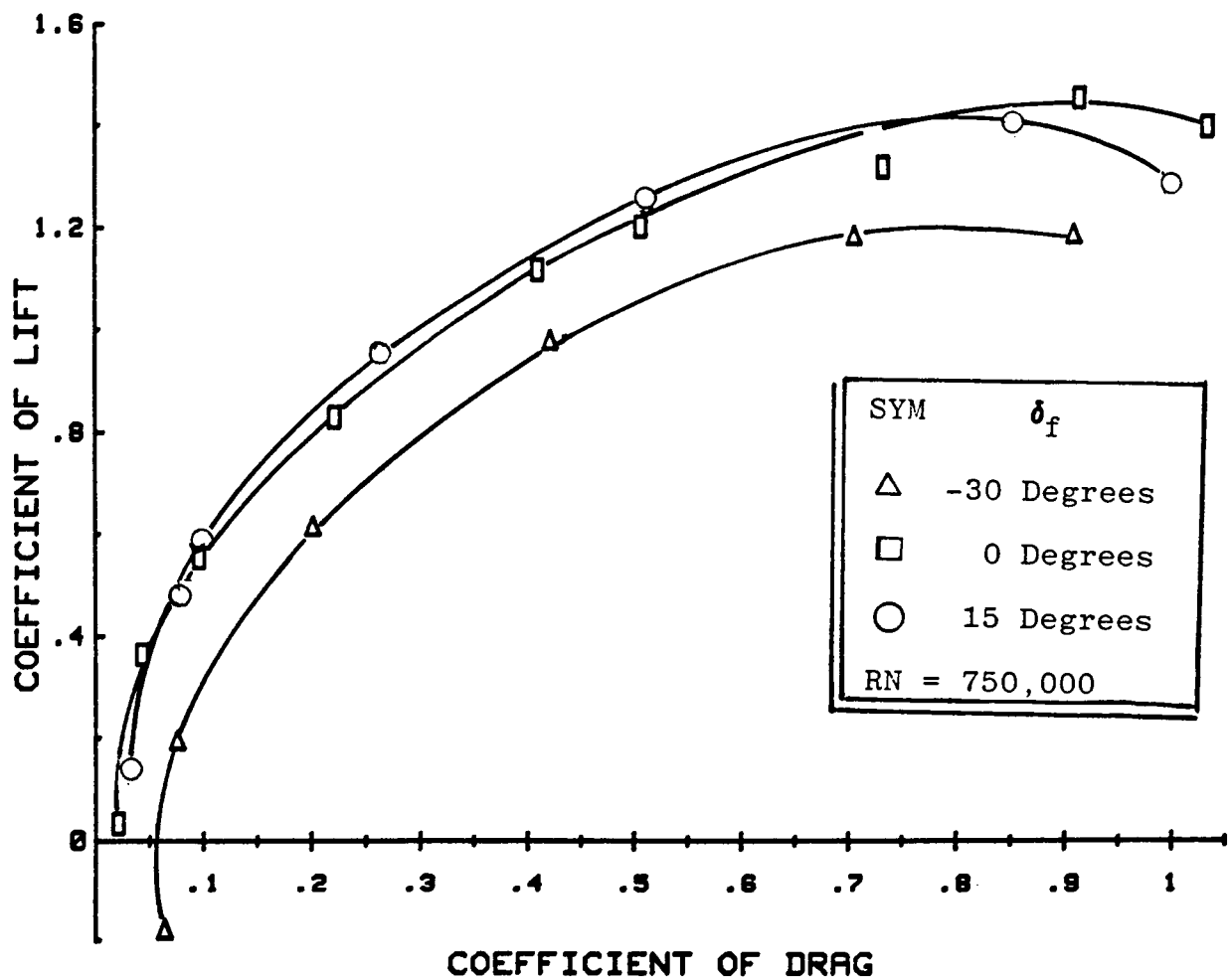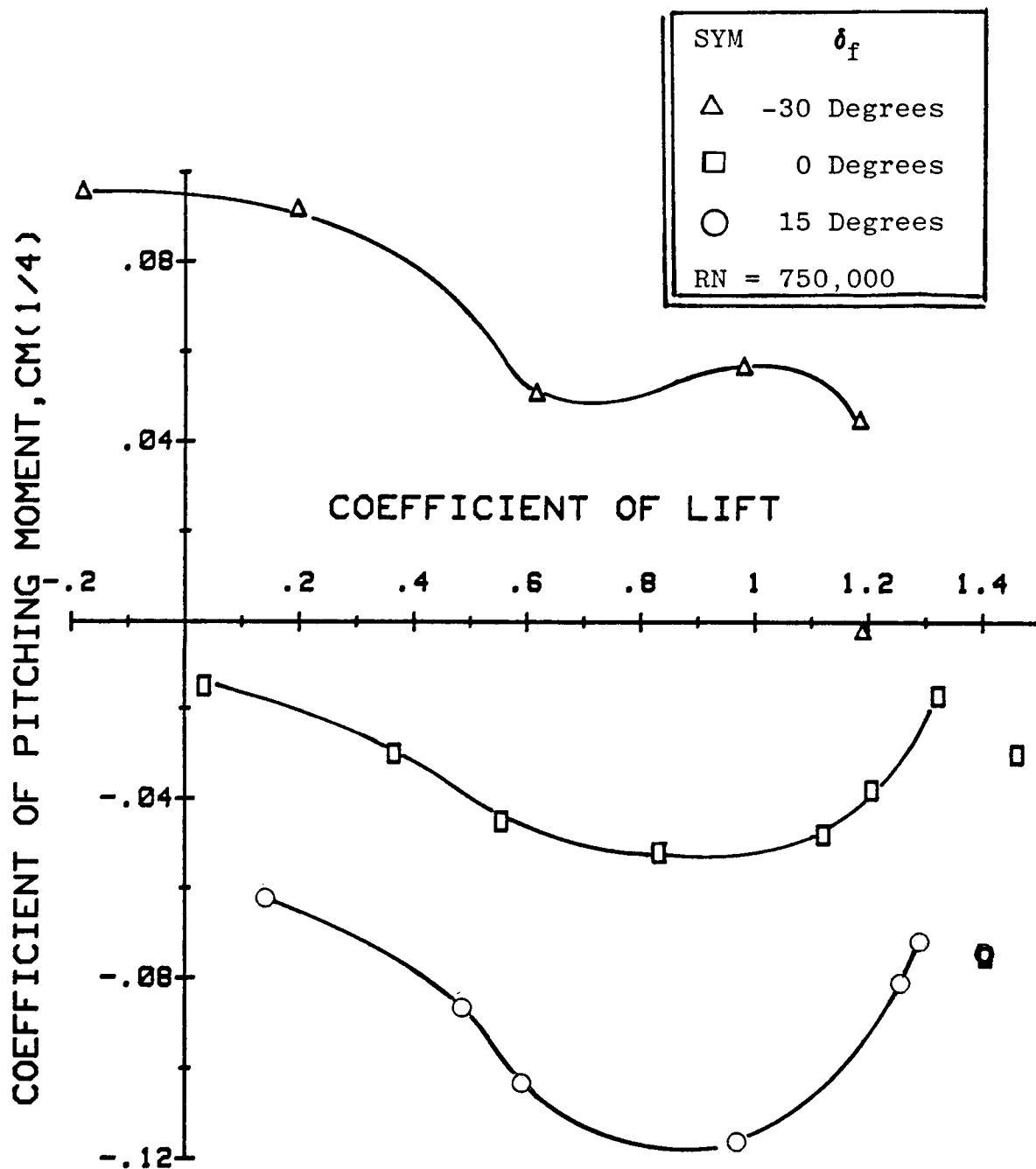Figure 22   Longitudinal Aerodynamic Characteristics for an XB-70-1 Model
(W + B + V + C) with Flap Deflections in Static Ground Effect.
H/b = 0.4.

(B) _CL   VS   CD_

Figure 22   Continued.

COEFFICIENT OF PITCHING MOMENT, CM(1/4)

COEFFICIENT OF LIFT

SYM	δ_f
△	-30 Degrees
□	0 Degrees
○	15 Degrees

RN = 750,000

(C) CM 1/4 VS CL

Figure 22   Concluded.

62

COEFFICIENT OF LIFT

H/b (A) CL vs H/b

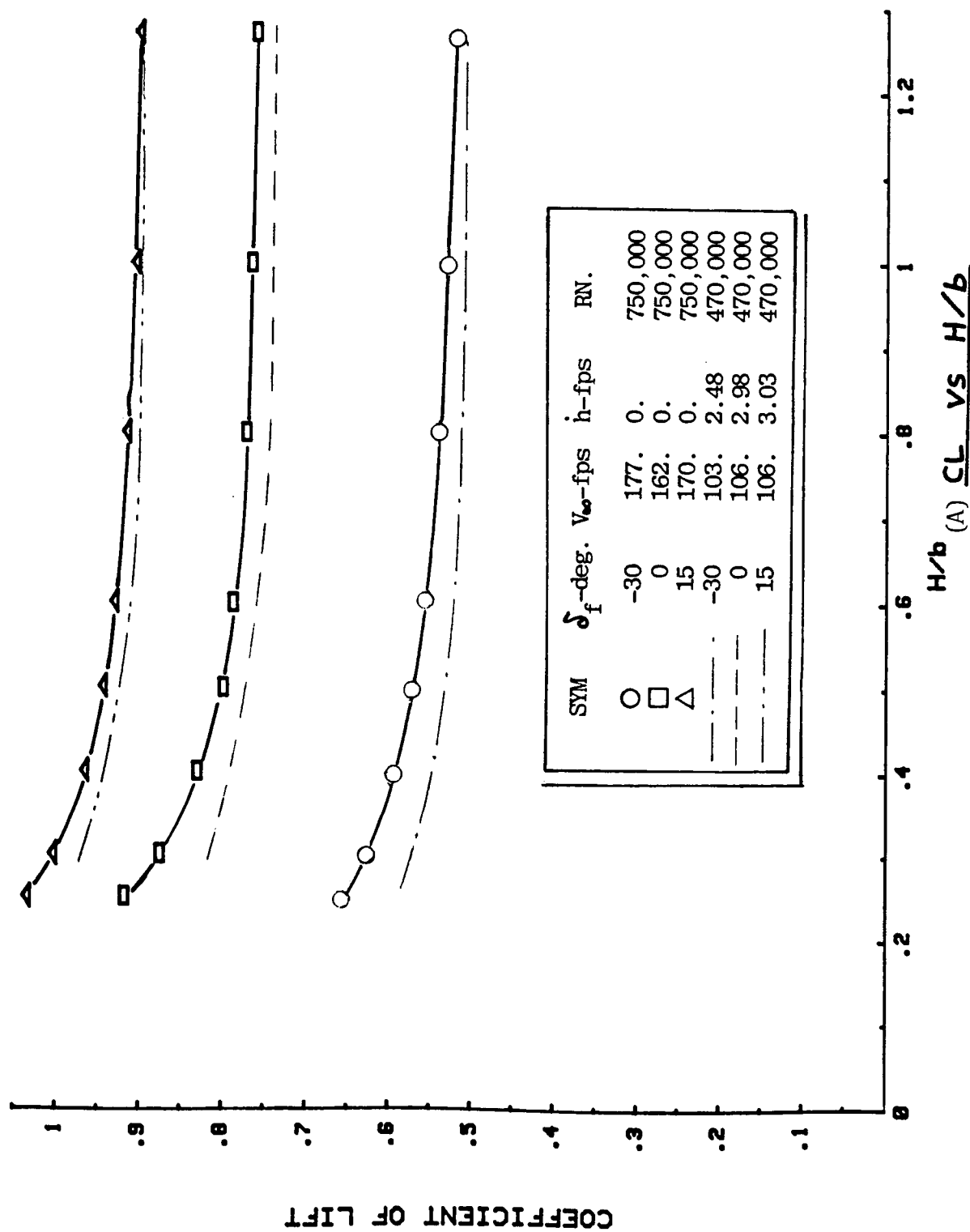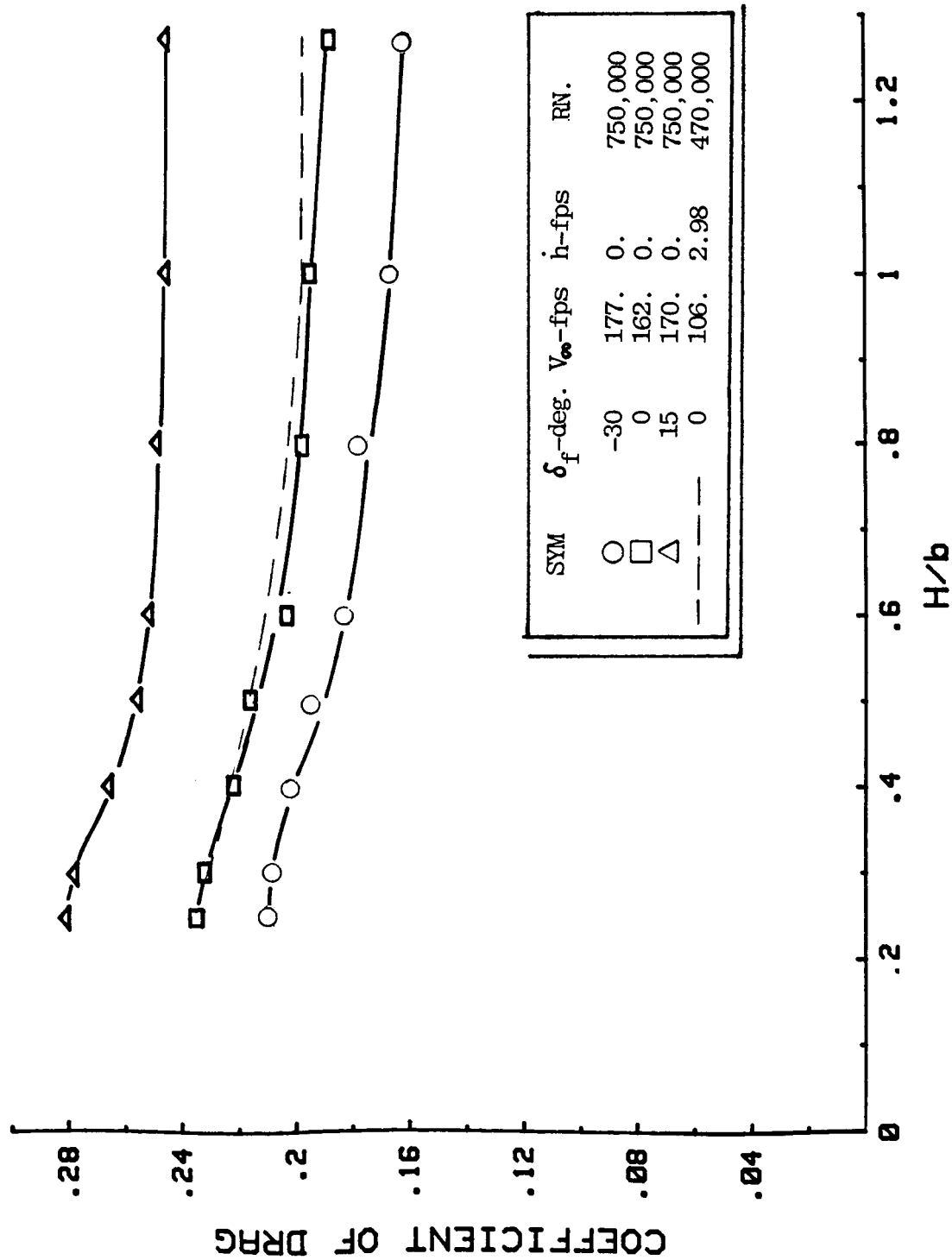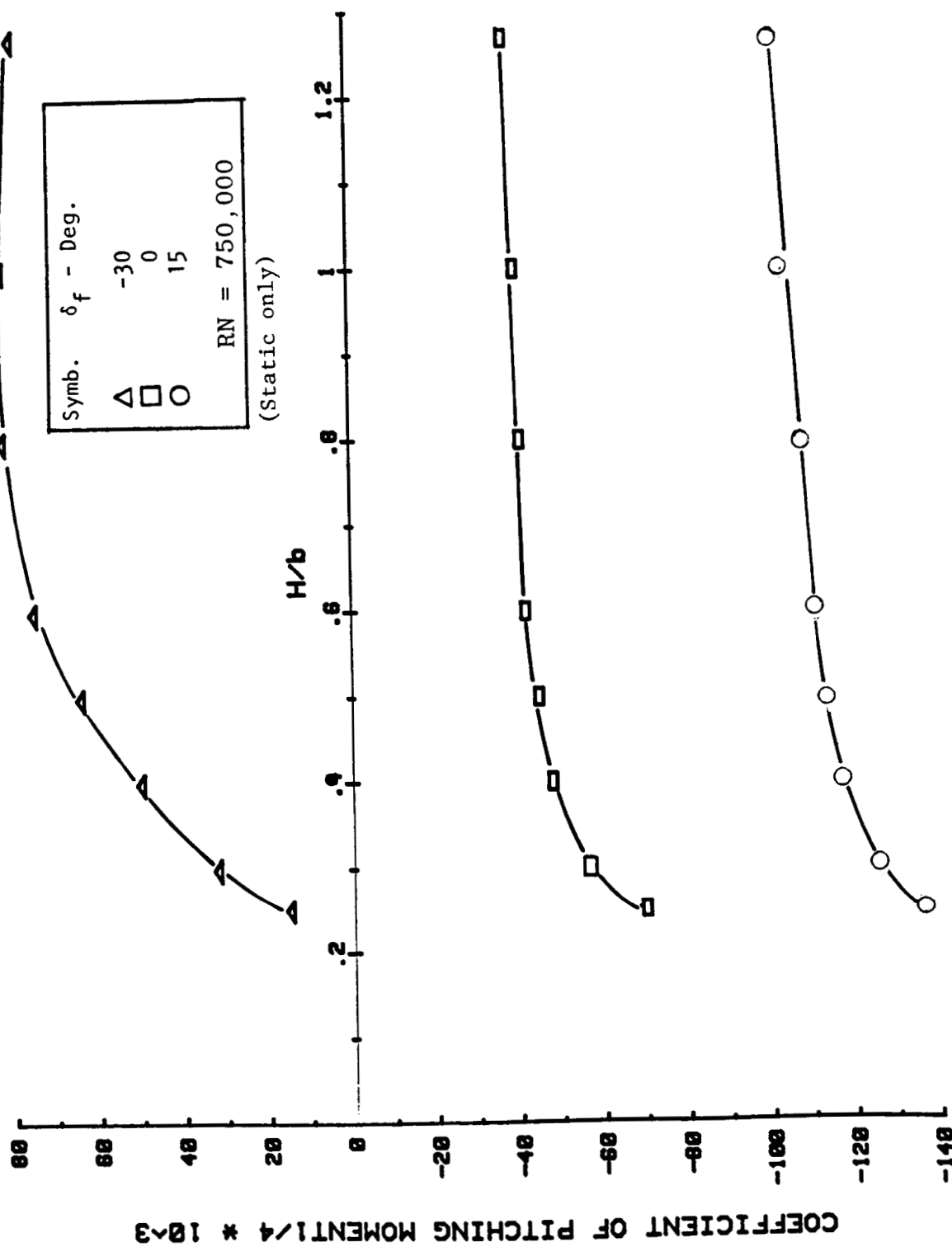| SYM	δ_f-deg.	V_∞-fps	$\dot{h}$-fps	RN.
◯	-30	177.	0.	750,000
☐	0	162.	0.	750,000
△	15	170.	0.	750,000
—··—	-30	103.	2.48	470,000
—·—	0	106.	2.98	470,000
———	15	106.	3.03	470,000

Figure 23   Effect of Flap Deflections on Longitudinal Aerodynamic
Characteristics for an XB-70-1 Model in Static and Dynamic
Ground Effect Testing, at $\alpha \simeq$ 14 Degrees.

63

(B) CD VS H/b Continued.

Figure 23

64

(C) $CM_{(1/4\bar{c})}$ VS H/b

Figure 23   Concluded.

SYM	δ_f-deg.	V_∞-fps	h-fps	RN.
O	-30	177.	0.	750,000
□	0	162.	0.	750,000
△	15	170.	0.	750,000
— · —	-30	103.	2.48	470,000
— —	0	106.	2.98	470,000
— · · —	15	106.	3.03	470,000

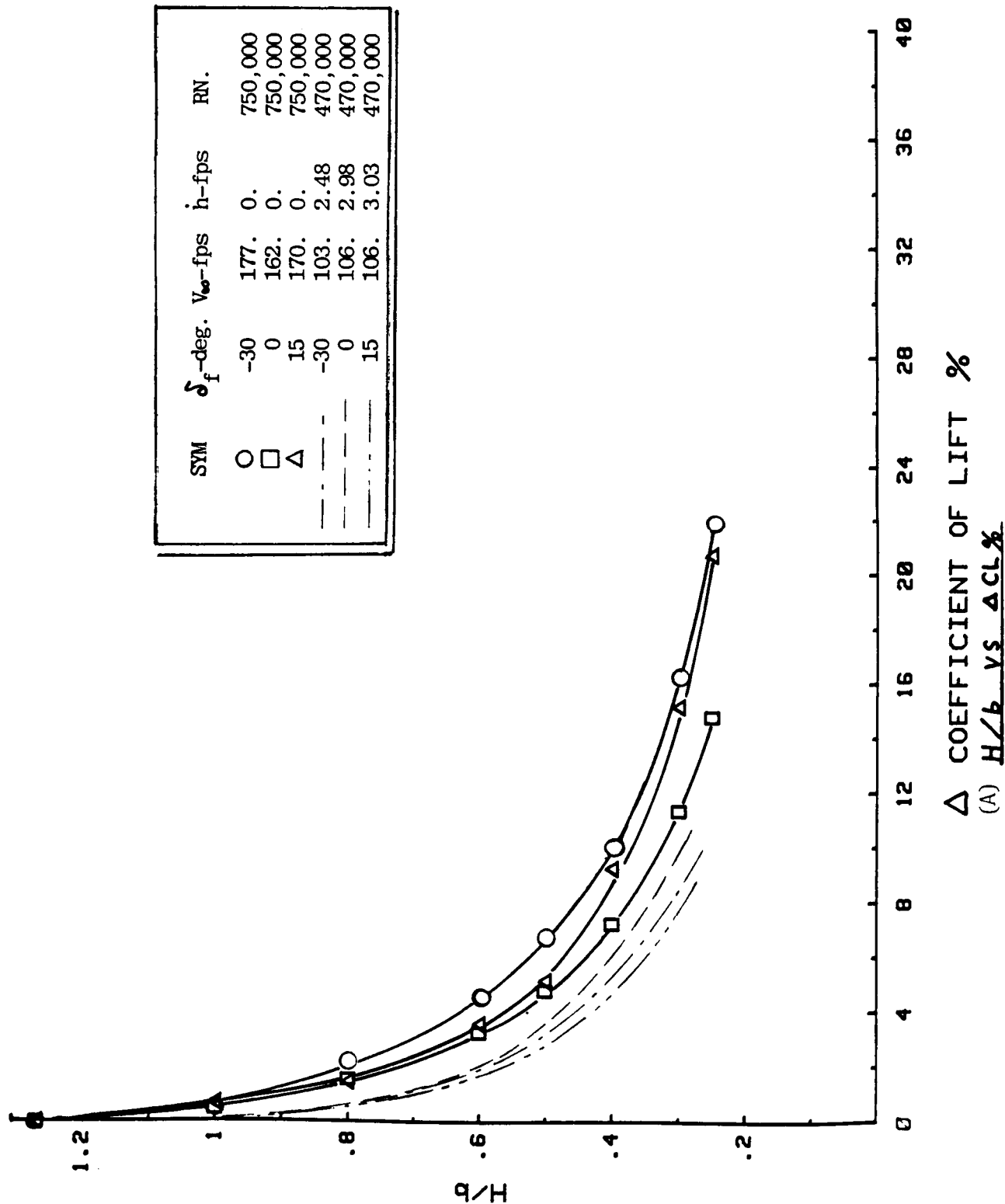$\triangle$ COEFFICIENT OF LIFT %

(A) **H/b vs △CL%**

H/b

Figure 24　Incremental Lift and Drag for an XB-70-1 Model with Flap Deflections in Static and Dynamic Ground Effect at $\alpha \simeq 14$ Degrees.

SYM	δ_f-deg.	V_∞-fps	$\dot{h}$-fps	RN.
□	-30	177.	0.	750,000
△	0	162.	0.	750,000
○	15	170.	0.	750,000
---	0	106.	2.98	470,000

H/b

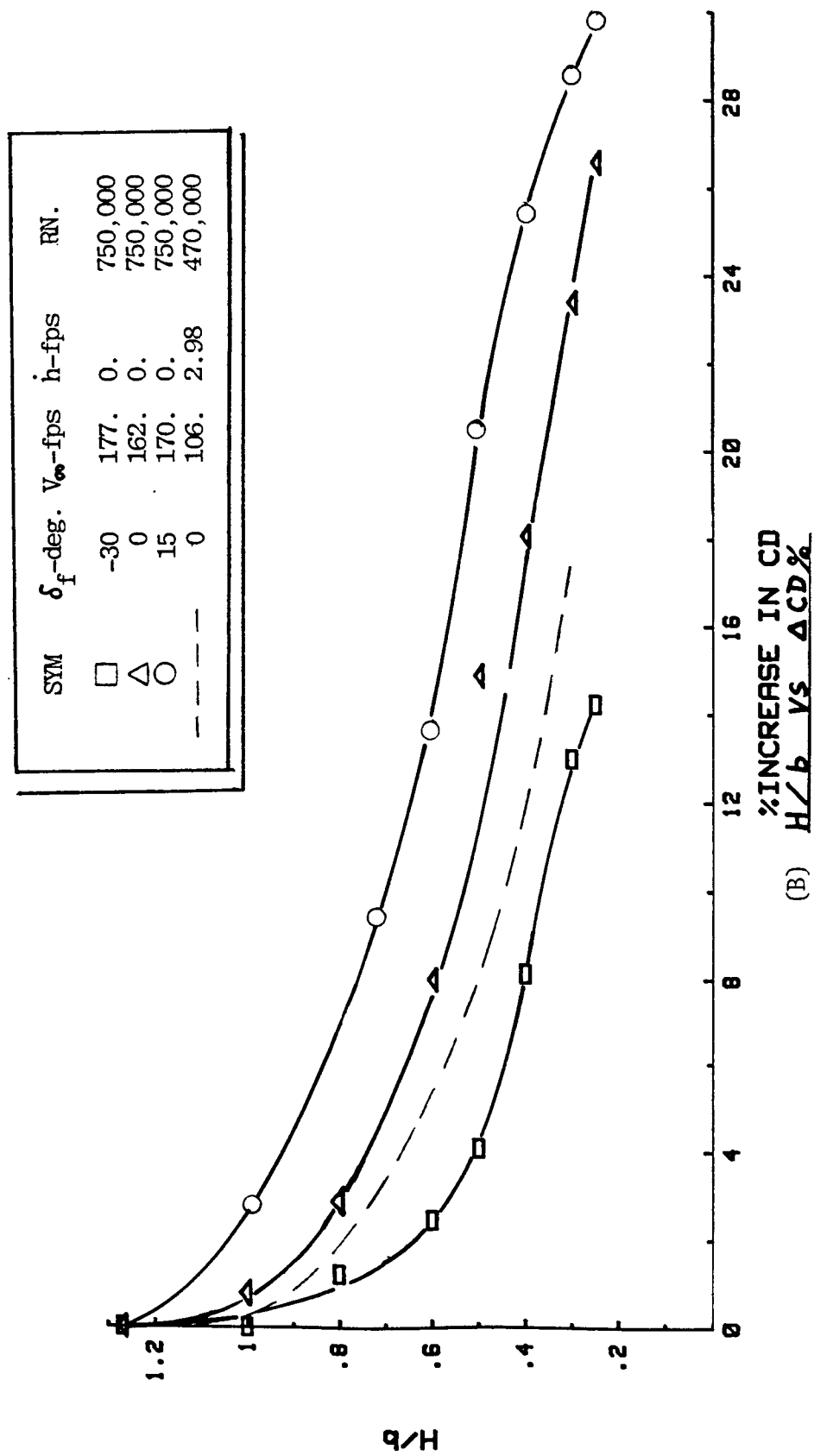%INCREASE IN CD

H/b vs ΔCD%

(B)

Figure 24   Concluded.
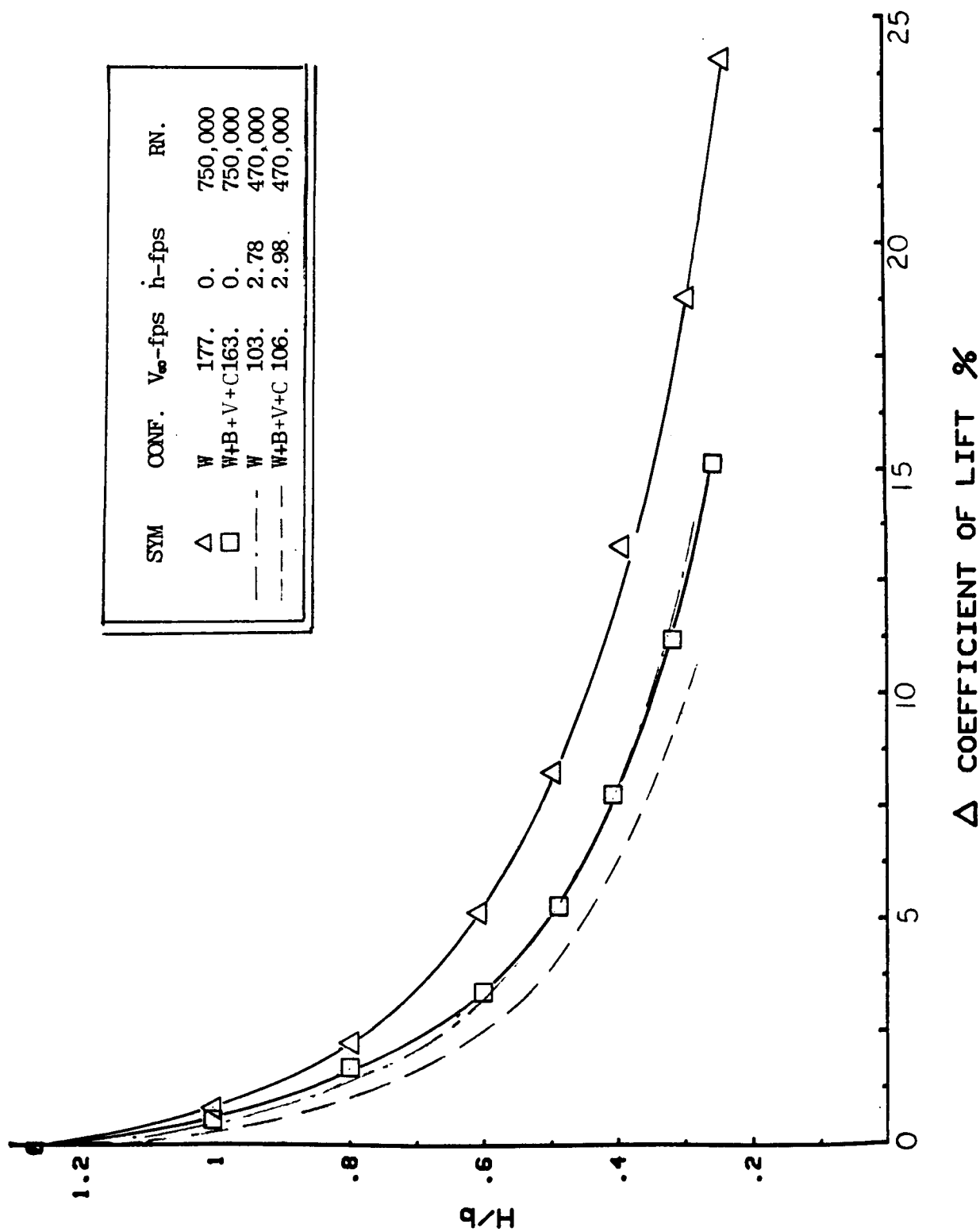
Figure 25   Incremental Lift for an XB-70-1 Model with and without Fuselage in Static and Dynamic Ground Effect at α = 14 Degrees.
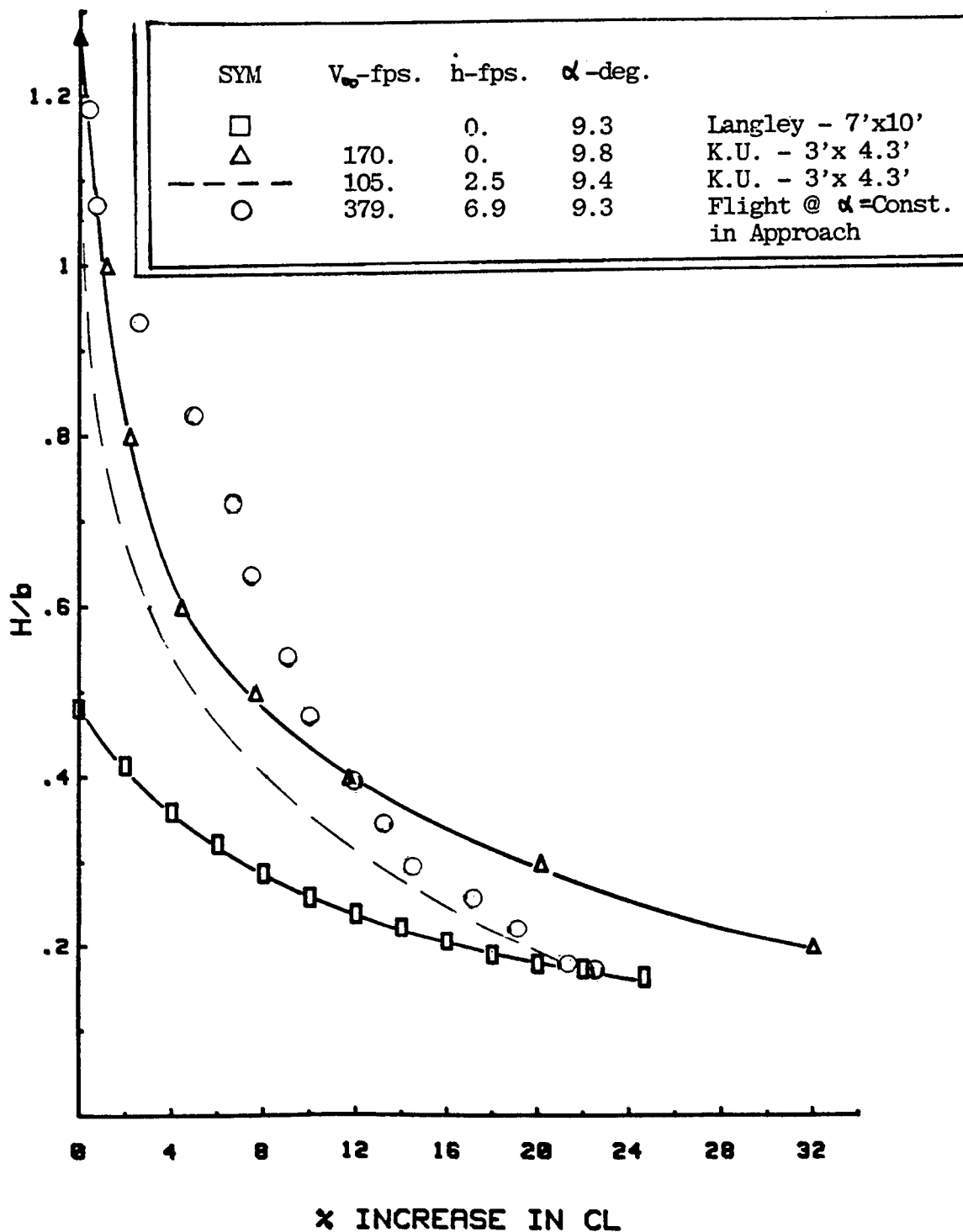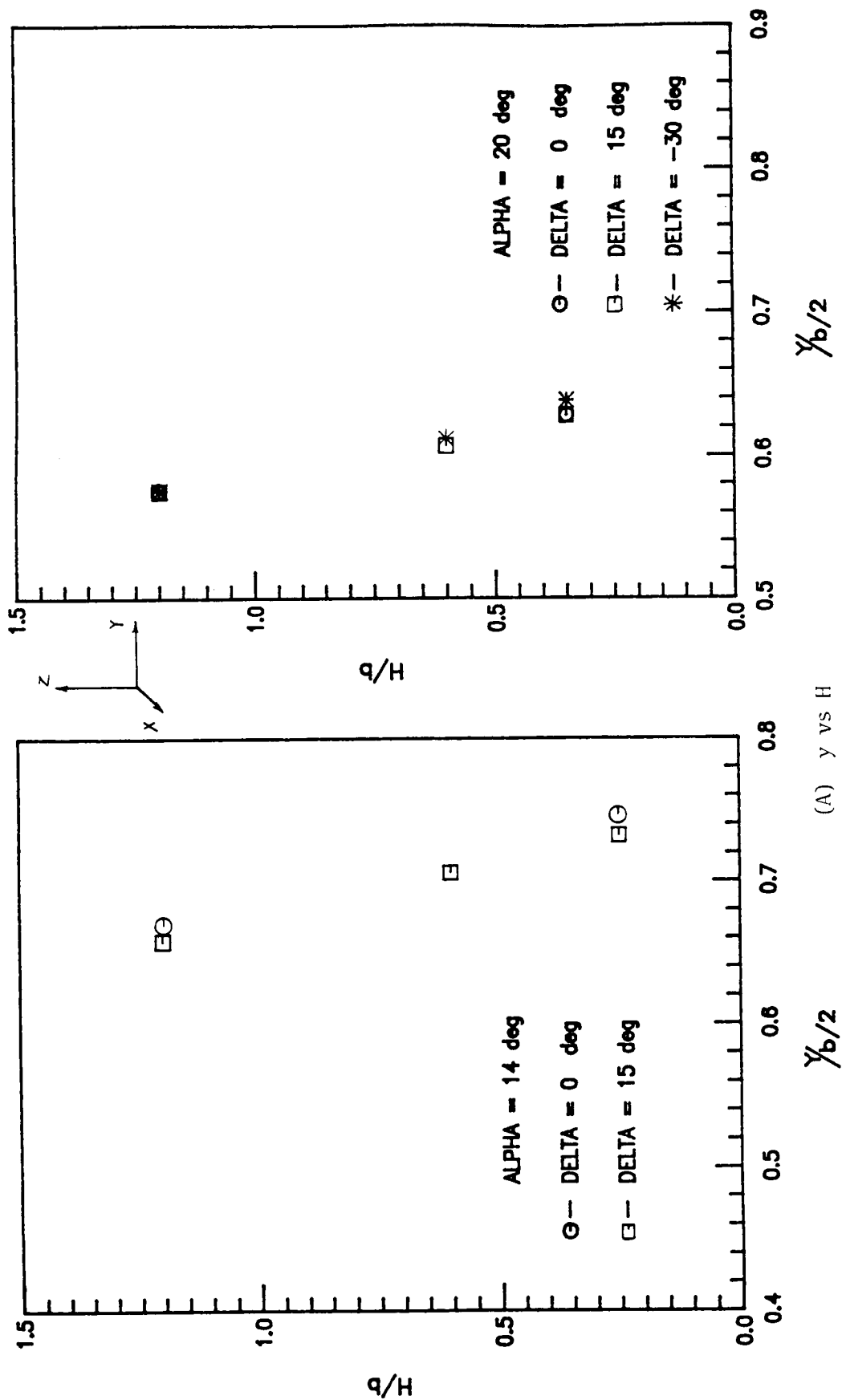
SYM	V_∞-fps.	$\dot{h}$-fps.	α-deg.	
□		0.	9.3	Langley - 7'x10'
△	170.	0.	9.8	K.U. - 3'x 4.3'
— — — —	105.	2.5	9.4	K.U. - 3'x 4.3'
○	379.	6.9	9.3	Flight @ α=Const. in Approach

Figure 26   Comparison of Ground Effect Data for the
XB-70-1 Configuration from Flight Test and
Wind-Tunnel Static and Dynamic Test.

Figure 27 Locations of the Vortex Core Center in Static Ground Effect for an F-106 Model at $x_r/c_r = 1.0$. x_r is Measured from Wing Apex.
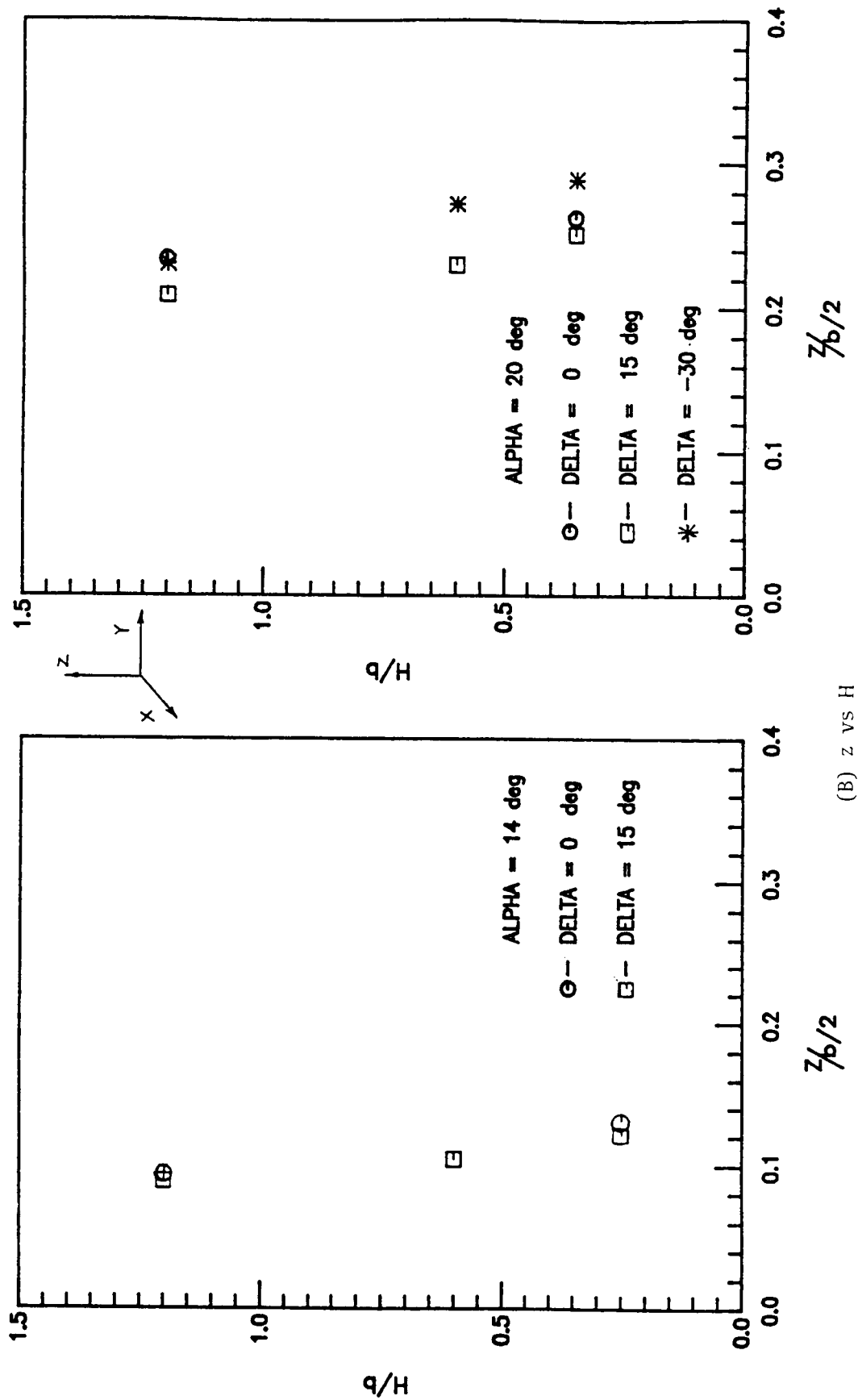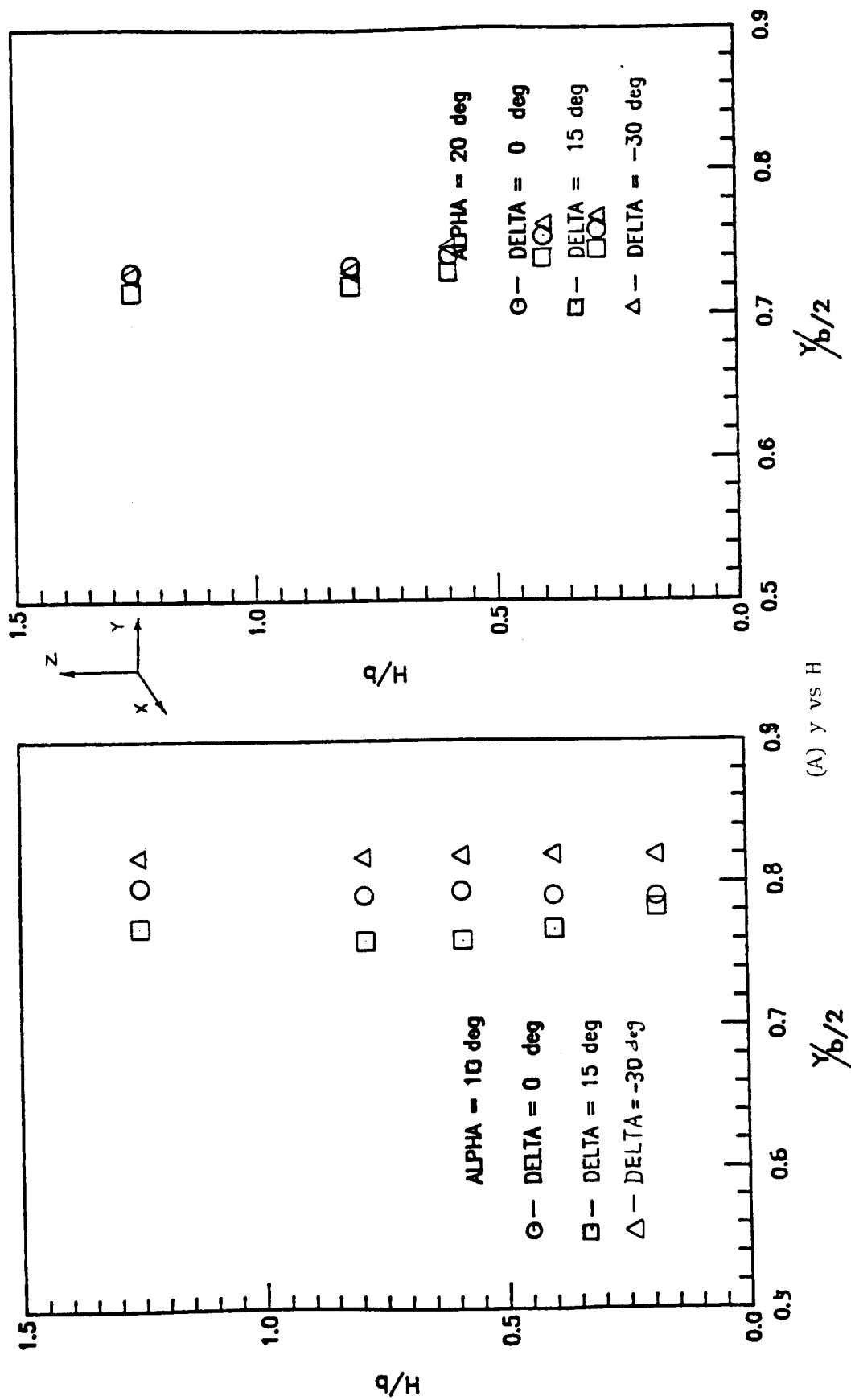
70

(B) z vs H
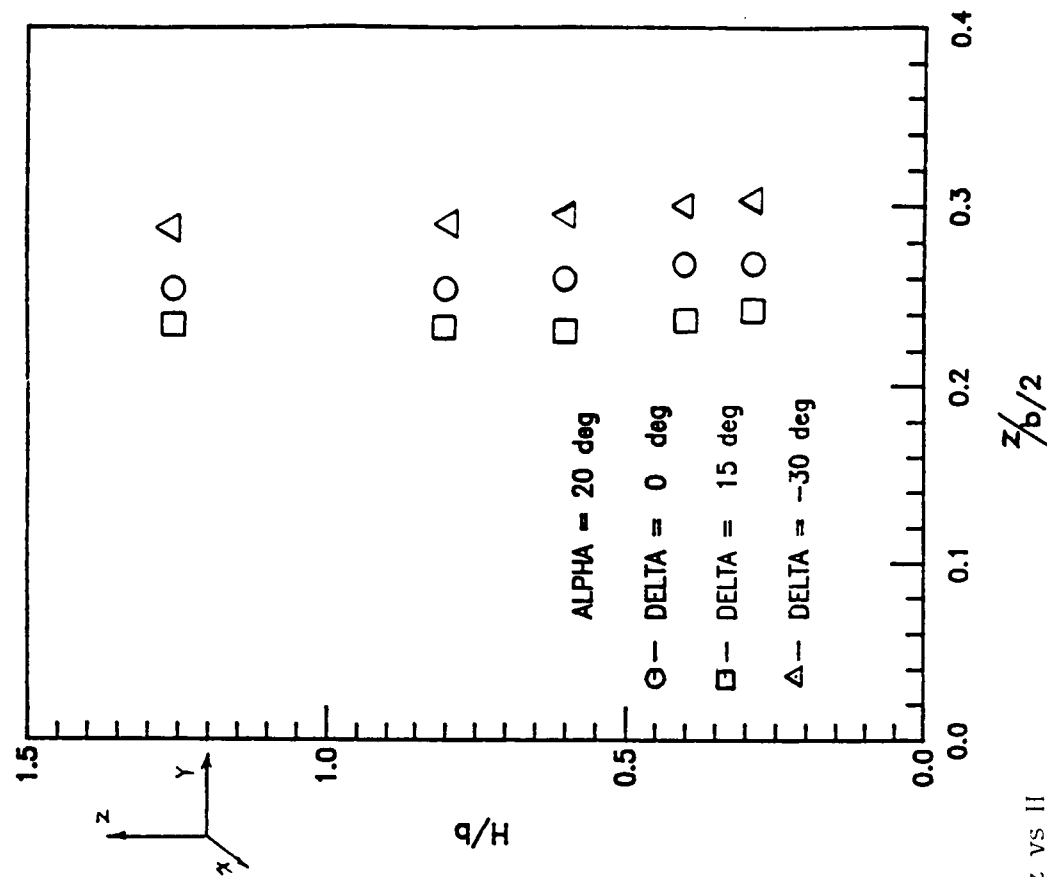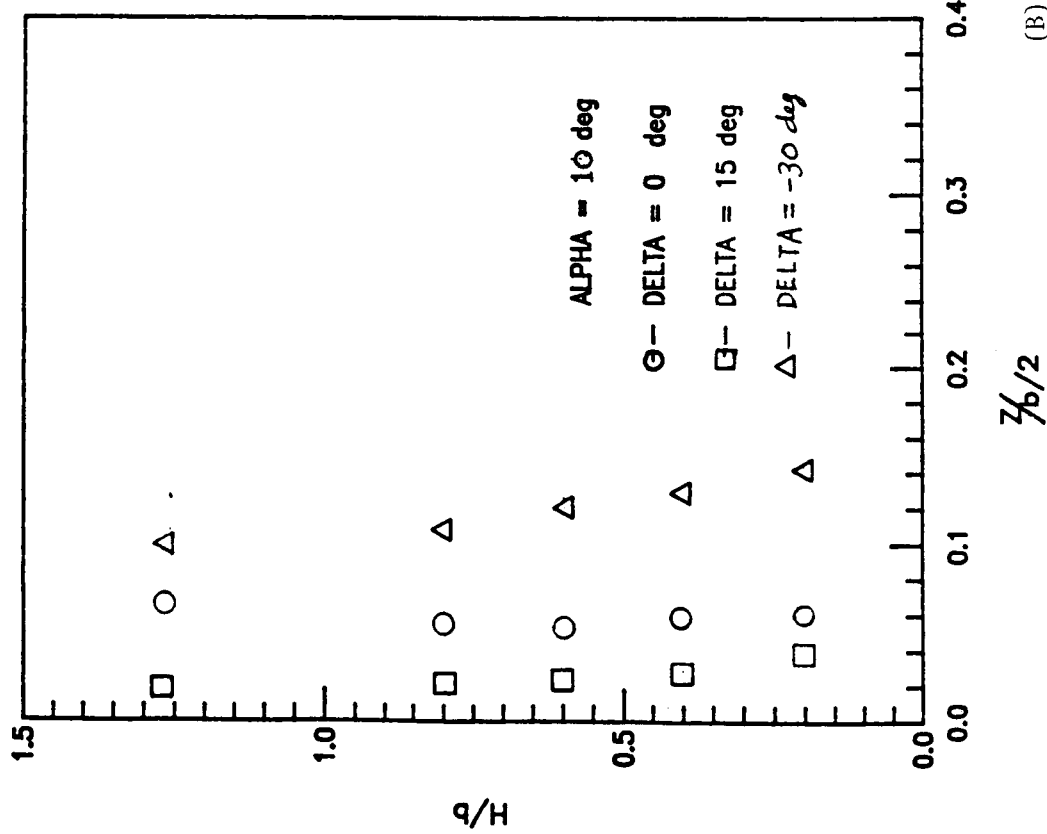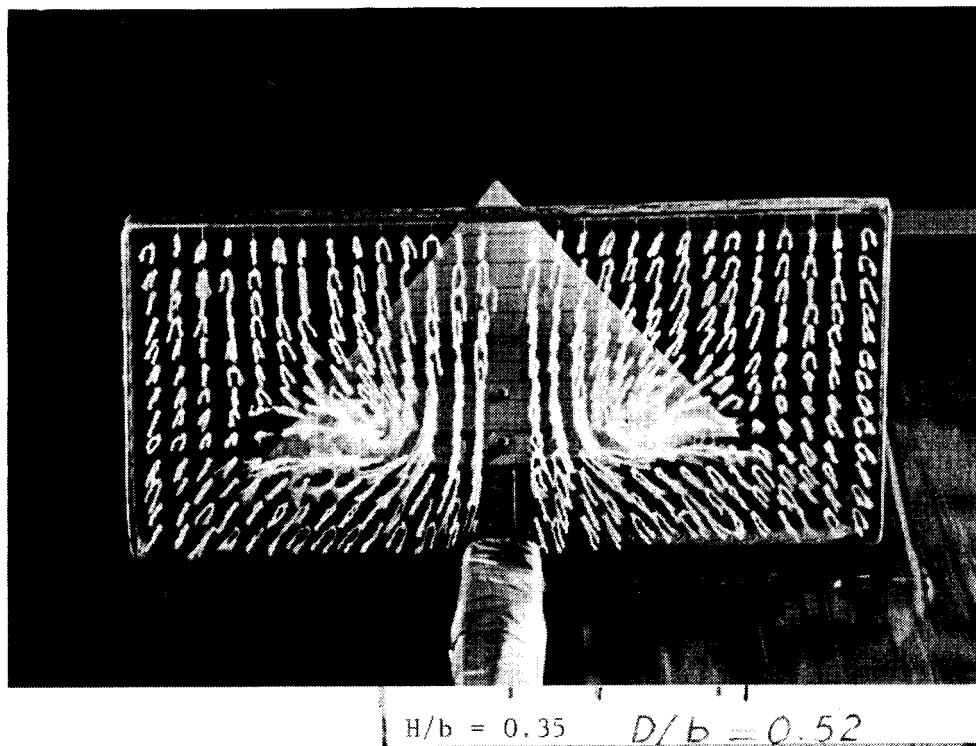
Figure 27   Concluded.

Figure 28 Locations of the Vortex Core Center in Static Ground Effect for an XB-70-1 Model at $x_r/c_r = 1.06$. x_r is Measured from Wing Apex.

(A) y vs H

(B) z vs II

Figure 28 Concluded.

H/b = 1.60   D/b = 0.48

H/b = 0.35   D/b = 0.52
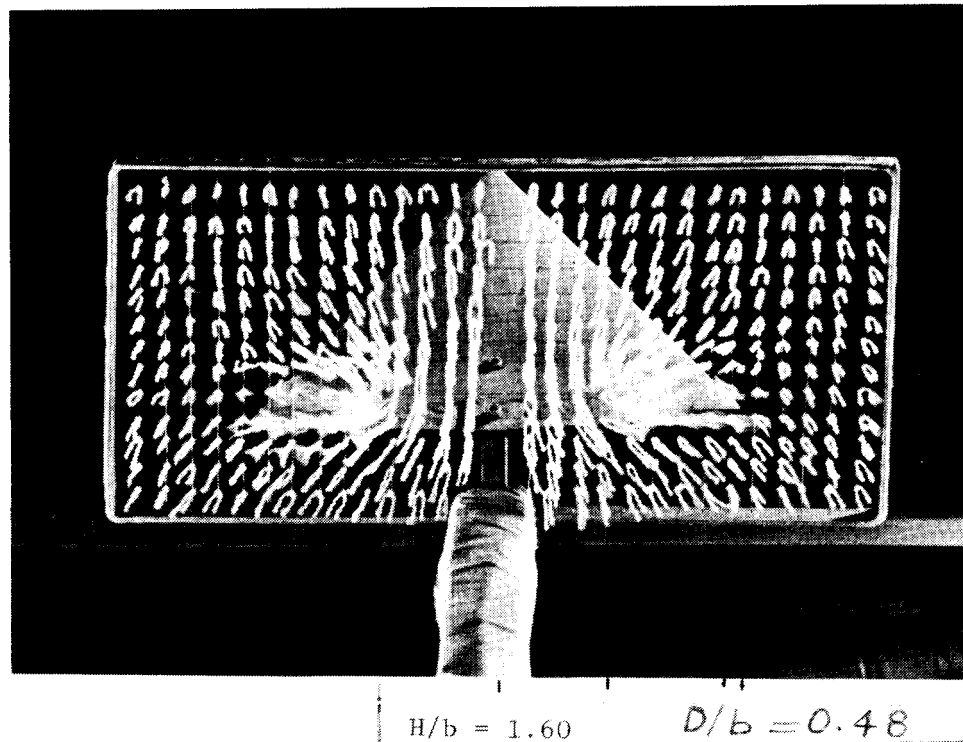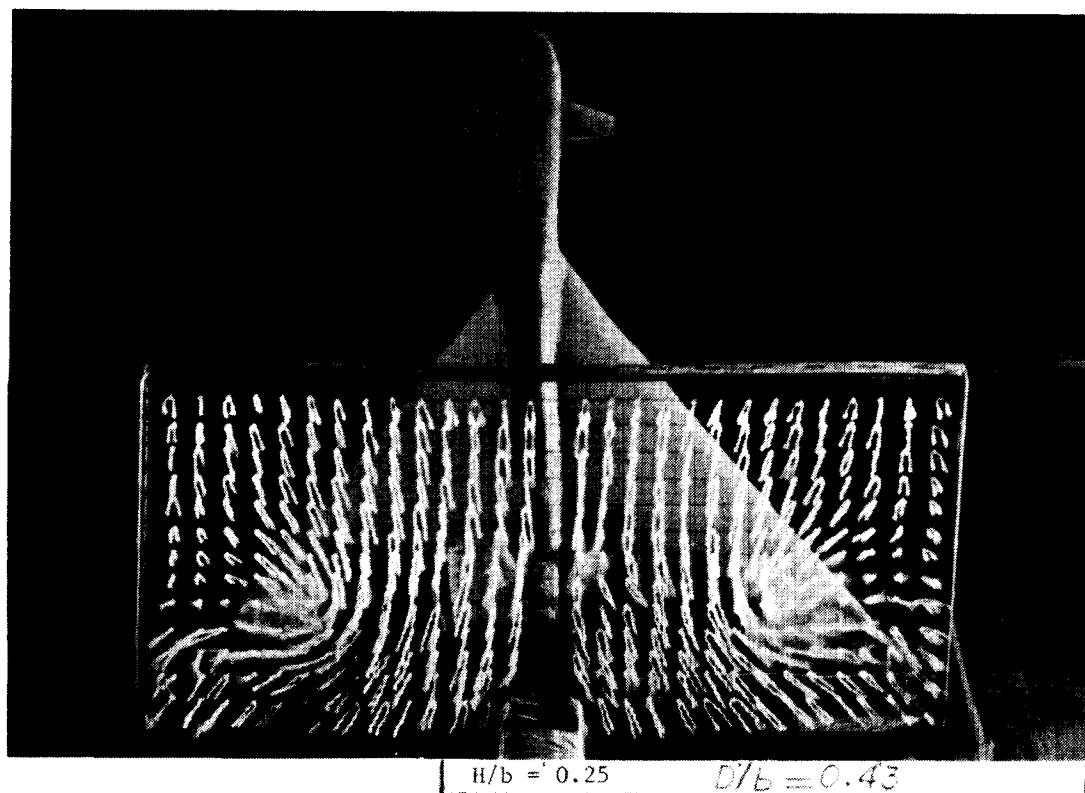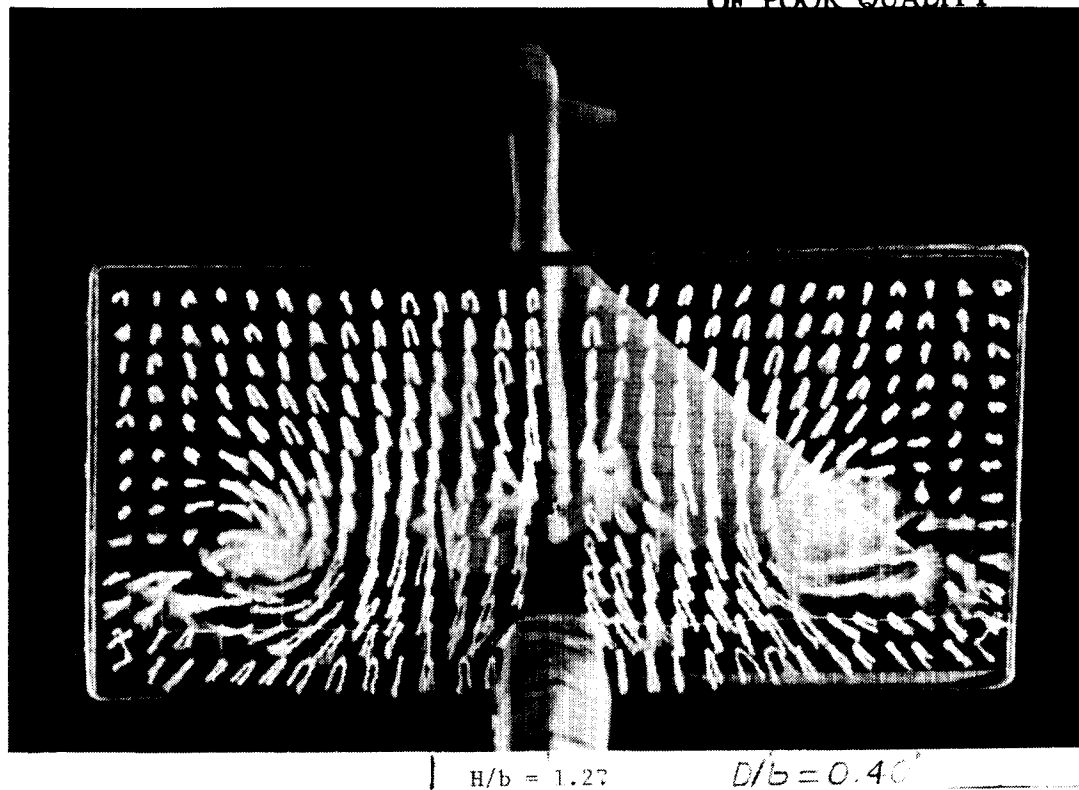
$\alpha = 20°$ $\delta_f = 0°$ $V_\infty = 80$ fps $X_r/C_r = 1.00$

Figure 29   Sizes of Vortex Cores in Static Ground Effect Effect from Flow
Visualization. F-106 Wing Alone.

74

H/b = 1.27   D/b = 0.46

H/b = 0.25   D/b = 0.43

$\alpha = 14°$ $\delta_f = 0°$ $V_\infty = 80$ fps $X_r/C_r = 1.06$

Figure 29   Concluded. XB-70 Model.

NASA
National Aeronautics and
Space Administration

Report Documentation Page

1. Report No. NASA CR-4105	2. Government Accession No.	3. Recipient's Catalog No.

4. Title and Subtitle	5. Report Date
An Experimental Investigation of Dynamic Ground Effect	December 1987
	6. Performing Organization Code

7. Author(s)	8. Performing Organization Report No.
Pai Hung Lee, C. Edward Lan, and Vincent U. Muirhead	CRING-FRL-717-1

9. Performing Organization Name and Address	10. Work Unit No. 505-61-71-02
Flight Research Laboratory The University of Kansas Center for Research, Inc. Lawrence, Kansas, 66045	11. Contract or Grant No. NAG1-616

12. Sponsoring Agency Name and Address	13. Type of Report and Period Covered
National Aeronautics and Space Administration Langley Research Center Hampton, Virginia 23665-5225	Contractor Report
	14. Sponsoring Agency Code

15. Supplementary Notes

Langley Technical Monitor: John W. Paulson, Jr.

Final Report

16. Abstract

A 60-degree delta wing, an F-106B, and an XB-70 models with and without flap deflections were tested in static and dynamic ground effect in the 36-by-51-inch subsonic wind tunnel at the University of Kansas. Dynamic ground effect was measured with movable sting support. For flow visualization, a tufted wire grid was mounted on the movable sting behind the model.

Test results showed that the lift and drag increments in dynamic ground effect were always lower than the static values. Effect of the trailing-edge flap deflections on lift increments was slight. The fuselage reduced the lift increments at a given ground height. From flow visualization under static conditions, the vortex core was seen to enlarge as the ground was approached.

17. Key Words (Suggested by Author(s))	18. Distribution Statement
Ground effect Static Dynamic Rate-of-descent Flow visualization	Unclassified-Unlimited Subject Category 02

19. Security Classif. (of this report)	20. Security Classif. (of this page)	21. No. of pages	22. Price
Unclassified	Unclassified	86	A05